Dissertation

Reliable detection of SARS-CoV-2 and prevention of SARS-CoV-2 variant infection with an ACE2-Fc fusion protein produced in *Nicotiana benthamiana*

Submitted by

Esther FÖDERL-HÖBENREICH

for the Academic Degree of

Doctor of Medical Science (Dr. scient. med.)

at the

Medical University of Graz

Institute of Pathology

under the Supervision of

Prof. I.R. Dr. Kurt ZATLOUKAL

2025

Statutory Declaration

I hereby confirm that the present thesis is the result of my own independent scholarly work. I also confirm that in all cases, where material from the work of others (in books, articles, essays, dissertations, and on the internet) is acknowledged, quotations and paraphrases are clearly indicated. No material other than that cited in the reference list has been used. I have read and understood the Medical University's regulations and procedures concerning plagiarism. Furthermore, I hereby declare that if artificial intelligence (AI) tools were used for the generation and/or correction of certain text passages in the creation of this work, such employment was conducted in compliance with ethical principles, academic integrity, and the regulations of my university. Additionally, it was ensured that this usage was transparently disclosed and appropriately attributed.

Graz, 06.08.2025 Esther Föderl-Höbenreich

Disclosure

Parts of this dissertation are published in the following peer-reviewed original research articles, and parts of the published work are being reproduced in this dissertation:

(1) **Esther Föderl-Höbenreich[1]***, Shiva Izadi[2]*, Lara Hofacker[2], Nikolaus F. Kienzl[2], Alexandra Castilho[2], Richard Strasser[2], Ferran Tarrés-Freixas[3,4], Guillermo Cantero[3,4], Núria Roca[3,4], Mònica Pérez[3,4], Cristina Lorca-Oró[3,4], Carla Usai[3,4], Joaquim Segalés[4,5], Júlia Vergara-Alert[3,4], Lukas Mach[2**], Kurt Zatloukal[1**]. An ACE2-Fc decoy produced in glycoengineered plants neutralizes ancestral and newly emerging SARS-CoV-2 variants and demonstrates therapeutic efficacy in hamsters. Scientific Reports. 2025 Apr 2; https://doi.org/10.1038/s41598-025-95494-w

[1] Diagnostic and Research Institute of Pathology, Medical University of Graz, Graz, Austria

[2] Institute of Plant Biotechnology and Cell Biology, Department of Biotechnology and Food Sciences, BOKU University, Vienna, Austria

[3] IRTA, Animal Health, Centre de Recerca en Sanitat Animal (CReSA), Campus de la Universitat Autònoma de Barcelona (UAB), 08193 Bellaterra, Catalonia, Spain

[4] Unitat mixta d'investigació IRTA-UAB en Sanitat Animal, Centre de Recerca en Sanitat Animal (CReSA), Campus de la Universitat Autònoma de Barcelona (UAB), 08193 Bellaterra, Catalonia, Spain

[5] Departament de Sanitat i Anatomia Animals, Facultat de Veterinària, Universitat Autònoma de Barcelona, 08193 Bellaterra, Catalonia, Spain

(2) Melina Hardt [1,*], **Esther Föderl-Höbenreich [1,*]**, Stephanie Freydl [1], Antonio Kouros [1], Martina Loibner [1], Kurt Zatloukal [1,*]. Pre-analytical sample stabilization by different sampling devices for PCR-based COVID-19 diagnostics. New Biotechnology. 2022 Apr 8; doi: 10.1016/j.nbt.2022.04.001.
[1]Diagnostic- and Research Center for Molecular Biomedicine, Diagnostic- and Research Institute of Pathology, Medical University of Graz, Graz, Austria.

(3) Tümay Capraz[1]† , Nikolaus F Kienzl[2]† , Elisabeth Laurent[3]† , Jan W Perthold[1] , **Esther Föderl-Höbenreich**[4] , Clemens Grünwald-Gruber[5] , Daniel Maresch[5] , Vanessa Monteil[6] , Janine Niederhöfer[7] , Gerald Wirnsberger[7] , Ali Mirazimi[6,8], Kurt Zatloukal[4], Lukas Mach[2*], Josef M Penninger[9,10*], Chris Oostenbrink[1*], Johannes Stadlmann[5,9*]. Structure-guided glyco-engineering of ACE2 for improved potency as soluble SARS-CoV-2 decoy receptor.

Elife. 2021 Dec 20;10:e73641. doi: 10.7554/eLife.73641. PMID: 34927585; PMCID: PMC8730730.

[1] Institute for Molecular Modeling and Simulation, University of Natural Resources and Life Sciences (BOKU), Vienna, Austria;

[2] Institute of Plant Biotechnology and Cell Biology, Department of Applied Genetics and Cell Biology, University of Natural Resources and Life Sciences (BOKU), Vienna, Austria;

[3] Institute of Molecular Biotechnology, Department of Biotechnology and Core Facility Biomolecular & Cellular Analysis, University of Natural Resources and Life Sciences (BOKU), Vienna, Austria;

[4] Diagnostic and Research Institute of Pathology, Medical University of Graz, Graz, Austria;

[5] Institute of Biochemistry, Department of Chemistry, University of Natural Resources and Life Sciences, Vienna, Austria;

[6] Karolinska Institute, Department of Laboratory Medicine, Stockholm, Sweden;

[7] Apeiron Biologics, Vienna, Austria;

[8]National Veterinary Institute, Uppsala, Sweden;

[9]IMBA - Institute of Molecular Biotechnology of the Austrian Academy of Sciences, Dr. Bohr, Vienna, Austria; [10]Department of Medical Genetics, Life Sciences Institute, University of British Columbia, Vancouver, Canada

Parts of the research presented in this thesis are protected by patent application A50477/2024, titled “Isolated polypeptides comprising an ACE2 moiety and a stability-increasing polypeptide moiety".

All ACE2-Fc constructs that were used in this study were designed and expressed by our collaboration partners at the Institute of Plant Biotechnology and Cell Biology of BOKU University, Vienna. Further, data shown in Figure 9b, Figure 10, Figure 13, Figure 18a and Figure 19 were produced by our collaboration partners at BOKU University. The *in vivo* study was performed at the Biosafety Level-3 facilities of the Biocontainment Unit of IRTA-CReSA in Barcelona, Spain.

During the preparation of this thesis, DeepL write (DeepL SE, https://www.deepl.com/writ) was used to enhance the language and readability. After using the tool, the content was thoroughly reviewed and edited.

Funding

This thesis was conducted at the Diagnostic and Research Institute of Pathology in Graz, Austria. The PhD student Esther Föderl-Höbenreich received funding from the Medical University of Graz through the Dr.med.sci. program “Sustainable health research”. Part of the thesis have been funded by a joint research project at the Diagnostic and Research Center for Molecular BioMedicine. The *in vivo* experiments have been funded by a Trans National Access grant within the EU-project ISIDORe (GA 101046133) granted to Zatloukal Innovations GmbH.

Acknowledgements

This dissertation would not have been possible without the support, encouragement, and guidance of many wonderful people.

First and foremost, I would like to thank my amazing family and friends. Your support in both happy and sad times means the world to me.

I would like to thank my supervisor, Kurt Zatloukal, for giving me the freedom to pursue and develop my own ideas. Your trust and encouragement have been instrumental in fostering my confidence and refining my expertise through independent work.

A special thanks goes to Lukas Mach for his generous investment of time, invaluable input, and constructive feedback. Your contributions have significantly enriched this dissertation.

I would also like to thank my colleagues for making this journey not only productive but also enjoyable. You made work feel like anything but work.

Furthermore, I would like to express my gratitude to our cooperation partners at BOKU University and highlight their valuable contributions to this dissertation.

Table of Contents

List of abbreviations

ACE2	angiotensin-converting enzyme 2
ADE	antibody dependent enhancement
ALI	air-liquid interface
Ang	Angiotensin
ARDS	acute respiratory distress syndrome
BE	artificial body excretion
BSL-3	Biosafety Level-3
CCL5	C-C Motif Chemokine Ligand 5
CoM	conditioned media

COVID-19	Coronavirus disease 2019
CPE	cytopathic effects
CXCL10	chemokine ligand 10
ELISA	Enzyme-linked immunosorbent assay
FcR	Fc receptor
FCS	fetal calf serum
FFPE	formalin-fixed paraffin-embedded
hMDM	human monocyte derived macrophages
hpi	hours post infection
HPRT1	Hypoxanthine Phosphoribosyltransferase 1
HRP	Horseradish Peroxidase
hrsACE2	human recombinant soluble ACE2
IC_{50}	half-maximal inhibitory concentrations
IFN	interferon
IFN-γ	Interferon gamma
Ig	Immune globulin
IL-1β	Interleukin-1 beta
IL-6	Interleukin-6
MEM	Minimal Essential Medium
MERS	Middle East respiratory syndrome
MOI	multiplicity of infection
MX2	MX Dynamin Like GTPase 2
N. benthamiana	Nicotiana benthamiana
PBS	Phosphate-buffered saline

PenStrep	Penicillin-Streptomycin
PF-332	PF-07321332
PFPE	PaxGene-fixed paraffin-embedded
pfu	plaque forming units
RAS	Renin-Angiotensin system
RBD	receptor binding domain
RT-qPCR	Reverse transcription quantitative polymerase chain reaction
SARS-CoV-1	Severe acute respiratory syndrome
SARS-CoV-2	Severe acute respiratory syndrome 2
sIgA	secretory IgA
$TCID_{50}$	Tissue Culture Infectious Dose 50
TMPRSS2	Transmembrane Serine Protease 2
TNF-α	Tumour Necrosis Factor alpha
UTM	Universal Transport Medium
VOC	Variant of Concern
VPM	Viral Preservative Medium
VTM	Viral Transport Medium

List of Figures

List of Tables

Abstract (German)

SARS-CoV-2 hat im Jahr 2019 eine weltweite Pandemie ausgelöst und eindrücklich gezeigt, welchen verheerenden Schaden neu auftretende Infektionskrankheiten anrichten können. Neben Maßnahmen wie Abstandhalten und dem Tragen von Masken wurden Massentestungen zu einer der zentralen Strategien, um die Verbreitung des Virus einzudämmen. Um zuverlässige Diagnostik zu gewährleisten, ist es wichtig den Einfluss präanalytischer Faktoren auf die Testergebnisse zu untersuchen. Ein Teil dieser Dissertation befasst sich mit den Auswirkungen präanalytischer Faktoren, wie Lagerzeit und Temperatur von Abstrichproben, auf die Nachweisbarkeit von SARS-CoV-2. Unsere Untersuchungen zeigen, dass sowohl die Wahl des Transportmediums als auch die Lagerzeit und Temperatur die RNA-Integrität signifikant beeinflussen.

Zusätzlich zu den genannten präventiven Maßnahmen wurde mit beispiellosem Tempo an therapeutischen Behandlungsansätzen und Impfstoffen geforscht. Der Schwerpunkt dieser Dissertation liegt auf der Entwicklung eines Rezeptor-Mimetika, welches für die Expression in glykoengineerten Pflanzen optimiert wurde. Der zelluläre Rezeptor ACE2 wurde mit der Fc-domäne von Immunglobulin G fusioniert und die Proteinsequenz adaptiert, um nicht-humane posttranslationale Modifikationen zu minimieren und so potenzielle Antigenizität zu reduzieren. Rezeptor-Mimetika bieten den Vorteil weniger anfällig für Escape-Varianten zu sein, da die Rezeptorerkennung essenziell für eine effiziente Infektion ist. In *in vitro*-Tests konnte gezeigt

werden, dass in Pflanzen exprimiertes ACE2-Fc, SARS-CoV-2 neutralisiert und zudem robust gegenüber Varianten ist. Darüber hinaus wurde die therapeutische Wirksamkeit in einem syrischen Goldhamster-Modell nachgewiesen. Die nasale Applikation von ACE2-Fc verringerte den Gewichtsverlust infizierter Tiere signifikant.

Weiters wurden immunmodulatorische Eigenschaften von ACE2-Fc untersucht, insbesondere das Potential von Fc-Domäne-vermittelter Infektion von Makrophagen. Unsere Ergebnisse liefern keine Hinweise auf ein ACE2-Fc induziert Infektion oder Stimulierung von Makrophagen *in vitro.*

Zusammenfassend wurde in dieser Arbeit die Bedeutung präanalytischer Faktoren für die SARS-CoV-2 Diagnostik und das Potenzial von ACE2-Fc als antivirales Therapeutikum gezeigt. Das in Pflanzen produzierte, optimierte ACE2-Fc Protein neutralisiert SARS-CoV-2 in sowohl *in vitro* als auch *in vivo* Experimenten und ist robust gegenüber Varianten.

Abstract (English)

SARS-CoV-2 caused a global pandemic in 2019, demonstrating the devastating impact that newly emerging infectious diseases can have. Beyond preventive measures such as social distancing and mask-wearing, mass testing became one of the central strategies to control the spread of the virus. To ensure reliable diagnostics, it is essential to investigate the influence of pre-analytical variables on the detectability of SARS-CoV-2. Our investigations demonstrate that both the choice of transport medium and storage conditions including duration and temperature, significantly impact RNA integrity.

In addition to the aforementioned preventive measures, research on therapeutic treatments and vaccines progressed at an unprecedented pace. The main focus of this thesis is on the development of a receptor mimetic that has been optimized for the expression in glycoengineered plants. The cellular receptor ACE2 was fused to the Fc-domain of immunoglobulin G and the protein sequence was adapted to minimize non-human post-translational modifications and thus reduce potential antigenicity.

Receptor mimetics offer the advantage of being less susceptible to escape variants, as receptor recognition is essential for efficient infection. We demonstrated in *in vitro* assays that *in planta* expressed ACE2-Fc efficiently neutralizes SARS-CoV-2 and is also robust against SARS-CoV-2 variants of concern. In addition, the therapeutic efficacy was demonstrated in a Syrian golden hamster model where daily nasal application of ACE2-Fc significantly reduced the weight loss of infected animals.

Furthermore, immunomodulatory properties of ACE2-Fc were investigated, in particular the potential of Fc domain-mediated infection of macrophages. Our results showed no evidence of ACE2-Fc-induced infection or stimulation of macrophages *in vitro*.

In conclusion, this work underscores the significance of pre-analytical factors in SARS-CoV-2 diagnostics an demonstrates the potential of *in planta* produced ACE2-Fc as an antiviral therapeutic. The, optimized ACE2-Fc variant effectively neutralizes SARS-CoV-2 in both *in vitro* and *in vivo* experiments and exhibits robustness's against viral variants.

1. Introduction

1.1. Emergence and Evolution of SARS-CoV-2

Throughout history there have been repeated outbreaks of pathogenic viruses, like the Spanish flu in 1918, severe acute respiratory syndrome (SARS-CoV-1) in 2002, Middle East respiratory syndrome (MERS) in 2015 or severe acute respiratory syndrome 2 (SARS-CoV-2) in 2019, the causative virus of the Coronavirus disease 2019 (COVID-19) pandemic (1).

Many pandemics were caused by viruses originating from animals, underscoring the significant role of zoonotic transmissions. Close contact between animals and humans through livestock farming and wildlife markets increases the risk of so-called spillover events, where zoonotic pathogens cross multiple barriers to become transmissible to humans (2). For example, the Spanish flu, one of the deadliest pandemics in recorded history, was caused by an adapted avian influenza virus (3). Similarly, bats have been identified to be the natural reservoir for many coronaviruses including those responsible for SARS-CoV-1 and MERS (4).

From bats, the virus is passed over to intermediate hosts – for example palm civet in case of SARS and dromedary camel in case of MERS (4). The emergence of SARS-CoV-2 followed a comparable pattern. In the case of SARS-CoV-2, the virus also originated from bats and subsequently spilled over to minks. Finally, close contact between market workers and minks paved the way to animal-to-human transmission (5).

Soon after onset of the COVID-19 pandemic, SARS-CoV-2 started to gather mutations in its genome, especially in the spike gene. In December 2020 the World Health Organization identified the Alpha variant as the first variant of concern (VOC). By early 2021, the Delta lineage had emerged and rapidly became the predominant variant globally. Later that year, in November 2021, the Omicron started to spread and replaced Delta as the prevailing variant (6).

During the virus replication cycle, genetic changes naturally occur, and determine the rate at which a virus evolves. For SARS-CoV-2 the mutation rate is estimated to be around 1×10^{-6} – 2×10^{-6} mutations per nucleotide per replication cycle. This rate is lower than that of most RNA viruses due to a 3' exonuclease proofreading mechanism. In contrast, viruses such as hepatitis C virus and human immunodeficiency virus lack this mechanism, resulting in higher mutation rates (7).

While most mutations are detrimental and hamper the virus's ability to replicate, some confer advantages. One notable example is the mutation D614G, which emerged in the early months of the pandemic and increased infectivity by improving the virus ability to bind to the host cell receptor (8). In general, mutations that persisted in the viral genome were associated with two main advantages: enhanced binding to the host cell receptor, which increased infectivity and transmissibility or mechanisms that facilitated immune evasion (9).

1.2. Diagnostic strategies & preanalytical challenges

Reliable, scalable, and widely accessible diagnostic methods were required to effectively manage the COVID-19 pandemic. Diagnostics played a crucial role in identifying cases and guiding public health interventions. However, the pandemic also exposed major challenges in implementing and scaling up these diagnostic strategies.

Reverse transcription quantitative polymerase chain reaction (RT-qPCR) was recommended by the World Health Organization as the gold standard for SARS-CoV-2 diagnostic due to its high sensitivity and specificity (10). RT-qPCR allows the detection of low viral loads; however, it is time—intensive, requires advanced equipment and trained personnel, which limits its accessibility in many regions. To address this limitations, rapid antigen tests were introduced as complementary approach. Their simplicity and rapid available results made them also suitable for at-home use, enabling early identification of infections. However, a study conducted between November 2022 and May 2023 reported that rapid antigen tests demonstrated a sensitivity of just 47 % compared to RT-qPCR (11). While these tests were more convenient, their lower sensitivity meant they were less reliable, particularly for detecting cases with lower viral loads. This highlights the trade-off between the easy handling and rapid turnaround of antigen tests and their comparatively lower sensitivity.

The accuracy of test results depends on the sensitivity of the test, as well as on pre-analytical factors such as sample collection and handling, shipping and storage conditions, and the choice of the transport medium. RNA instability caused by RNases and hydrolysis can lead to false-negative results and decays in sample processing could further exacerbate RNA

degradation (12). The use of RNA stabilization media in swab tubes has been shown to effectively preserve RNA integrity, facilitating reliable and efficient batch testing (13). The World Health Organization recommended storing SARS-CoV-2 samples at 2-8°C with long-term storage requiring temperatures of -70°C (14).

1.3. SARS-CoV-2 virion structure and replication cycle

The SARS-CoV-2 virion consists of four structural proteins, namely spike (S), nucleocapsid (N), membrane (M) and envelope (E). The positive-sense, single-stranded RNA genome is wrapped with N proteins forming a helical structure inside the virion, whereas M, E, and S proteins are incorporated in the membrane. The genome is 30 kilobases in size and encodes 29 proteins, which can be divided in structural and non-structural proteins (15).

The initial step of host cell infection involves binding of the S protein to the host cell receptor angiotensin-converting enzyme 2 (ACE2). Upon binding, conformational changes expose a cleavage site in a subunit of the S protein, which can then be cleaved by host proteases. Depending on the entry route, the S protein is cleaved by either cellular transmembrane protease serine 2 (TMPRSS2) or by endosomal cathepsin L (16). Cell surface entry is TMPRSS2-dependent and triggers fusion between the virus and the cell membrane, resulting in a direct release of the viral genome into the cytoplasm, where it is uncoated and replicated. If TMPRSS2 is not or only weakly expressed, SARS-CoV-2 – ACE2 complexes are internalized via endocytosis and the viral S protein is processed by cathepsin L in a pH-dependent manner. Once viral RNA is released into the cytoplasm, it is uncoated and translated into polyproteins, which are then cleaved into structural and non-structural proteins (16).

The non-structural proteins form the transcription and the replication complex. The replication complex synthesizes complementary negative-sense RNA, which serves as a template to produce additional positive-sense genomic RNAs. The newly synthesized proteins are then transported to the endoplasmic reticulum and the golgi apparatus where they are assembled into new virions and are finally released by exocytosis (17).

1.4. ACE2 receptor

ACE2 is a transmembrane glycoprotein composed of an extracellular domain, a transmembrane domain, and a short intracellular tail. The extracellular domain consists of a carboxypeptidase domain (residues 19-615) and a collectrin-like domain (residues 616-740). The collectrin-like domain consists of a neck domain (residues 616-726) and a linker to the transmembrane domain (18). The dimeric structure of ACE2 is shown in Figure 1.

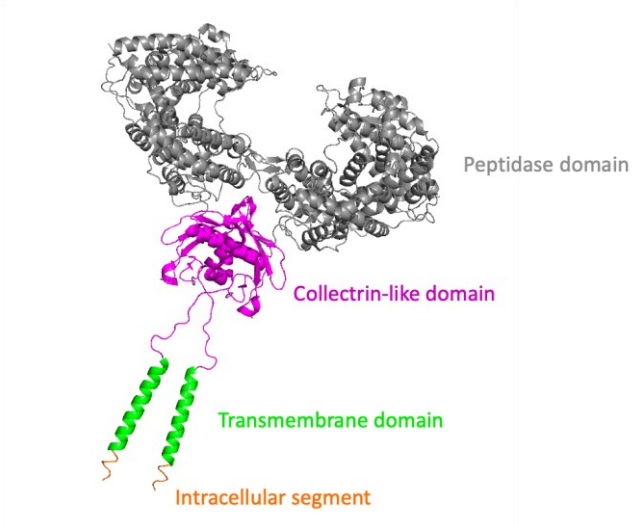

Figure 1 Structure of dimeric ACE2 [PDB 6M18] and its domains: peptidase domain (grey), collectrin like domain (magenta), transmembrane domain (green), intracellular segment (orange). The structural model was generated with Pymol.

The primary physiological role of ACE2 is to regulate the renin-angiotensin system, which is essential for controlling blood pressure and electrolyte balance. ACE2 converts Angiotensin (Ang) II to Ang 1-7, a peptide that exerts protective effects by promoting vasodilation and decreasing fibrosis, inflammation, and cell proliferation (19).

In addition to its role in the renin angiotensin system, ACE2 also acts as entry receptor for several viruses of the Coronaviridae family including the Human Coronavirus NL63, the betacoronaviruses SARS-CoV, and SARS-CoV-2 (20).

The distribution of ACE2 expression is particularly relevant for its role in viral pathogenesis, as it determines the susceptibility of different tissues to infection. ACE2 was found to be highly expressed on nasal ciliated cells in the upper respiratory tissue and on type II alveolar cells in the lungs (16). However, highest expression levels of ACE2 were found in the small intestine, testis, kidney, heart, and colon (21).

Beside different expression levels, the glycosylation of ACE2 profoundly affects its structure and interaction with SARS-CoV-2 spike proteins and subsequently virus entry and infectivity (22). Human ACE2 contains seven N-glycosylation sites of which the majority is occupied with complex-type glycans. These glycans contribute to the proper folding and trafficking of ACE2 to the cell surface. However, they shield large areas of the protein, including the binding site of the receptor binding domain (RBD) of the spike protein (22). Understanding how glycosylation affects the binding affinity for viral proteins is crucial for developing therapeutic interventions.

1.5. Pathophysiology of SARS-CoV-2

The pathophysiology of COVID-19 is characterized by a spectrum of clinical manifestations, ranging from asymptomatic cases to severe acute respiratory distress syndrome (ARDS), and multiorgan failure (23). The severity of disease is influenced by factors such as host immune response, age, and pre-existing comorbidities like hypertension, cardiovascular disease, and diabetes (24). In most individuals SARS-CoV-2 infection is limited to the upper respiratory tract, which can be accompanied by fever, dry cough, and malaise (25).

SARS-CoV-2 initially infects nasal epithelial cells with subsequent local replication and propagation. During this early stage of infection, there is a limited immune response. Affected individuals develop common-cold symptoms and are highly contagious. If the virus cannot be cleared, infection progresses to the lower respiratory tract, where it primarily infects alveolar type II cells and triggers immune cell infiltration in the infected pulmonary tissues (23). During the early phase of the pandemic, in about 20 % of all infected patients, SARS-CoV-2 progressed to the lower respiratory tract (23).

Autopsy tissues from patients with COVID-19 revealed massive infiltration of immune cells, such as macrophages, dendritic cells, and natural killer cells (26). Furthermore, increased levels of pro-inflammatory cytokines, including interleukin-6 (IL-6), interleukin-1 beta (IL-1β), chemokine ligand 10 (CXCL10), interferon gamma (IFN-γ) and tumour necrosis factor alpha (TNF-α), have been associated with disease severity (27). While these cytokines are essential for mounting an effective immune response, their overproduction can result in a detrimental feedback loop also known as “cytokine storm” (28). The produced cytokines attract more and more immune cells from the periphery to the site of infection (29). The massive release of cytokines by hyperactivated immune cells, cause sever pulmonary inflammation, severe tissue damage and contributes to the development of ARDS (25,30).

ARDS is characterized by impaired gas exchange due to increased capillary permeability and alveolar edema, caused by inflammatory lung injury (31). Analysis of lungs from ARDS patients revealed a histological pattern known as diffuse alveolar damage, which is associated with interstitial and intra-alveolar oedema, alveolar type II cell hyperplasia and dying pneumocytes (25).

1.6. Innate immune response in SARS-CoV-2 infection

The innate immune system is the first line of defence encountered by invading pathogens and must be tightly regulated in order to maintain the balance between protective and pathogenic responses. SARS-CoV-2 can trigger excessive release of proinflammatory cytokines through

hyperactivation of immune cells, supporting the development of clinical complications such as ARDS (31). Complications observed in patients with severe disease progression are closely linked to a dysregulated immune response (32,33).

Role of Macrophages in COVID-19

Macrophages represent a diverse group of tissue-resident, phagocytic cells within the innate immune system and are found in various organs such as the brain (microglia), liver (Kupffer cells), and lungs (alveolar and interstitial macrophages) (34). These cells play a crucial role in maintaining tissue balance and providing immune defence. During an infection, macrophages identify invading pathogens and tissue damage through a wide range of pattern recognition receptors. Once macrophages detect a pathogen, they release inflammatory mediators to and recruit additional immune cells (35).

Macrophages can shift between pro-inflammatory and anti-inflammatory states, depending on the surrounding signals (36). Macrophages act as a critical link between innate and adaptive immunity by detecting and engulfing pathogens, presenting antigens, and producing cytokines. Their dual role in inflammation and tissue repair is central to many diseases (37–39).

In severe cases of COVID-19, macrophages can contribute to the development of immunopathology by becoming hyperactivated and producing excessive levels of cytokines, which can lead to a cytokine storm. This unchecked inflammatory response can cause extensive tissue damage, vascular permeability, and systemic organ failure (35,36). Furthermore, macrophage polarization, which encompasses both pro-inflammatory and anti-inflammatory states, appears to be imbalanced in COVID-19, potentially exacerbating tissue damage (40).

Interferon signalling and complement activation

Upon infection, various innate immune pathways are activated. Mononuclear phagocytes, including dendritic cells, monocytes and macrophages can be activated either directly by recognizing pathogen-associated molecular patterns, or indirectly by detecting damage-associated molecular patterns released from infected epithelial cells (41).

Pattern recognition receptors, such as Toll-like receptors and retinoic acid inducible gene I – like receptors, sense viral RNA replication intermediates and proteins and initiate the production of type I & III interferons (IFNs) (42). IFNs secreted by infected cells, confer an antiviral state to surrounding cells by triggering the transcription of IFN-stimulated genes, thereby further strengthening the host defence (43).

SARS-CoV-2 has evolved different mechanisms to evade the innate immune response. These include blocking of interferon signalling, evading host recognition by e.g., masking inflammatory RNA or blocking recognition by pattern recognition receptors (44). A genetic study of COVID-19 patients revealed that mutations in genes involved in type I IFN pathways were more prevalent among patients who developed life-threatening symptoms compared to those with asymptomatic or mild infections (45). These findings highlight the crucial role of IFN signalling in combatting SARS-CoV-2 infection.

The complement system is also part of the innate immune system, alongside physical barriers, and immune cells. Initially synthesized in the liver, complement proteins circulate through the bloodstream, ready to respond to pathogens. The complement system contributes to the elimination of viruses through several mechanisms, including the direct neutralization of free viral particles, the lysis of infected host cells and the induction of an antiviral state in surrounding cells (46). However, in the context of SARS-CoV-2 infection, excessive activation of the complement system has been associated with disease severity and higher mortality rates (47).

A central player in the complement cascade is C1q, which activates the classical complement system and also acts as a bridge between the innate and the adaptive immune response by interacting with antibodies. When antibodies opsonize invading pathogens, C1q recognizes and binds to the Fc-domains in the immune complexes (48). Subsequent activation of the classical pathway leads to the production of opsonin (C3b), potent anaphylatoxins (C3a, C4a and C5a) and the formation of the membrane attack complex. C3b can bind to the surface of pathogens, marking them for engulfment by phagocytes, whereas anaphylatoxins induce acute inflammation by attracting and activating immune cells. The membrane attack complex forms pores in the plasma membrane, leading to direct lysis of virions or infected cells, and marks the endpoint of the complement cascade. Elevated levels of complement components have been found in patients with severe disease. Extensive deposition of C1q was identified in lung autopsy material, suggesting a significant role in the inflammatory damage observed in severe cases (49,50). Additionally, high levels of C5a in plasma have been found to be a distinct feature of severe COVID-19 (51).

Interplay between viral strategies and host defences underscores the complexity of the immune response to SARS-CoV-2 and highlights the need for further investigation of the complement system's function during COVID-19.

Antibody-dependent enhancement

In general, antibodies are elicited upon natural infection or vaccination and protect against re-infection by targeting epitopes expressed on the surface of invading pathogens. However, not all binding antibodies also have a neutralizing capacity, and under certain circumstances they can even facilitate virus uptake and replication (52). This mechanism is known as antibody dependent enhancement (ADE) and was observed for several viruses, with the most prominent example being Dengue virus. ADE can either occur during initial infection or upon re-infection when there is already a pre-existing immunity (53). Non-neutralizing antibodies or antibodies at sub-neutralizing concentrations can interact with Fc receptors (FcR) expressed on immune cells and build a bridge between the cells and the virus, thereby facilitating infection.

Sera from COVID-19 convalescent and vaccinated individuals, was shown to trigger ADE at sub-neutralizing concentrations in *in vitro* experiments (54–56). In addition to the direct interaction between Fc domains and FcR, the Fc domain of virus-bound antibodies can engage with complement factor C1q, promoting C1q receptor mediated uptake. This C1q-mediated ADE could have significant clinical implications, as C1q is found at high concentrations in the plasma and receptors for C1q are widely expressed on the surface of various cell types (56).

1.7. Antibody response and mucosal immunity

Upon infection, the immune system generates specific antibodies targeting viral antigens, primarily spike and nucleocapsid proteins present on the virus surface. Within two weeks of symptom onset, most individuals develop measurable levels of immunoglobulins (Ig), including IgM, IgG and IgA. IgM antibodies are typically the first immunoglobulins that appear, followed by IgG. Serum neutralizing antibody titers peak two weeks after symptom onset and then gradually decline over time (57) .

Neutralizing antibodies recognize specific epitopes on invading viruses, preventing them from binding to the host cells. However, non-neutralizing antibodies can mediate protective effects by activating FcR-dependent pathways, like antibody-dependent cellular cytotoxicity, phagocytosis and complement deposition, which lead to the resolution of infected cells. These mechanisms can also enhance the potency of neutralizing antibodies (58).

During antibody-dependent cellular cytotoxicity, the Fc domain of IgG antibodies, which coat infected cells or pathogens, engages with FcRs expressed on the surface of natural killer cells. This mediates the release of granzymes and perforin, which kill the infected cell. During antibody-dependent phagocytosis, pathogens or infected cells that are opsonized with IgA, IgG or IgM can be recognized by FcRs present on monocytes, macrophages, or dendritic cells, inducing phagocytosis. The Fc domain may also trigger antibody-dependent complement

deposition, leading to the lysis of opsonized cells (58). Furthermore, it was shown that adding components of the complement system to neutralization assays significantly increases the neutralisation titers of vaccinee serum samples (59).

While circulating antibodies play an essential role in controlling systemic viral spread, mucosal antibodies provide a local protection at the mucosal surface which is the first site that is encountered by SARS-CoV-2 (57). Secretory IgA (sIgA) is the most abundant antibody isotype in mucosal secretions including saliva, tears, and nasal fluids. It is well-adapted to the mucosal environment and is more resistant to enzymatic degradation. It directly neutralizes pathogens at the mucosal surface and is considered a non-inflammatory antibody that prevents infection via immune exclusion. By binding to multiple epitopes on invading pathogens, sIgA cross-links these pathogens facilitating agglutination and trapping within the mucus. Moreover, neutralization at mucosal surfaces, minimizing viral shedding (60).

While IgG transudes from the circulation to mucosal surfaces, IgA is synthesized locally. Monomeric IgAs can be linked by J-chains to form polymeric IgA, which is then transported across epithelial cells to the mucosal lumen via receptors located on the basal membrane of epithelial cells. After reaching the luminal side, parts of the receptor stay attached to the polymeric IgA, forming the secretory component. The secretory component provides resistance to degradation by proteases present in the harsh mucosal environment (60). Viruses opsonized by sIgA are effectively cleared from the upper respiratory tract through mucociliary mechanisms (61).

1.8. Animal models in SARS-CoV-2 research

Animal models are fundamental to COVID-19 research, providing crucial insights into the disease's progression and treatment. While *ex vivo*, *in vitro*, and organoid models have contributed to understand virological features of SARS-CoV-2, they lack the complexity of whole-organism interactions. Therefore, the use of animal models that closely mirror the clinical and pathological manifestations of COVID-19 in humans is essential for investigating viral pathogenesis, transmission dynamics, and developing effective therapeutics and vaccines (62). Several animal species have been evaluated for their susceptibility to SARS-CoV-2 infection and their ability to develop COVID-19-like symptoms. Each model presents distinct advantages and limitations.

Mice were found to be naturally resistant to SARS-CoV-2 infection due to inappropriate receptors. They must either be genetically modified by replacing the viral entry receptor, ACE2, with its human homologue, or SARS-CoV-2 must be adapted to bind to the mouse ACE2 (63).

However, the emergence of later SARS-CoV-2 variants has altered these dynamics. Later evolved Omicron variants gathered the ability to infect wild-type mice without the need for genetic modifications. Although Omicron variants can successfully establish infection in mice, they typically do not cause major clinical symptoms (64)

Ferrets have proven to be a valuable model for studying the pathogenicity and transmission of human respiratory viruses like respiratory syncytial virus and influenza virus (65). They are also susceptible to SARS-CoV-2 and develop mild-to-moderate respiratory symptoms, like those observed in humans. They efficiently support viral replication in the upper respiratory tract and exhibit viral shedding, making them particularly useful for transmission studies (66). Additionally, their immune response to infection shares similarities with that of humans. However, ferrets do not consistently develop severe lung pathology and systemic illness, which limits their utility for studying severe COVID-19 cases (63). Furthermore, their use may be constrained by factors such as higher housing costs compared to that of smaller rodent models.

Non-human primates, including rhesus macaques, cynomolgus macaques, and African green monkeys, are among the most suitable models for SARS-CoV-2 research due to their genetic, physiological, and immunological similarities to humans (67). In general, infected animals develop mild-to moderate disease and are a vital platform for evaluating safety and efficacy of vaccines and therapeutic agents before progressing to clinical trials (62). However, the use of non-human primates is limited by ethical considerations, high maintenance costs, and the necessity of specialized research facilities. Despite these challenges, they remain one of the most informative models, as they provide a more accurate prediction of the drug and vaccine efficacy compared to small animal models (68).

The Syrian golden hamster has gained recognition as an important model organism for SARS-CoV-2 research due to its natural susceptibility to the virus and its ability to develop disease manifestations resembling mild-to-moderate human COVID-19. Furthermore, Syrian golden hamsters efficiently transmit SARS-CoV-2 through direct contact as well as through aerosols, serving as an effective model for researching viral transmission dynamics (69) . Upon infection, hamsters experience noticeable weight loss, lung inflammation, and significant viral replication in the respiratory tract. Weight loss typically begins within one to two days post-infection, reaching its peak at around six days post infection. Maximum weight loss ranges from 6.1 % to 15.4 % upon infection with early SARS-CoV-2 strains, depending on the infection dose (69,70). After 14 days they return to their original weight. Later emerged VOCs such as Delta

still induce significant weight loss, whereas Omicron isolates fail to do so, even when administered at high doses (71,72). Additionally, hamsters infected with Omicron variants exhibit less severe lung pathology and have lower viral loads in the lungs than those infected with Wuhan or Delta strains (71). Their small size, ease of handling, and cost-effectiveness further enhance their suitability for preclinical studies. However, one limitation of this model is that the disease course remains mild, failing to fully replicate severe COVID-19 cases observed in humans (69).

1.9. Therapeutic antiviral strategies

The emergence of SARS-CoV-2 has prompted extensive research into therapeutic and preventive antiviral strategies. Antivirals against SARS-CoV-2 can be categorized into two types: virus-targeting (direct) and host-targeting agents (indirect). Direct acting antivirals specifically target viral components and interfere with the viral replication cycle, whereas indirect acting agents modulate the host immune response. Both strategies have advantages and drawbacks (73).

Directly acting agents, such as monoclonal antibodies and small molecules are highly selective but are also sensitive to escape mutants. By contrast, indirect acting agents target host proteins and are considered to have a broad antiviral spectrum and are less prone to emerging virus variants. However, their non-specific mechanism of action raises concerns about their safety profile (74).

In general, intervention with direct acting agents like viral RNA polymerase inhibitors (e.g., Remdesivir), viral main protease inhibitors (e.g., Nirmatrelvir) and monoclonal antibodies are recommended to be administered as soon as possible after infection. In contrast, immunomodulators and anti-inflammatory drugs (e.g., corticosteroids, Janus kinase inhibitors, cytokine antagonists) should be administered at an advanced stage of disease progression (74).

Monoclonal antibodies directed against SARS-CoV-2 have a dual function. On the one hand, they block virus entry by binding to the viral spike protein and on the other, they can elicit antibody effector functions like antibody-dependent cellular phagocytosis supporting clearance of opsonized virions and activation of the complement system (75). Several monoclonal antibodies have reached market authorization, however as the pandemic progressed, clinical use was no longer recommended because newly arising VOCs became resistant against them (74).

ACE2-based decoys offer a promising alternative to monoclonal antibodies. By mimicking the natural target of SARS-CoV-2, they competitively inhibit SARS-CoV-2 infection. These decoys can be designed as soluble receptors, loaded onto extracellular vesicles, or designed as antibody-based constructs (76). Several ACE2-based decoys have been engineered to enhance their affinity towards the spike protein or to improve their pharmacokinetic properties. Modifications, such as the removal of specific glycans from ACE2, have been shown to significantly increase the binding affinity to the spike protein (77,78). However, the clinical applicability of soluble ACE2 is limited by its short serum half-life, which is typically only a few hours (79). To address this limitation, the serum half-life of therapeutic proteins can be extended by fusion to an Fc domain of human IgG (80). This strategy takes advantage of the natural recycling mechanism mediated by neonatal FcR. Endothelial cells internalize serum proteins via pinocytosis and within the acidic environment of endosomes, the Fc domain of the fusion protein binds to the neonatal FcR. This interaction prevents the protein from being degraded by the lysosome and supports its recycling to the cellular surface, where it re-enters the circulation (80).

1.10. Therapeutic protein expression in plants

Therapeutic protein expression in plants has emerged as a promising platform to produce biopharmaceuticals, offering several advantages over traditional expression systems. Plants can be rapidly engineered to produce complex proteins, including antibodies, enzymes, and vaccine candidates, with proper post-translational modifications. Compared to mammalian cell culture systems, plant-based expression systems are more cost-effective, scalable, and pose a lower risk of contamination with human pathogens (81).

The first therapeutic compound produced in plants was approved by the U.S. Food and Drug Administration to treat Gaucher disease in 2012. Since then, multiple therapeutics including vaccines and antibodies reached clinical trials including an antibody cocktail for the treatment of Ebola virus (82) and vaccine candidates against malaria (83) and COVID-19 (84,85).

Plants can be utilized for recombinant protein production through two primary methods: stable transformation and transient expression (86,87). Stable transformation involves cloning of the target gene into an expression vector, which is then integrated into the plant genome. This results in the development of transgenic plants with the gene permanently integrated into either the nuclear or chloroplast genome. These plants pass the transgene to future generations, allowing for long-term protein production and seed storage for large-scale manufacturing (87).

In contrast, transient expression does not require stable integration into the plant genome. Instead, recombinant agrobacterium strains are used to deliver the gene of interest, which is also known as agroinfiltration. This method provides the advantage of higher protein yields and significantly faster production times. Recombinant proteins can typically be harvested from leaves within one to two weeks after infiltration. In comparison, generating and selecting stable transgenic plants may take up to a year, making transient expression a much more time-efficient strategy (86).

Variouse plant species are utilized for recombinant protein production, each with distinct advantages. Tobacco plants, particularly *Nicotiana benthamiana (N. benthamiana)* and *Nicotiana tabacum* are popular due to their fast growth and suitability for transient expression. Crops like maize and rice but also fruits and vegetables including tomatoes, lettuce and potatoes are also used for recombinant protein expression (87).

Advances in glycoengineering have refined the N-glycosylation processes in plant-produced proteins, aligning them more closely with human glycosylation patterns and enhancing their compatibility for therapeutic applications (88). Plants can generate an N-glycan core structure like that of mammalian cells; however, the terminal sugar residues of their N-glycans differ. Unlike mammalian complex N-glycans, which contain β1,4-galactose and core α1,6-fucose, plant N-glycans contain β1,2-xylose and core α1,3-fucose. Consequently, monoclonal antibodies produced in plants tend to have N-glycan profiles enriched with those plant-specific residues. The presence of β1,2-xylose and core α1,3-fucose remains a concern due to their potential immunogenicity, as they are not found on human proteins. Therefore, glycoengineered *N. benthamiana* plants have been developed, in which the β1,2-xylosyltransferase and α1,3-fucosyltransferase genes have been knocked out or knocked down. These glycoengineered plants enable the expression of recombinant proteins without plant-specific N-glycan residues (89).

1.11. Rationale of the study

The primary objectives of this dissertation are:

- Improving the reliability of SARS-CoV-2 detection as prerequisite for specific therapeutic intervention
- Providing proof-of-concept that an ACE2 decoy can block SARS-CoV-2 variants of concern from infection

Secondary objectives are:

- Investigating the influence of glycosylation on the neutralization activity of ACE2-Fc, with an emphasis on identifying modifications that enhance the neutralization potential.
- Optimization of ACE2-Fc for expression in glycoengineered *N. benthamiana* to improve its stability, reduce its propensity to form higher oligomers, and to minimize non-human post-translational modifications.
- Examining the neutralization spectrum against SARS-CoV-2 variants of concern.
- Evaluating the therapeutic applicability of ACE2-Fc *in vivo* and determine its efficacy, safety, and potential as a treatment for SARS-CoV-2 infections.
- Exploring the impact of ACE2-Fc on the infection of human monocyte-derived macrophages, providing insights into its immunomodulatory effects.

2. Methods

2.1. Ethics declaration

The animal experiments were approved by the Institutional Animal Welfare Committee of the Institut de Recerca i Tecnologia Agroalimentàries (CEEA-IRTA, registration number CEEA 365/2023) and by the Ethical Commission of Animal Experimentation of the Autonomous Government of Catalonia (registration number CEA-OH/12069/1) and were conducted by certified staff. Animal studies were carried out in compliance with the ARRIVE guidelines and under the approval of the biosafety committee (registration number CBS 116/2023). Convalescent sera were collected at the Medical University of Graz from adult volunteers after written informed consent and were approved by the ethics committee of the Medical University of Graz (EK number: 34-203 ex 21/22).

2.2. Biosafety

All *in vitro* experiments involving live SARS-CoV-2 were performed in a Biosafety Level-3 (BSL-3) facility at the Diagnostic and Research Institute of Pathology at the Medical University of Graz.

The BSL-3 laboratory operates under negative pressure and is equipped with a - 30 Pascal air lock. Inside the laboratory, the pressure is - 60 Pascal to contain hazardous agents. SARS-CoV-2 handling requires advanced personal protective equipment consisting of a Tychem 2000C suite (Cat. III, Type 3/4/5/6) that is impermeable to liquids and particles and provides robust protection against biological agents. Chemical-resistant boots as well as the inner layer of gloves are attached to the suite with adhesive tape. The second pair of gloves is of a different colour to facilitate spotting of holes in the outer layered gloves. Further, powered air-purifying respiratory systems with a hood covering head, face, and shoulders were used. The personnel

protective equipment worn while working with live SARS-CoV-2 is shown in Figure 2a. Personnel exit the BSL-3 laboratory through a chemical shower (Figure 2b), which nebulizes 2 % peracetic acid solution for decontamination.

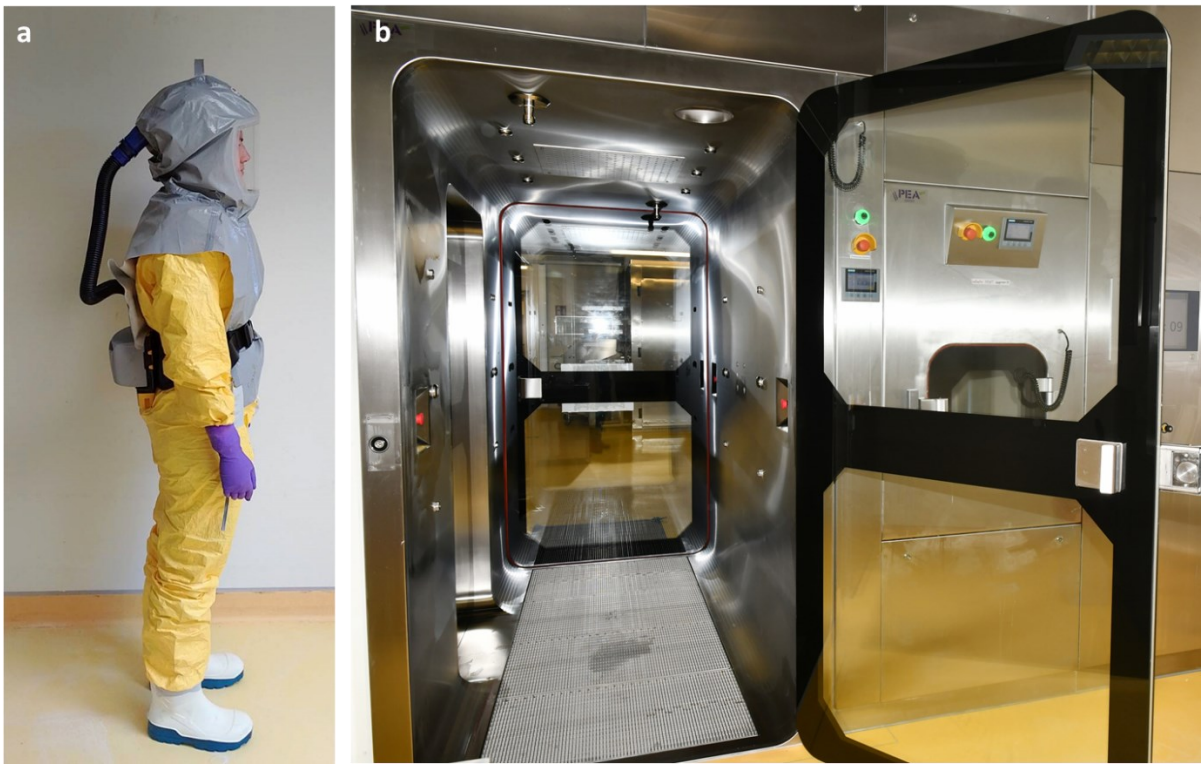

Figure 2 Biosafety measures at the BSL-3 laboratory at the Diagnostic and Research Institute of Pathology at the Medical University of Graz. a) Personnel protective equipment consisting of a Tychem 2000C suite, chemical resistant boots, double layered gloves and a powered air-purifying respiratory systems with a hood covering head, face, and shoulders. b) The chemical shower is used to exit the laboratory and nebulizes 2 % peracetic acid for decontamination. Adapted from Loibner et al. (2022).

In vitro assays involving live SARS-CoV-2 were conducted within a Class II biosafety cabinet within the BSL-3 laboratory. Samples processed in the BSL-3 laboratory must be properly inactivated before they can be transferred to a lower biosafety environment for further processing. The Center for Disease Control and Prevention confirmed that the AVL buffer used for viral RNA extraction from cell culture supernatants adequately inactivates SARS-CoV-2 (90). Welch et al (91) reported on the inactivation properties of the RLT buffer used for intracellular RNA extraction. Samples used for Bioplex measurements were inactivated by UV irradiation followed by a sterility control. Therefore, 200 µl of cell culture supernatant was transferred to a 48-well plate, which was placed on ice. The plate was then irradiated with a UV lamp (VL-215.G) at 254 nm for 30 minutes, with the lamp placed approximately 10 cm

above the plate. After UV-irradiation, the supernatant was transferred to a clean Eppendorf tube and 10 % v/v was used to control for efficient inactivation. Therefore, 20 µL of each sample was added to confluent VeroE6 cells in a 96-well plate and monolayers were controlled for cytopathic effects (CPE) after 96 hours. UV-inactivated samples were stored at -80°C in the BSL-3 laboratory until inactivation was confirmed.

Inactivated samples were placed in a decontamination lock and decontaminated by nebulization of 2 % peracetic acid to prevent contamination of the external environment.

In-vivo experiments with SARS-CoV-2 were performed at the BSL-3 facilities of the Biocontainment Unit of IRTA-CReSA (Barcelona, Spain) by certified staff.

2.3. SARS-CoV-2 RNA stability testing

Information on swab collection devices including recommended storage conditions is listed in Table 1 and was cited from the suppliers' homepages including relevant instructions for use.

Artificial body excretion (BE) was prepared with 2.5 mg/mL BSA (Carl Roth GmbH, Karlsruhe, Germany), 3.5 mg/mL tryptone (Becton Dickinson, Le Pont de Claix, France) and 0.8 mg/mL mucin (Merck KGaA, Germany) as described previously (92). BE was spiked with SARS-CoV-2 to achieve final concentrations of 10,000 copies/ml and 1,000 copies/ml collection solution. Therefore, 100 µL of spiked BE were applied onto each swab, which was directly transferred into the respective collection medium. Spiked swab collection devices were stored at room temperature (RT; 20.6°C – 22.4°C) and at 37.0°C – 37.4°C. Directly after spiking (= t0), after 24 and 96 hours, swabs were vortexed, 140 µl were collected, and viral RNA was quantified as described in *2.18 Extracellular virus RNA isolation and quantification*.

A SARS-CoV-2 RNA copy number standard (VR-1986D, ATCC, UK) was used to generate a standard curve to calculate viral copy numbers as described in *2.6 Viruses*. The limit of detection was estimated to be three copies per reaction, which corresponds to 170 copies/ml of collection solution.

Table 1 Transport swab systems and respective manufacturer claims. Taken from Hardt et.al (2022).

Device	Abbreviation	Storage Condition	Regulatory Status
Copan eSwab™ 480C + Single Regular Size Nylon® Flocked Swab	eSwab	INTENDED USE Copan Liquid Amies Elution Swab (ESwab®) Collection and Transport System is intended for the collection and transport of clinical specimens containing aerobes, anaerobes and fastidious bacteria from the collection site to the testing laboratory. Swab specimens for bacterial investigations collected using ESwab® should be transported directly to the laboratory, preferably within 2 hours of collection to maintain optimum organism viability. If immediate delivery or processing is delayed, then specimens should be refrigerated at 4 – 8ºC or stored at room temperature (20 – 25°C) and processed within 48 hours.	EU: CE IVD Outside EU: FDA cleared
Copan UTM-RT® Universal Transport Medium 359C + Single Regular Size Nylon® Flocked Swab	UTM	INTENDED USE UTM® is an FDA cleared collection and transport system suitable for collection, transport, maintenance and long-term freeze storage of clinical specimens containing viruses, including COVID-19, chlamydia, mycoplasma or ureaplasma organisms. Using the UTM-RT® System, collected specimens can be stored for up to 72h at 2-8°C (according to CDC recommendations https://www.cdc.gov/coronavirus/2019-ncov/lab/guidelines-clinical-specimens.html)	EU: CE IVD Outside EU: FDA cleared
IMPROVIRAL™ Viral Preservative Medium (8110111) + ImproSwab® (550040A)	VPM	Widely used for the collection, preservation and transportation of nasopharyngeal pathogen specimens such as influenza, pneumonia, avian influenza, hand-foot-mouth disease, measles and other viruses. Storage and transport under 0-8℃ and no more than 30 days at room temperature.	EU: CE IVD
Viral transport medium*	VTM	As recommended by CDC: Store respiratory specimens at 2 - 8°C for up to 72 hours after collection. If a delay in testing or shipping is expected, store specimens at -70°C or below.	not specified

*(HBSS (Life Technologies Europe, Bleiswijk, Netherlands) + 2% FCS (Thermo Fisher Scientific, Waltham, US) + 0,2% PenStrep (Thermo Fisher Scientific, Waltham, US). Taken from Hardt et al. (2022).

2.4. Protein expression

ACE2-Fc proteins were designed and produced by our partners at BOKU University (Vienna, Austria) as described previously (93,94).

Expression in HEK293-6E cells

Recombinant ACE2-Fc fusion proteins that were used to study the impact of specific N-glycosylation on the neutralization activity, were expressed using transiently transfected HEK293-6E cells following the protocol described in Capraz et. al (77).

Expression in *N. benthamiana* ΔXT/FT

Recombinant ACE2-Fc fusion proteins were produced by agrobacterium-mediated transient expression in leaves of *N. benthamiana* ΔXT/FT (89). Extraction from 30 g wet leaves with subsequent purification by affinity chromatography using a protein A column yielded 20 mg ACE2-728H-Fc (95).

2.5. Cells

African green monkey kidney epithelial cells (VeroE6) were obtained from Biomedica (VC-FTV6, Vienna, Austria) and were grown in Minimal Essential Medium (MEM) supplemented with Earle's Salts and L-Glutamine (ThermoFisher Scientific, US), 1 % Penicillin-Streptomycin (PenStrep, Thermo Fisher Scientific, Waltham, MA, USA) and 5 % fetal calf serum (FCS; ThermoFisher Scientific, US). Human lung adenocarcinoma cells (Calu-3) cells were obtained from the Center for Medical Research, Medical University Graz, Austria and were grown in MEM (Thermo Fisher Scientific, US) supplemented with Earle's Salts and L-Glutamine, 1 % PenStrep and 10 % FCS.

Human monocytes were kindly provided by Dr. Sabine Wagner-Lichtenegger. Briefly, human monocytes were obtained from leukocyte depletion chambers by negative selection using the RosetteSep kit (Stemcell Technologies, Germany) according to the manufacturer's instructions. For macrophage differentiation, primary human monocytes were cultivated in RPMI-1640 (Gibco, US), supplemented with 100 µg/ml granulocyte-macrophage colony stimulating factor (Peprotech, Germany) and 5 % human heat inactivated serum (Sigma Aldrich, US). Cells were cultured for six days at 37°C. Differentiated human monocyte derived macrophages (hMDMs) were harvested by trypsinization and gentle scratching. hMDMs were seeded in OptiPro Serum free medium (Gibco, US) supplemented with 2 % L-glutamine (Gibco, US) and were rested overnight before use.

2.6. Viruses

All experimental procedures involving SARS-CoV-2 were performed in a BSL-3 laboratory. Wild type SARS-CoV-2 Wuhan-Hu-1 (wh19: Human 2019-nCoV Isolate, Ref-SKU 026V-03883), was obtained from Charité Universitätsmedizin Berlin, Germany. Omicron isolate lineage B.1.1.529 was purchased from EVAg (om21: SKU: 010V-04425). Delta isolate (de21: hCoV-19/Austria/Graz-MUG21/2021) and Omicron isolate (om23, linage EG5.1) were isolated at the Medical University of Graz from nasopharyngeal swabs.

Virus Isolation

Nasal swabs were collected from volunteers with a SARS-CoV-2 infection confirmed by RT-qPCR or lateral flow assay. Nasal swabs were stored at -80°C until use. Nasal swab solution was filtered through a 0.2 µm syringe filter (ThermoFisher Scientific, US) and subsequently 1 % PenStrep was added to avoid bacterial growth. 100 µl was added to VeroE6 cells seeded in 24-well plates and incubated until CPE was visible. The supernatant was centrifuged for 5 minutes at 3000 x g to remove cellular debris. SARS-CoV-2 replication was confirmed by RT-qPCR as described in *2.18 Extracellular virus RNA isolation and quantification*. The supernatant was stored at -80°C and was used for stock production.

Virus propagation

Virus strains were propagated in VeroE6 cells at 37°C and 5 % CO_2 for 72 - 96 hours. Cells were lysed by a freeze and thaw cycle, followed by a centrifugation step at 10 minutes for 3000 × g to remove cellular debris. Supernatants were filtered with 0.2 µm syringe (ThermoFisher Scientific, US), aliquoted, and stored at − 80°C until use.

Quantification of infectious virus titer

SARS-CoV-2 virus titers were determined by calculating the tissue culture infectious dose 50 ($TCID_{50}$). The $TCID_{50}$ describes the dilution factor of a virus stock at which 50 % of the wells develop CPE. Therefore,1 x 10^4 VeroE6 cells were seeded in 96-well plates to reach 100 % confluency. VeroE6 monolayers were infected in six replicates with serial 10-fold dilutions of virus stock and incubated for 96 hours at 37°C and 5 % CO_2. Subsequently, cells were fixed with 4 % neutral-buffered formalin (SAV Liquid Production GmbH, Germany) and CPE was visualized by crystal violet staining. Therefore, fixed cells were stained with a 1:100 dilution of a 0,05 % gentian violet solution (solved in 20 % methanol) for 30 minutes. $TCID_{50}$ was calculated by Reed-Munch method (96). Briefly, the infection rate is calculated as followed:

$$Infectionrate(IR) = \frac{number\ of\ cumulative\ positive\ wells}{number\ of\ cumulative\ positive\ wells + number\ of\ cumulative\ negative\ wells}$$

Next, the two dilutions in which the cumulative percentage straddles 50 % are identified (IR1 < 50 > IR2) and the proportional difference (PD) between those two dilutions is calculated as followed:

$$proportional\ difference(PD) = \frac{IR2 - 50\%}{IR2 - IR1}$$

The PD is used to interpolate the dilution corresponding to the 50 % endpoint, which is defined as (ID50) and is calculated as followed:

$$ID50 = 10^{log(dilution\ IR2) + PD * - log(dilution\ factor)}$$

The $TCID_{50}$ is defined as the reciprocal of ID50 and has to be divided by the volume added to each well:

$$\frac{TCID50}{ml} = \frac{\frac{1}{ID50}}{Vol[ml]\ per\ Well}$$

The virus titer is then defined as $TCID_{50}$/ml.

Quantification of virus copy numbers

SARS-CoV-2 RNA copy number standard (VR-1986D genomic RNA from 2019 Novel Coronavirus, Lot: 70035624, ATCC, Glasgow, UK) was used to generate a standard curve to estimate virus copies. Ct-values were plotted against the natural logarithm of copy numbers followed by linear regression analysis.

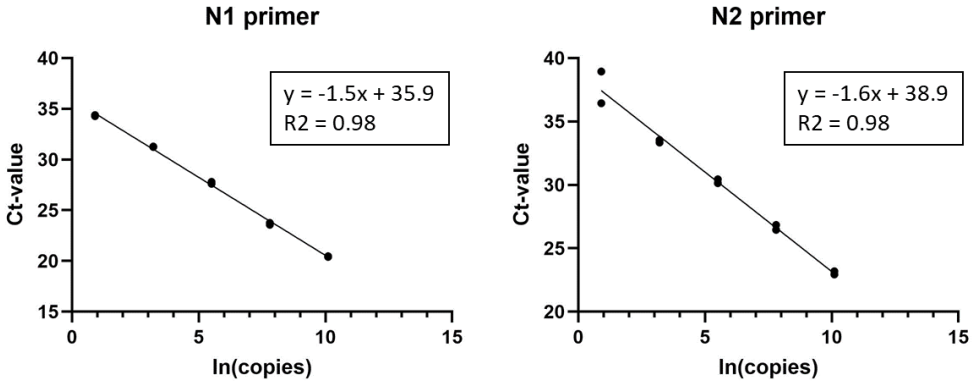

Figure 3 Linear regression analysis for the quantification of virus copy numbers

Viral copy numbers were calculated from the following equations:

N1 primer: y = -1.5x + 35.9

N2 primer: y = -1.6x + 38.9

Details from virus stock batches produced and used throughout this dissertation are listed in Table 2.

Table 2 Virus stock characteristics

Description	Passage	Date	copies/µl	$TCID_{50}$/µl	CPE	filtered
wuhan 2019	2	18.10.2022	3,59E+07	1609	100%	yes
wuhan 2019	2	19.03.2024	3,15E+07	1368	100%	yes
delta 2021	2	18.10.2022	9,00E+07	850	100%	yes
delta 2021	2	19.03.2024	5,74E+07	426	100%	yes
delta 2021	2	30.07.2024	1,26E+07	8518	5%	no
omicron 2021	2	18.10.2022	2,92E+07	413	100%	yes
omicron 2021	2	19.03.2024	3,17E+07	290	100%	yes
omicron 2023	2	19.03.2024	9,17E+07	274	100%	yes

Viral genome sequencing

Virus RNA was isolated as described in *2.18 Extracellular virus RNA isolation and quantification.* Sequencing was performed at the Division of Molecular pathology at the Medical University of Graz as described previously (50).

Primers targeting the entire SARS-CoV-2 genome were designed to produce approximately 2 kb amplicons. For each sample, 2.5 µl of RNA were used for RT-qPCR reaction using oligonucleotide primers at a concentration of 400 nM. The following cycling conditions were used: 55°C for 15 minutes, 95°C for 3 minutes; 35 cycles consisting of 95°C for 15 seconds and 57°C for 3 minutes; final extension at 72°C for 10 minutes. The PCR products were pooled and purified using 1.8X Ampure XP beads (Beckman Coulter), with subsequent washes in 75 % ethanol and elution. Amplicons were eluted in 30 µL of water and fragmented to a size range of 150-250 bp. Ion Torrent barcode and sequencing adapters were attached using the NEBNext Fast DNA Fragmentation & Library Prep Set for Ion Torren kit (New England Biolabs). Sequencing was carried out on an Ion Torrent S5XL system with a 540 Chip Kit and the 200 bp sequencing Kit (ThermoFisher). The obtained sequences were aligned to the SARS-CoV-2 reference genome (accession number: NC_045512.2).

2.7. Antivirals

ACE2-Fc decoys were produced as described in *2.4 Protein expression* and provided by Lukas Mach, BOKU University. Main protease inhibitor PF-07321332 (PF-332) was purchased from Selleckchem (Catalog No. S9866). Convalescent sera from four different donors were

collected at Medical University Graz between August 2021 and July 2022. Sera were heat inactivated and pooled for neutralization assays.

2.8. Enzyme-linked immunosorbent assay

Enzyme-linked immunosorbent assays were carried out by our cooperation partners at BOKU University Vienna, Austria according to standard protocols. Briefly, 96-well plates (Nunc MaxiSorp; Thermo Fisher Scientific, Waltham, MA, USA) were coated overnight at 4°C with 200 ng per well of in-house produced Wuhan RBD (97) in 100 µl phosphate-buffered saline (PBS). Plates were then washed three times with PBS containing 0.05 % Tween 20 (PBST). From an initial concentration of 1 µg/ml, twofold serial dilutions of the ACE2-Fc samples were prepared in PBST containing 1 % bovine serum albumin (dilution buffer), and 50 µl then added per well. After incubation for 1 hour at 37°C, the plates were washed three times with PBST prior to addition of 50 µl of 0.03 µg/ml peroxidase-conjugated goat antibodies to human Fc (Sigma-Aldrich, St. Louis, MO, USA) in dilution buffer prior to incubation for 1 hour at 37°C. After washing of the plates, bound peroxidase activity was detected by the addition of 100 µl of ELISA substrate solution (0.1 mg/ml tetramethylbenzidine (Sigma-Aldrich) in 100 mM citric acid/sodium phosphate buffer (pH 5.0) containing 0.006 % H_2O_2). After 5-15 minutes, the reaction was stopped by addition of 100 µl 0.18 M H_2SO_4 prior to measurement of the optical density at 450 nm (reference wavelength: 620 nm) using a Spark multi-channel spectrophotometer (Tecan, Grödig, Austria).

2.9. Differential scanning calorimetry

Differential scanning calorimetry experiments were performed by our cooperation partners at BOKU University as described in (77). A MicroCal PEAQ-DSC Automated system (Malvern Panalytical, Malvern, UK), using 5-10 µM protein solutions in PBS was used. The heating was performed from 20°C to 100°C at a rate of 1°C/min. The protein solution was cooled *in situ* and an identical thermal scan was run to generate the baseline for subtraction from the initial scan. All measurements were performed in triplicates. Fitting was done with Origin 7.0 for DSC software using the non-2-state transition model.

2.10. Metabolic activity assay

Cytotoxicity was assessed prior to neutralization assays to ensure that the antivirals do not exhibit inherent toxicity to host cells, which could confound the results and lead to misinterpretation of their antiviral activity. To assess cytotoxicity, a resazurin-based assay was performed. VeroE6 cells were seeded in 96-well plates at a density of 1 x 10^4 cells per well and allowed to adhere overnight. Culture medium was replaced with medium containing

serially diluted test compounds and was incubated for 24 hours. A cell control, without any compound added and serially diluted DMSO as toxicity control were included. After 72 hours, substances were removed, and fresh medium was added to all wells. Subsequently, 20 µl of a freshly prepared resazurin solution (final concentration 10 µM) was added using an automated dispenser integrated in the plate reader. Plates were incubated for 60 minutes at 37°C wit 5 % CO_2 to allow reduction of resazurin to resorufin by dehydrogenase enzymes from metabolic active cells. Fluorescence was measured using a microplate reader at an excitation wavelength of 485 nm and an emission wavelength of 590 nm on a Synergy 4 plate reader (BioTek, US). Background fluorescence from wells containing medium without cells was subtracted from all readings. Metabolic activity was expressed relative to untreated control cells. All assays were performed in triplicates. The metabolic activity of VeroE6 cells was not altered by any of the compounds within the tested concentration range (Figure 4).

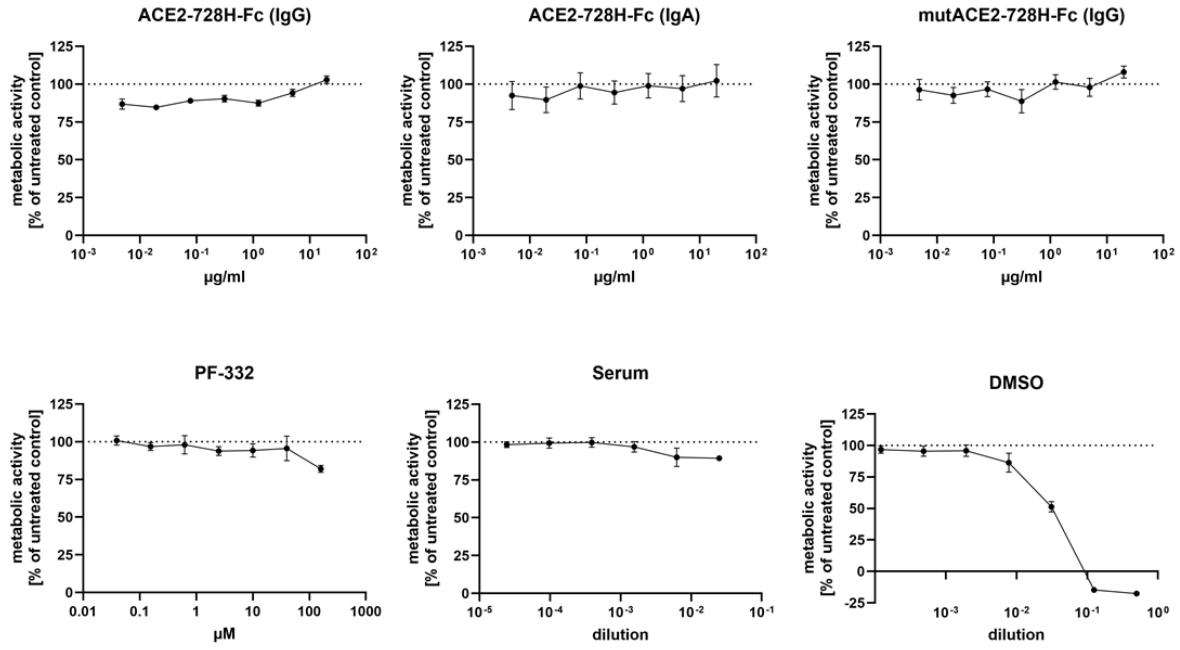

Figure 4 Evaluation of the concentration range of antivirals for neutralization assays. VeroE6 cells were incubated with serially diluted antivirals for 72 hours. Metabolic activity was measured using a resazurin assay. Values were corrected for background signal (medium without cells) and normalized to a cell control (cells without substance). Data are shown as mean ± SEM and refer to a single experiment performed in triplicates.

2.11. Virus neutralization assay by RT-qPCR

ACE2-Fc decoys were produced as described in *2.4 Protein expression* and provided by Lukas Mach, BOKU University Vienna, Austria. ACE2-Fc variants were preincubated at the indicated concentrations with 60 plaque forming units (pfu) SARS-CoV-2 for 30 minutes at 37°C. VeroE6

and Calu-3 cells were seeded in 48-well plates at a density of 3 x 10^4 cells/well. After preincubation, cells were infected for 1 hour at 37°C. Subsequently, virus inoculum was replenished with fresh media and 24 hours post infection (hpi) extracellular viral RNA was isolated from cell culture supernatants and quantified by RT-qPCR as described *in 2.18 Extracellular virus RNA isolation and quantification.*

2.12. Virus neutralization assay by monitoring of cytopathic effects

Neutralizing activity was assessed by CPE assays, as described previously (95). VeroE6 cells were seeded in 96-well plates at a density of 1 x 10^4. Antiviral compounds were serially diluted (4-fold) and incubated with SARS-CoV-2 for 15 minutes at 37°C. Subsequently, compound-virus mixtures were added to VeroE6 cells in triplicates and incubated for 72 - 96 hours at 37°C. Cells were fixed with 4 % neutral buffered formalin and CPE was visualized by crystal violet staining. Therefore, fixed cells were stained with a 1:100 dilution of a 0,05 % gentian violet solution (solved in 20 % methanol) for 30 minutes. After staining, washing and drying, plates were scanned before the stain was dissolved in 10 % glacial acetic acid. Optical density was read at 595 nm. Data were normalized to a virus control (0 % Inhibition, no-compound) and a cell control (100 % inhibition, no virus). Half-maximal inhibitory concentrations (IC_{50}) values were calculated by nonlinear regression analysis with variable slopes in GraphPad PRISM Version 9.

2.13. Virus neutralization assay in air-liquid interface cultures

Primary human air-liquid interface (ALI) cultures (MucilAir, Epithelix) were washed once with PBS prior to infection and the basal medium was replenished with MucilAir culture medium containing 20 µg/ml ACE2-Fc. 5 x 10^3 pfu SARS-CoV-2 (wh19) were incubated with ACE2-Fc (20 µg/ml) and subsequently added to the apical side of the ALI culture. After one hour incubation at 37°C, the virus inoculum was removed, and the apical side was washed three times with PBS to remove residual extracellular virus. Virus release was assessed 24 hpi by washing the apical side with 200 µl PBS (apical wash). Viral RNA was then isolated from the apical wash and was quantified as described in *2.18 Extracellular virus RNA isolation and quantification.*

Transwell membranes were fixed in PAXgene Tissue Fix (PreAnalytiX, Switzerland) for 0.5 - 4 hours and were maintained in PAXgene Tissue STABILIZER Concentrate (PreAnalytiX, Switzerland) for 24 hours. Subsequently, transwell membranes were cut in half. One half was used for quantification of intracellular virus loads as described in *2.19 Intracellular RNA*

isolation and quantitative real-time PCR. The second half was used for immunohistochemical analysis. Fixed samples were dehydrated through graded series of ethanol to remove water. The histokinet program included the following steps: 70 % ethanol for 30 minutes, 80 % ethanol for 30 minutes at 30°C, 90 % ethanol for 1 hour at 50°C, 96 % ethanol for 1h at 60°C, 96 % ethanol for 1 h ourat 90°C, 100 % ethanol for 1 hour at 96°C, 100 % ethanol for 1 hour at 98°C, xylen for 2 hours and finally 3 hours at 55°C in paraffin. Subsequently membranes were embedded in tissue infiltration/embedding medium Paraplast Plus (Leica, US). Blocks were stored at room temperature until sectioning. Immunohistochemical staining was performed as described in *2.20 Immunohistochemistry*.

2.14. *In-vivo* experiment

Six- to eight-week-old Syrian hamsters were housed at the animal BSL-3 facilities at IRTA-CReSA. After a week of acclimatization, hamsters were challenged intranasally with 10^4 $TCID_{50}$/animal (50 µl/nostril) of SARS-CoV-2 (Human 2019-nCoV – hCoV-19/France/GE1973/2020, clade G, D614G (S)). To evaluate the *in vivo* therapeutic efficacy of ACE2-Fc, the initial dose of 2.5 mg/ml (~2.5 mg/kg) was administered intranasally 24 hpi. Subsequent treatments were given daily for a total of five consecutive days. Virus challenge as well as treatment were conducted under anaesthetics (4 % isoflurane). Animals were evaluated clinically and weighted daily. At five days post infection all animals were euthanised by intraperitoneal administration of sodium pentobarbital (not exceeding a dose of 60 mg/kg). Lung, spleen, heart, kidney, and liver were collected for pathological analysis. To quantify the viral burden, dilutions from lung homogenates were applied to confluent VeroE6 cells. After 96 hours CPE was assessed, and $TCID_{50}$/ml was determined as described in *2.6 Viruses.*

Further, RNA from lungs was isolated as described in *2.19 Intracellular RNA isolation and quantitative real-time PCR*. Relative expression of CXCL10, MX Dynamin Like GTPase 2 (MX2), C-C Motif Chemokine Ligand 5 (CCL5) and the viral N gene were analysed using the primers listed in Table 3 and Table 4.

Table 3 RT-qPCR Primer sequences

Primer	**Sequence**
hmstr_ActB_fw	GGC CAG GTC ATC ACC ATT
hmstr_ActB_rev	GAG TTG AAT GTA GTT TCG TGG ATG
hmstr_MX2_fw	CCA GTA ATG TGG ACA TTG CC
hmstr_MX2_rev	CAT CAA CGA CCT TGT CTT CAG TA
hmstr_CCL5_3_fw	TCAGCTTGGTTTGGGAGCAA

hmstr_CCL5_3_rev	TGAAGTGCTGGTTTCTTGGGT
hmstr_CXCL10_fw	GCC ATT CAT CCA CAG TTG ACA
hmstr_CXCL10_rev	CAT GGT GCT GAC AGT GGA GTC T

2.15. hMDM infection assay

hMDMs and Calu-3 cells were seeded in cell culture plates for RNA isolation and were infected at a multiplicity of infection (MOI) = 1 $TCID_{50}$/cell and MOI 0.01 $TCID_{50}$/cell, respectively. After one hour, virus inoculum was replaced with fresh medium. Immediately afterwards, intracellular RNA was harvested (= t0), or cells were further incubated for 24 hours, 48 hours and 72 hours to monitor viral RNA levels over time. Intracellular virus RNA loads were determined as described in *2.19 Intracellular RNA isolation and quantitative real-time PCR.*

For immunofluorescent staining hMDM and Calu-3 cells were seeded on cover slips (Ø 10 mm) and infected at a MOI = 1 $TCID_{50}$/cell and MOI = 0.01 $TCID_{50}$/cell, respectively. Cells were incubated for 24 hours without removing the virus inoculum. Cells were fixed with 4 % formaldehyde and SARS-CoV-2 nucleocapsid and double-stranded RNA were detected by immunofluorescent staining as described in *2.21 Immunofluorescent staining* .

2.16. Fc-receptor mediated uptake of SARS-CoV-2 in hMDMs

hMDM were infected at a MOI = 0.1 $TCID_{50}$/cell in the presence of 10-fold serially diluted ACE2-728H-Fc (0.02 – 20 µg/ml). After 24 hours, intracellular RNA was isolated and viral RNA was quantified by RT-qPCR quantified as described *2.19 Intracellular RNA isolation and quantitative real-time PCR.*

To examine C1q mediated effect, hMDM were infected in the presence of single compounds (ACE2-728H-Fc (5 µg/ml), mutACE2-Fc (5 µg/ml), convalescent serum (1:50)) and in combination with C1q (20 µg/ml). After 24 hours, intracellular RNA was isolated and viral RNA was quantified by RT-qPCR as described in *2.19 Intracellular RNA isolation and quantitative real-time PCR.*

2.17. Treatment with conditioned media

Production of conditioned media

Calu-3 and VeroE6 cells were cultivated in DMEM + 10 % FCS + 1% PenStrep and DMEM + 2 % FCS + 1 % PenStrep, respectively. Before infection, the medium was exchanged with OptiPro SFM + 2 % L-glutamine medium. Calu-3 and VeroE6 cells were mock-infected with PBS or infected with SARS-CoV-2 at a MOI = 0.01 $TCID_{50}$/cell and incubated for 24 hours,

until a minimal CPE was observed, and cell monolayers were mostly intact. Supernatants were harvested and centrifuged at 2,000 x g for 10 minutes to remove cellular debris. Conditioned media (CoM) was collected from infected Calu3-cells (CoM $Calu3_{inf}$), infected VeroE6 cells (CoM $Vero_{inf}$), mock infected Calu-3 cells (CoM $Calu_{mock}$), and mock infected VeroE6 cells (CoM $Vero_{mock}$) and were stored at -80°C until use.

Treatment with conditioned media

hMDM from three different donors were treated with CoM or OptiPro SFM for 24 hours. Intracellular RNA was isolated and quantified as described in *2.19 Intracellular RNA isolation and quantitative real-time PCR.* Supernatants were collected and UV UV inactivated as described in *2.2 Biosafety.*

2.18. Extracellular virus RNA isolation and quantification

Extracellular RNA was isolated using QIAamp® Viral RNA Mini Kit (QIAGEN GmbH, Germany), according to the manufacturer's instructions. Briefly, 140 µl cell culture supernatant was added to 560 µl AVL buffer. Subsequently, 560 µl ethanol (96-100 %) was added, vortexed, and loaded on a QIAamp Mini spin column. After centrifugation, the flow-through was discarded and the column was washed with 500 µl of AW1 buffer, followed by 500 µl AW2 buffer. Finally, the RNA was eluted in 40 µl nuclease free water. Isolated RNA was stored at -80°C until use.

SARS-CoV-2 RNA was quantified by using N1 or N2 primers and a TaqMan probe with a FAM reporter and a BHQ-1 quencher (Eurofines, Germany) together with the one-step QuantiTect® Multiplex RT-qPCR Kit (QIAGEN GmbH, Germany) on a Rotor Gene® Q cycler (QIAGEN GmbH, Germany). Reactions were performed in a total volume of 25 µl at 50°C for 30 minutes followed by 95°C for 15 minutes and 45 cycles of 95°C for 3 seconds and 55°C for 30 seconds. Primer and probe sequences are listed in Table 4.

Table 4 Primers and probe sequences for the SARS-CoV-2 N gene

Name	Sequence (5′ > 3′)	Label
2019-nCoV_N1-F	GAC CCC AAA ATC AGC GAA AT	none
2019-nCoV_N1-R	GAC CCC AAA ATC AGC GAA AT	none
2019-nCoV_N1-P	ACC CCG CAT TAC GTT TGG TGG ACC	FAM, BHQ-1
2019-nCoV_N2-F	TTA CAA ACA TTG GCC GCA AA	none
2019-nCoV_N2-R	GCG CGA CAT TCC GAA GAA	none
2019-nCoV_N2-P	ACA ATT TGC CCC CAG CGC TTC AG	FAM, BHQ-1

2.19. Intracellular RNA isolation and quantitative real-time PCR

Intracellular RNA was isolated using RNeasy Mini Kit (QIAGEN GmbH, Germany), according to the manufacturer's protocol. Briefly, cells were directly lysed by the addition of 350 µl RLT buffer. The cell lysate was loaded on a QIAshredder spin column for homogenization. 350 µl 70 % ethanol was added to the homogenate, vortexed, and loaded on a RNeasy spin column. The column was centrifuged to bind the RNA to the membrane. Subsequently on-column DNase digestion was performed. The bound RNA was washed with RW1 buffer and twice with RPE buffer. Finally, RNA was eluted in nuclease free water and stored at – 80°C until use.

cDNA was synthesized using LunaScript RT SuperMix Kit (New England Biolabs, Germany) and RT-qPCR was performed using Luna Universal qPCR Master Mix (New England Biolabs, Germany) on a QuantStudio 7 Flex System. Reactions were performed in a total volume of 10 µl at 50°C for 2 minutes followed by 95°C for 10 minutes and 40 cycles of 95°C for 15 seconds and 60°C for 30 seconds. Genes of interest were normalized to Hypoxanthine Phosphoribosyltransferase 1 (HPRT1) and relative changes in gene expression were determined by the ΔΔCt method (98). The primers used are listed in Table 5.

Table 5 Primer sequences for RT-qPCR

Target	Forward sequence	Reverse sequence
HPRT1	TCAGGCAGTATAATCCAAAGATGGT	AGTCTGGCTTATATCCAACACTTCG
IL6	ACTCACCTCTTCAGAACGAATTG	CCATCTTTGGAAGGTTCAGGTTG
MX1	GTTTCCGAAGTGGACATCGCA	CTGCACAGGTTGTTCTCAGC
CXCL8	ACTGAGAGTGATTGAGAGTGGAC	AACCCTCTGCACCCAGTTTTC
Siglec-1	CAGGTGACAGAGACTCTTGGGA	GGCAATCCTACAGCCAAGAGCT
SARS-CoV-2 N	TTA CAA ACA TTG GCC GCA AA	GCG CGA CAT TCC GAA GAA

TNF (qHsaCED0037461), CXCL10 (qHsaCED0046619), IFN1b (qHsaCED0046851), IFIT1 (qHsaCED0034841), and CCL5 (qHsaCID0011644) qPCR primers were purchased from Biorad (US).

2.20. Immunohistochemistry

Formalin-fixed paraffin-embedded (FFPE) tissues or PaxGene-fixed paraffin-embedded (PFPE) tissues were sectioned at 3 µm. Sections were deparaffinized by immersing the slides in xylene for 15 minutes, followed by rehydration through graded ethanol series starting with 100 % ethanol for 2 minutes, 90 % ethanol for 2 minutes, 70 % ethanol for 2 minutes and 50 % ethanol for 2 minutes. Subsequently, sections were rinsed in distilled water. Antigen retrieval

was conducted in Natriumcitrat-buffer, pH = 6 (Glatt Koller, Austria) in a microwave for 40 minutes at 270 Watt. Slides were cooled at room temperature for 20 minutes before being rinsed with distilled water. Endogenous peroxidases were blocked with 10 % H_2O_2 (Merck KGaA, Germany) in methanol for 10 minutes. SARS-CoV-2 was detected by anti-coronavirus nucleocapsid antibody (R019, Sino Biological, China) diluted 1:500 or SARS-CoV-2 spike antibody (1A9, GeneTex, US) diluted 1:500 and a horseradish peroxidase (HRP)-conjugated secondary antibody (Dako REAL EnVision, HRP Rabbit/Mouse; Agilent Dako, Denmark). DAB+ Chromogen (Agilent Dako, Denmark) was applied for 3 minutes. FFPE and PFPE sections were countersained with mayer hematoxylin (Glatt Koller, Austria) and Gill II hematoxylin (Merck, Germany), respectively. Sections were washed for 3 minutes, with warm running tap water. Sections were dehydrated through graded ethanol series starting with 90 % ethanol for 2 minutes, 100 % ethanol for 2 minutes and were cleared in butylacetat for 2 minutes. Sections were mounted with Entellan (Merck, Germany).

2.21. Immunofluorescent staining

hMDM and Calu-3 cells were grown on cover slips (Ø 10 mm) and were fixed with 4 % formaldehyde after treatment. Fixed cells were rinsed with PBS and permeabilized with 0.1 % Triton-X (Sigma) in PBS for 10 minutes. Following permeabilization, cells were blocked in 2 % goat serum (Cell Signalling, MA, USA) for 30 minutes. Primary antibodies were diluted in 1 % BSA (Roth, Germany) and incubated for 1 hour. Conjugated secondary antibodies were diluted 1:400 in 1 % BSA and incubated for 30 minutes. Nuclei were stained with 1 µg/ml DAPI (Life Technologies, US) for 5 minutes and subsequently mounted with ProLong Gold antifade reagent (Life Technologies, US). The following primary antibodies were used: rabbit anti-SARS-CoV-2 nucleocapsid (#80026-1-RR, Proteintech, UK) and mouse anti-double stranded RNA J2 (# 10010200, Nordic, Denmark). The following secondary antibodies were used: goat anti-rabbit IgG Alexa Fluor Plus 594 (#A32740, Thermo Fisher, US) and goat anti-mouse Alexa Fluor Plus 488 (#A32723, Thermo Fisher, US). Samples were imaged using an Olympus IX83 inverted wide field microscope and cellSens Dimension 4.2.1 software.

2.22. Immunoblotting

Cells were lysed in M-Per Mammalian Protein Extraction Reagent (Thermo Fisher, US) supplemented with 5 µg/ml Pierce protease and phosphatase inhibitor mini tablets (Thermo Fisher, US). Protein lysates were pulse sonicated for approximately 10 seconds and total protein concentration was assessed by Pierce BCA protein assay kit (Thermo Fisher, US). Proteins were boiled in Laemmli buffer (Biorad, US) + 10 % beta mercaptoethanol for 5 minutes at 95°C. 6 µg protein were loaded and separated in 4 -12 % Bis-Tris gels (Biorad, US) in

running buffer (200 mM glycine, 25 mM Tris, 0.1 % SDS). Proteins were transferred to PVDF membranes (Merck, Germany) in transfer buffer (192 mM glycine, 25 mM Tris, 20 % MetOH). Subsequently, membranes were blocked with 5 % non-fat milk (ITW Reagents, Italy) in TBS-T (20mM Tris, 137 mM NaCl, 0,1 % Tween-20, pH = 7.6) for 30 minutes. Washes were performed with TBS-T buffer. Antibodies were diluted in TBS-T + 5 % non-fat milk. Primary antibodies were incubated overnight at 4°C and a secondary antibody linked to HRP was incubated for 1 hour at room temperature. HRP signals were visualized by Clarity Max Western ECL Substrate with a Chemidoc MP instrument (Biorad, US). Primary antibodies: ACE2 (#HPA000288; Sigma, US) 1:100, CD35 (Abcam, UK.) 1:250 and beta actin (#4967S, Cell Signaling, US). Secondary antibody: 1:10,000 and Anti-rabbit HRP-linked (#7074, Cell Signaling, US).

2.23. Cytokine quantification

Secreted cytokines were measured using the Bio-Plex Pro Human Cytokine 8-plex kit (Biorad, US) by the ZMF Core facility Bioimaging and Flow Cytometry according to the manufacturer's instructions.

2.24. Statistical analysis

Statistical analysis was performed using GraphPad Prism 10. Data were assumed to be normally distributed and analysed for statistical significance by ANOVA or t-tests. Multiple comparisons were corrected with Dunnett's, Tukey or Bonferroni post-hoc-test. Significance levels were determined as ns = $p > 0.05$; * = p 0.01–0.05; ** = p 0.001–0.01; *** = p 0.0001–0.001; **** = $p \leq 0.0001$.

3. Results

Parts of this dissertation have been published as original research articles in New Biotechnology (99), eLife (77) and Scientific Reports (95).

3.1. Sample collection system and storage temperature impact SARS-CoV-2 RNA integrity

Quantitative RT-qPCR is considered the diagnostic gold standard for the detection of SARS-CoV-2 (100), both in terms of sensitivity and specificity. Pre-analytical handling of patient specimens is critical to ensure reliable and valid test results. Therefore, the effect of storage time and temperature on the quantification of SARS-CoV-2 by RT-qPCR was investigated. SARS-CoV-2 RNA stability was monitored in different commercially available sample collection systems for nasal/oropharyngeal swabs. Five different collection solutions including PBS, viral

transport medium (VTM), universal transport medium (UTM), viral preservative medium (VPM) and eSwabs were tested. Collection solutions were spiked with different SARS-CoV-2 loads (10,000 and 1,000 copies/ml collection medium) and stored at room temperature or 37°C, respectively. Viral copy numbers were determined directly after spiking (= t0), after 24 hours (= t24) and 96 hours (= t96) of storage. In PBS, VTM, VPM, and UTM, no significant decrease of viral RNA levels was observed over 96 hours when stored at room temperature. In contrast, in eSwab solution, viral RNA levels significantly decreased from an average median of 7,800 copies/ml at t0 to 1,300 copies/ml at t96 hours at room temperature (Figure 5).

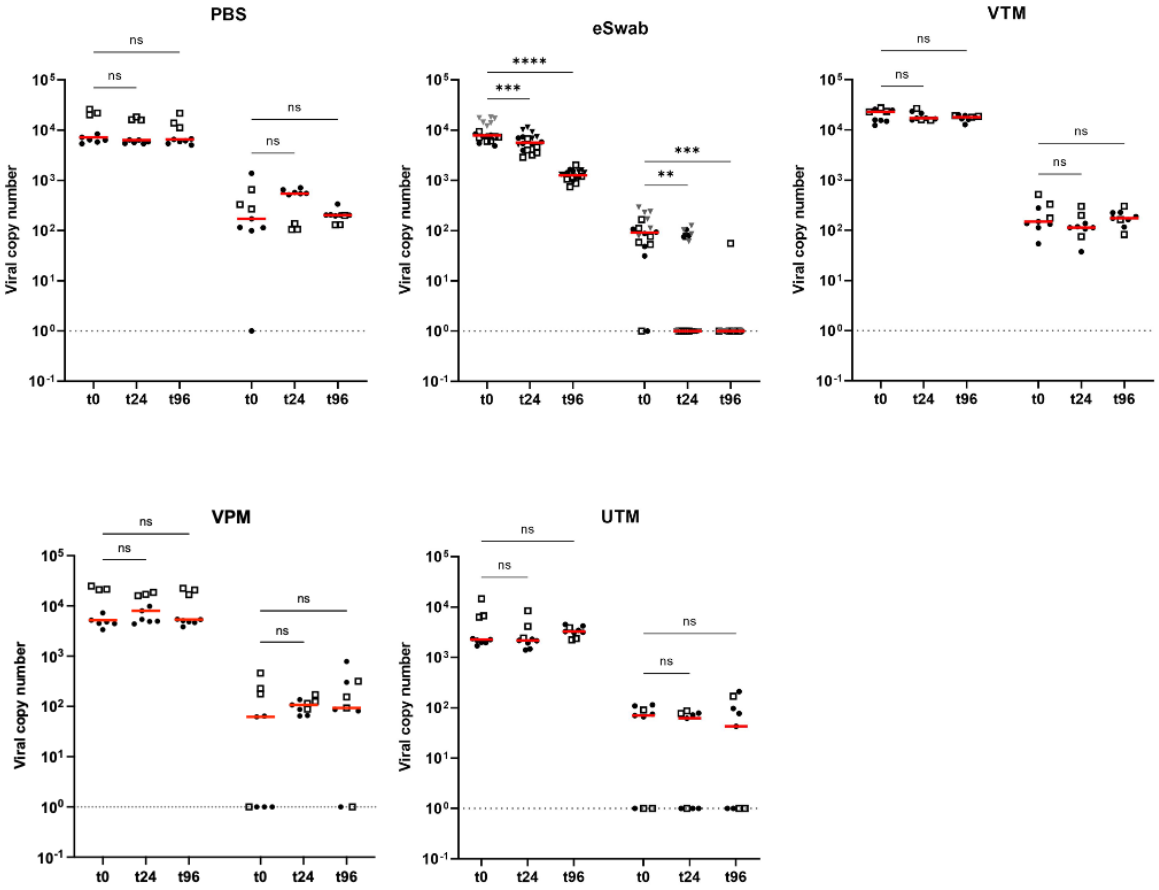

Figure 5 Stabilization of SARS-CoV-2 RNA by sample collection systems at room temperature. Five different collection solutions were spiked with 10,000 and 1,000 SARS-CoV-2 copies/ml and stored at room temperature**.** Viral copy numbers were determined directly after spiking (= t0), after 24 hours (= t24) and 96 hours (= t96) by RT-qPCR**.** Data shown refer to one to three independent experimental series (indicated by symbol shape) with either three or six replicates. Bars represent median values. P values were determined by 2-way ANOVA followed by Dunnett's post hoc test. *ns = p > 0.05; * = p 0.01–0.05; ** = p 0.001–0.01; *** = p 0.0001–0.001; **** = p ≤ 0.0001.* Adapted from Hardt et al. (2022).

Sample quality may be compromised if cooling chains are not maintained, and recommended storage temperatures are exceeded. Therefore, sample collection systems were stored at elevated temperatures and the effect on viral RNA quantification was determined. Increasing the storage temperature to 37°C had a profound effect on the integrity of viral RNA in some of the collection solutions. After 24 hours at 37°C, viral copies were significantly reduced in eSwab and VTM. After 96 hours, viral RNA was undetectable in PBS and eSwab collection solution. However, in VPM viral copy numbers remained stable over 96 hours (Figure 6).

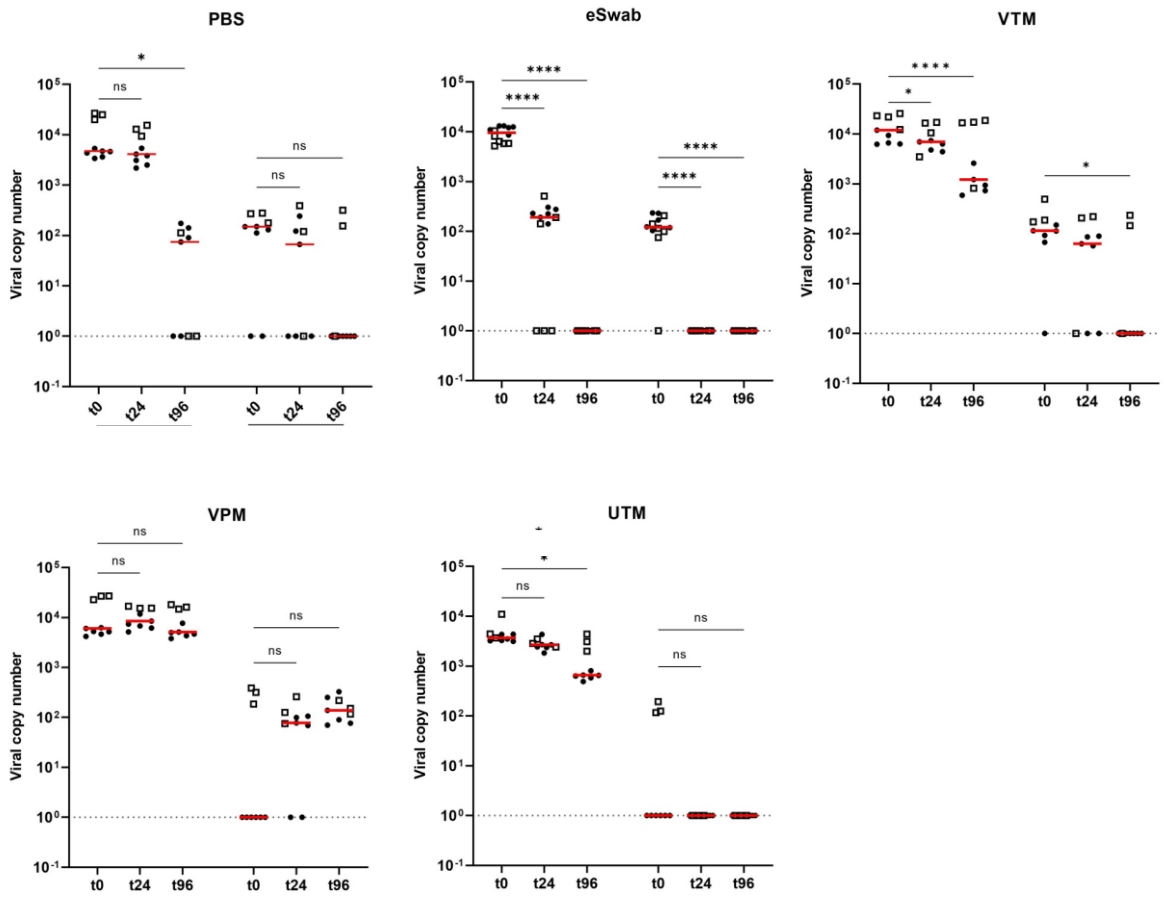

Figure 6 Stabilization of SARS-CoV-2 RNA by sample collection systems at 37°C. Five different collection solutions were spiked with 10,000 and 1,000 SARS-CoV-2 copies/ml and stored at 37°C**.** Viral copy numbers were determined directly after spiking (= t0), after 24 hours (= t24) and 96 hours (= t96) by RT-qPCR**.** Data shown refer to one to three independent experimental series (indicated by symbol shape) with either three or six replicates. Bars represent median values. P values were determined by repeated measures 2-way ANOVA followed by Dunnett's post hoc test. *ns = p > 0.05; * = p 0.01–0.05; ** = p 0.001–0.01; *** = p 0.0001–0.001; **** = p ≤ 0.0001.* Adapted from Hardt et al. (2022).

3.2. Antiviral activity of recombinant ACE2-Fc

3.2.1. Glycosylation of ACE2-Fc impacts the neutralizing activity

Human ACE2 is heavily glycosylated and comprises seven N-glycosylation sites (N53, N90, N103, N322, N432, N546, and N690) (101). Molecular dynamics simulations suggested that glycosylation and sialylation critically affect the binding affinity between ACE2 and the RBD of the spike protein of SARS-CoV-2 (77). Based on the results obtained from molecular dynamics simulations, the glycans at position N90 and N322 were eliminated, and the impact of their removal on the neutralization activity was investigated. Therefore, asparagine at position 322 was substituted with glutamine to prevent glycosylation (ACE2-N332Q-Fc). Glycosylation of asparagine at position 90 was eliminated by replacing threonine at position 92 with glutamine (ACE2-T92Q-Fc) (78,102). Additionally, a construct carrying both mutations (ACE2-DM-Fc) was designed. Further, wild-type (wt)-ACE2-Fc was enzymatically deglycosylated with peptide-N4-(N-acetyl-beta-glucosaminyl)asparagine amidase F (DeGlyco ACE2-Fc) or desialylated with neuraminidase (Desial ACE2-Fc).

The impact of deglycosylation and desialylation of ACE2-615-Fc – a fusion protein consisting of the soluble protease domain (amino acids 18 - 615) and a human IgG1 Fc domain – on its SARS-CoV-2 neutralization activity was assessed by virus neutralization assays. Therefore, VeroE6 cells were infected with SARS-CoV-2 in the presence of varying concentrations of ACE2-Fc (10 µg/ml, 20 µg/ml, 50 µg/ml) and the neutralization activity was assessed by quantification of viral RNA levels in the culture supernatants 24 hpi (Figure 7). We observed concentration-dependent neutralization with all ACE2-Fc constructs. Incubation with 50 µg/ml wt-ACE2-Fc resulted in an average increase of 3.1 Ct-values, corresponding to an approximately 8.5-fold reduction in viral RNA. The single mutant ACE2-N322Q-Fc demonstrated enhanced neutralization activity, with a 6.5 Ct-value increase at the same concentration, equivalent to a 90-fold reduction in viral RNA. ACE2-T92Q-Fc exhibited even greater neutralization activity, with a Ct-value increase of 14.9, which is comparable to the neutralization activity of the enzymatically deglycosylated construct ACE2-DeGlyco-Fc. Notably, at the lowest tested concentration (10 µg/ml), only ACE2-DeGlyco-Fc significantly increased Ct-values by 6.5, equivalent to a 90-fold reduction of viral RNA.

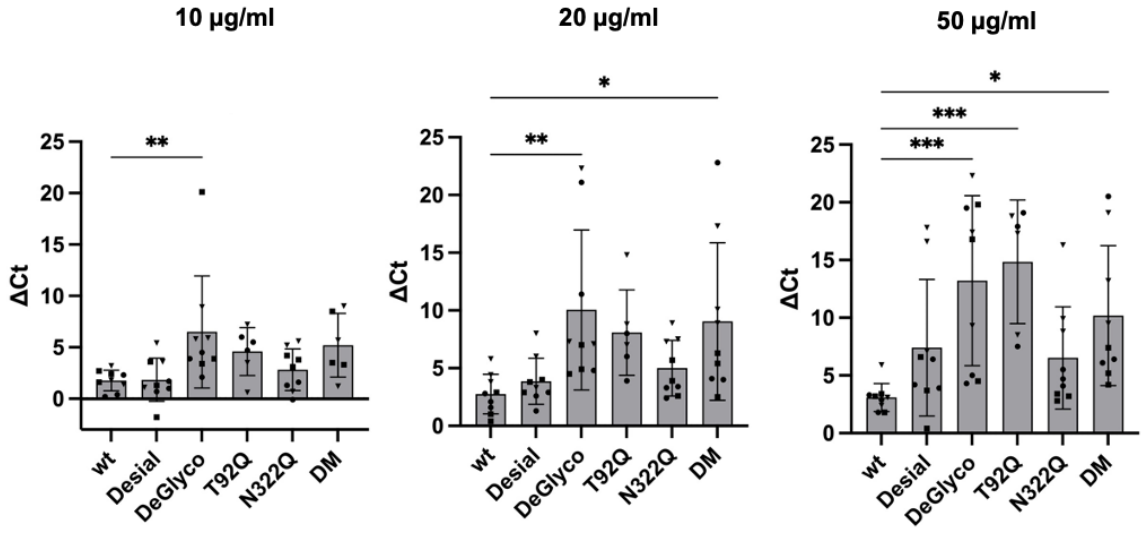

Figure 7 Glycosylation of ACE2-Fc affects SARS-CoV-2 neutralization activity. Wild-type ACE2-Fc decoy (containing ACE2 amino acids 18-615) and glyco-engineered variants thereof were incubated with SARS-CoV-2 (wh19) at different concentrations (10 µg/ml, 20 µg/ml, 50 µg/ml) prior to infection of VeroE6 cells. Viral RNA loads in cell culture supernatants were quantified by RT-qPCR 24 hpi. DeGlyco, deglycosylated wild-type ACE2-Fc; T92Q, mutant ACE2-615L-Fc lacking N-glycans at N90; N322Q, mutant ACE2-615L-Fc lacking N-glycans at N322; DM, mutant ACE2-615L-Fc lacking N-glycans at N90 and N322. Data are presented as mean ± SD of two to three experimental series (symbol shapes) performed in triplicates. P values were determined by one-way ANOVA followed by Dunnett's post hoc test. *ns = P > 0.05; * = P 0.01–0.05; ** = P 0.001–0.01; *** = P 0.0001–0.001; **** = P ≤ 0.0001.* Adapted from Capraz et al. (2021).

Since we observed that glycosylation has a substantial impact on the neutralization activity of ACE2-615-Fc, and given that different expression systems produce distinct glycan profiles, we compared the neutralization activity of ACE2-615-Fc produced in glycoengineered *N. benthamiana* plants with that expressed in a human embryonic kidney cell line (HEK293).

At high concentrations, ACE2-615-Fc expressed in *N. benthamiana* and HEK293 cells exhibited comparable neutralization activities. Notably, ACE2-615-Fc derived from *N. benthamiana* showed significantly higher neutralization activity at lower concentrations (Figure 8). We suggest that this effect could most likely be attributed to different glycosylation patterns resulting from the respective expression system.

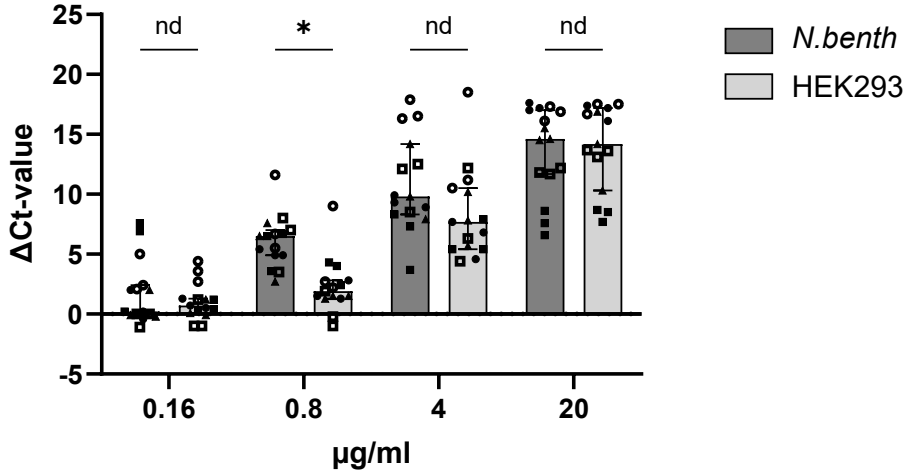

Figure 8 Neutralization activity of ACE2-Fc expressed in *N. benthamiana* and HEK293 cells. ACE2-615H-Fc was pre-incubated with SARS-CoV-2 (de21) prior to infection of Calu-3 cells. Supernatants were harvested 48 hpi and viral RNA was quantified by RT-qPCR. Ct-values were normalized to the corresponding infected, untreated control. Data refer to five independent experimental series (symbol shape), each performed in triplicates. Bars represent median values with 95 % CI. P values were determined by repeated multiple unpaired t-test followed by Bonferroni post hoc test. *ns = P > 0.05; * = P 0.01–0.05; ** = P 0.001–0.01; *** = P 0.0001–0.001; **** = P ≤ 0.0001.*

3.2.2. Optimization of ACE2-Fc for the expression in *N. benthamiana*

We observed substantial fragmentation of the ACE2-615-Fc decoy by endogenous proteases of *N. benthamiana*, which cleave the fusion protein within or in close proximity of the linker region (Figure 9b). ACE2-615-Fc consists of a truncated ACE2 ectodomain (amino acids 18-615), that lacks the collectrin-like domain. We hypothesized that expression of the full-length ACE2 ectodomain (amino acids 18-740, later referred to as ACE2-740-Fc) could enhance resistance to proteolytic cleavage. Furthermore, we evaluated the impact of different linker sequences connecting the ACE2 domain to the Fc domain of IgG1, specifically the endogenous IgG1 hinge region (H: EPKSCDKTHTCPPCPAPELLGGP) and a synthetic linker sequence (L: GGGGSGGGGS).

We found that the truncated ACE2-615L-Fc decoy containing the synthetic linker, was less prone to proteolytic cleavage as compared to ACE2-615H-Fc containing the natural hinge region. Moreover, our findings indicate that the ACE2-740-Fc decoy, which includes the collectrin-like domain, exhibits significantly greater resistance to proteolytic fragmentation *in planta* compared to the truncated version ACE2-615-Fc (Figure 9b). In addition, ACE2-740-Fc has enhanced neutralization activity compared to ACE-615-Fc (Figure 9a). The different linker peptides did not affect the neutralization activity. Given that the hinge region is a sequence

naturally occurring in humans, it is less likely to provoke immunogenic reactions. Therefore, we selected the hinge region as preferred linker peptide.

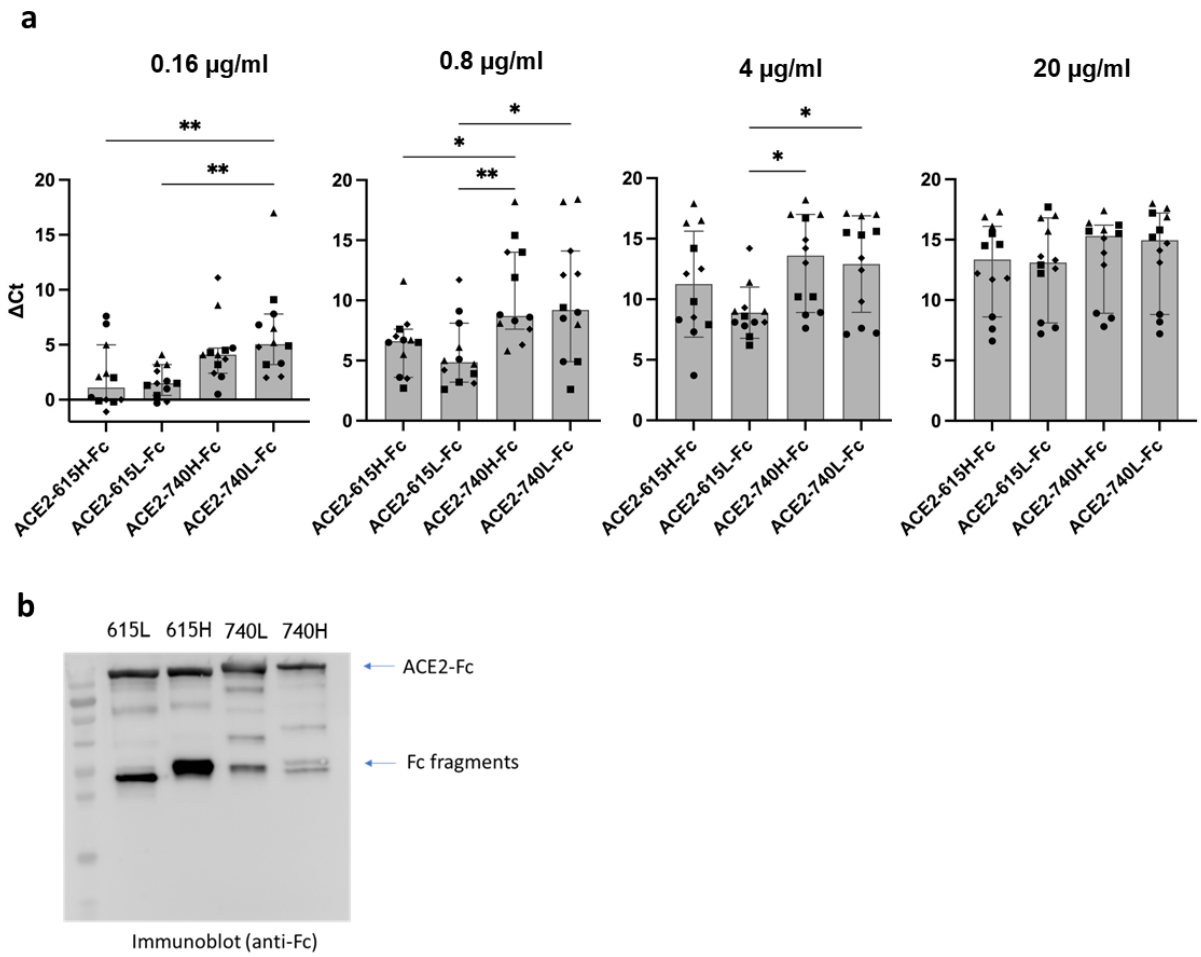

Figure 9 ACE2-740-Fc demonstrates enhanced neutralization activity and resistance to proteolytic cleavage compared to ACE-615-Fc. The constructs differ in the length of the ACE2 domain (615aa, 740aa) and in the linkers connecting the ACE2 and Fc domain (L, synthetic GGGGSGGGGS linker; H, IgG1 hinge region). a) ACE2-Fc decoys were pre-incubated with SARS-CoV-2 (de21) prior to infection of Calu-3 cells. Supernatants were harvested 48 hpi and viral RNA was quantified by RT-qPCR. Ct-values were normalized to the corresponding infected, untreated control. Data refer to three independent experiments (symbol shape) performed in triplicates. Bars represent median values with 95 % CI. b) Western blot: ACE2-740-Fc is less sensitive to proteolysis than ACE2-615-Fc, as evident from the reduction in Fc fragments. P values were determined by one-way ANOVA followed by Tukey post hoc test. *ns = p > 0.05; * = p 0.01–0.05; ** = p 0.001–0.01; *** = p 0.0001–0.001; **** = p ≤ 0.0001.* The data presented in Figure 9b were kindly provided by Alexandra Castilho (BOKU University).

Nevertheless, the hinge region and parts of the C-terminal ectodomain of ACE2 are subject to unwanted non-human post-translational modifications when expressed *N. benthamiana*, which could lead to adverse immunogenic reactions. Up to three of six proline residues are hydroxylated when produced in *N.benthamiana* (Figure 10), whereas these modifications are not observed when the fusion protein is expressed in HEK293 cells.

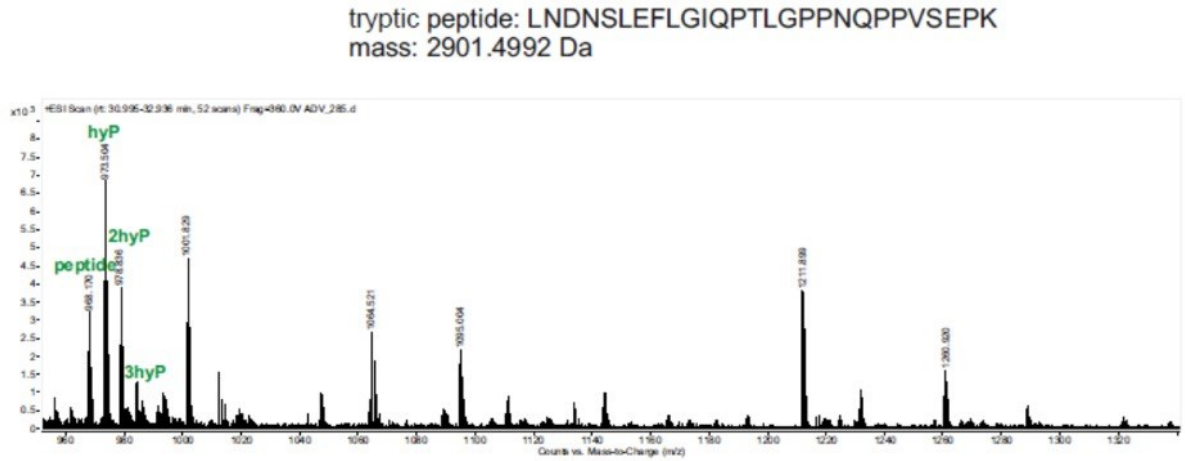

Figure 10 ACE2-740H-Fc expressed in *N. benthamiana* contains up to three hydroxylated proline residues (hyP). Analysis of ACE2-740H-Fc by tryptic fingerprinting was performed by the BOKU Core Facility Mass Spectrometry. The data presented in Figure 10 were kindly provided by Alexandra Castilho and Richard Strasser (BOKU University).

Hence, we developed an ACE2-Fc variant that is optimized for the expression in glycoengineered *N. benthamiana*, namely ACE2-728H-Fc. ACE2-728H-Fc lacks twelve structurally flexible amino acids of the full-length ACE2 ectodomain (residues 729-740), which include four proline residues (P733, P734, P737, P738) and a potential O-glycosylation site (T730). Furthermore, ACE2-728H-Fc also lacks the first seven amino acids of the hinge region (EPKSCDK), containing an additional proline (P742) and an unpaired cysteine (C745) residue (Sequence 1). The structure of ACE2-728H-Fc with its domains is shown in Figure 11.

Sequence 1: Sequence of ACE2-740H-Fc. The human IgG1 Fc-domain (italics) and the hinge region of human IgG1 (underlined) are highlighted. Proline residues P733, P734, P737, P738, P742, cysteine residue C745 and the O-glycosylation site T730 are shown in bold. The residues removed in ACE2-728H-Fc are highlighted in yellow.

QSTIEEQAKTFLDKFNHEAEDLFYQSSLASWNYNTNITEENVQNMNNAGDKWSAFLKEQSTLAQMYPL
QEIQNLTVKLQLQALQQNGSSVLSEDKSKRLNTILNTMSTIYSTGKVCNPDNPQECLLLEPGLNEIMA
NSLDYNERLWAWESWRSEVGKQLRPLYEEYVVLKNEMARANHYEDYGDYWRGDYEVNGVDGYDYSRGQ
LIEDVEHTFEEIKPLYEHLHAYVRAKLMNAYPSYISPIGCLPAHLLGDMWGRFWTNLYSLTVPFGQKP
NIDVTDAMVDQAWDAQRIFKEAEKFFVSVGLPNMTQGFWENSMLTDPGNVQKAVCHPTAWDLGKGDFR

ILMCTKVTMDDFLTAHHEMGHIQYDMAYAAQPFLLRNGANEGFHEAVGEIMSLSAATPKHLKSIGLLS
PDFQEDNETEINFLLKQALTIVGTLPFTYMLEKWRWMVFKGEIPKDQWMKKWWEMKREIVGVVEPVPH
DETYCDPASLFHVSNDYSFIRYYTRTLYQFQFQEALCQAAKHEGPLHKCDISNSTEAGQKLFNMLRLG
KSEPWTLALENVVGAKNMNVRPLLNYFEPLFTWLKDQNKNSFVGWSTDWSPYADQS[615]IKVRISLKSA
LGDKAYEWNDNEMYLFRSSVAYAMRQYFLKVKNQMILFGEEDVRVANLKPRISFNFFVTAPKNVSDII
PRTEVEKAIRMSRSRINDAFRLNDNSLEFLGIQ[728]P**T**LG**PP**NQ**PP**VS[740]*E**P**KS**C**DKTHTCPPCPAPEL*
LGGPSVFLFPPKPKDTLMISRTPEVTCVVVDVSHEDPEVKFNWYVDGVEVHNAKTKPREEQYNSTYRV
VSVLTVLHQDWLNGKEYKCKVSNKALPAPIEKTISKAKGQPREPQVYTLPPSRDELTKNQVSLTCLVK
GFYPSDIAVEWESNGQPENNYKTTPPVLDSDGSFFLYSKLTVDKSRWQQGNVFSCSVMHEALHNHYTQ
KSLSLSPGK

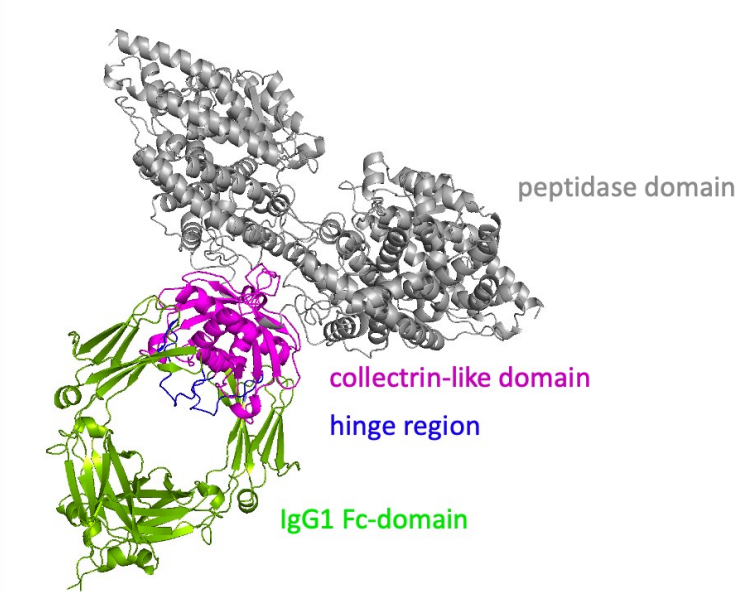

Figure 11 Structure of ACE2-728H-Fc and its domains: peptidase domain (grey), collectrin like domain (magenta), hinge region (blue), IgG1 Fc domain (green). The structural model was generated with Pymol.

Notably, removal of the 12 amino acids did not affect the neutralization activity of ACE2-728H-Fc (Figure 12).

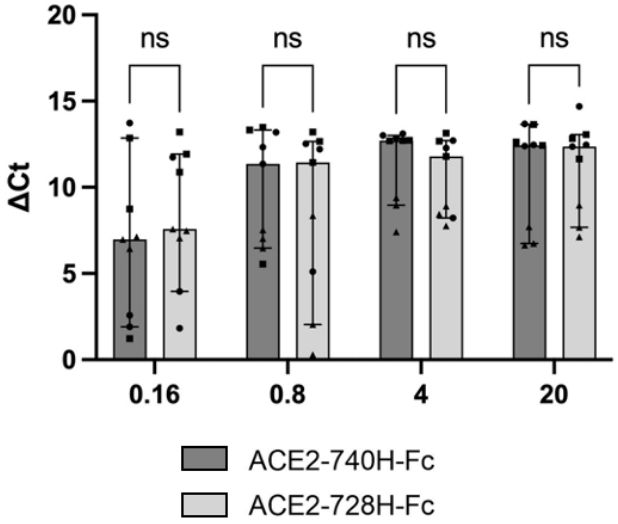

Figure 12 ACE2-728H-Fc and ACE2-740H-Fc have similar neutralization activities. ACE2-Fc decoys were pre-incubated with SARS-CoV-2 (de21) prior to infection of Calu-3 cells. Supernatants were harvested 48 hpi and viral RNA was quantified by RT-qPCR. Ct-values were normalized to the corresponding infected, untreated control. Data refer to three independent experiments (symbol shape) performed in triplicates. Bars represent median values with 95 % CI. P values were determined by two-way ANOVA followed by Bonferroni post hoc test. *ns = p > 0.05; * = p 0.01–0.05; ** = p 0.001–0.01; *** = p 0.0001–0.001; **** = p ≤ 0.0001.*

Moreover, removal of the twelve amino acids significantly increased the proportion of dimeric ACE2-728H-Fc while markedly reducing its propensity to form higher oligomers compared to ACE2-740H-Fc (Figure 13). This effect is likely due to the elimination of the unpaired cysteine residue C745. The dimeric form is advantageous over higher oligomers in terms of product stability, in particular in terms of its lower tendency to form precipitates upon prolonged storage and repeated freeze-thaw cycles.

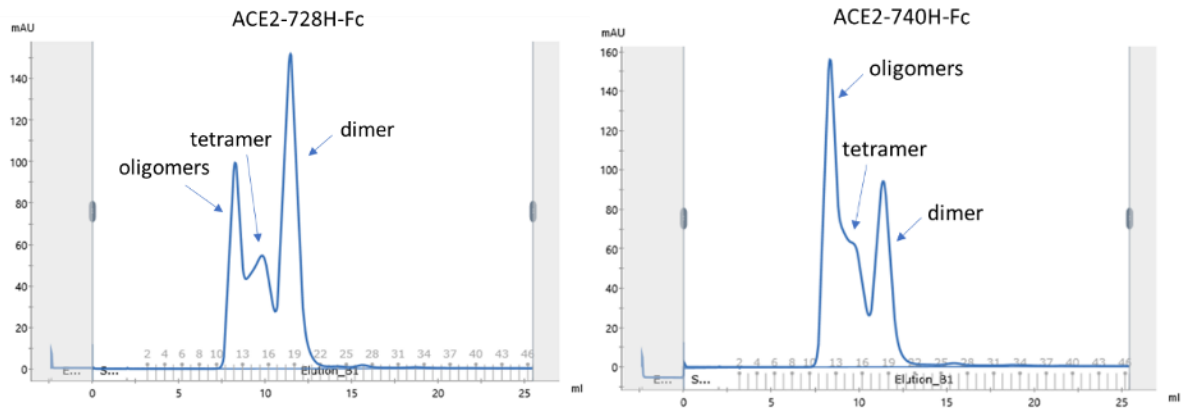

Figure 13 ACE2-728H-Fc has a significantly lower propensity to form undesirable higher-order oligomers compared to ACE2-740H-Fc. Affinity-purified ACE2-728H-Fc and ACE2-740H-Fc expressed in *N. benthamiana* was analyzed using size-exclusion chromatography. The oligomer peak elutes in the void volume of the column. These data were kindly provided by Richard Strasser (BOKU University).

We compared the neutralization activity of the oligomeric fraction (containing tetrameric and higher oligomeric forms), the dimeric fraction and unfractionated ACE2-728H-Fc. As shown in Figure 14, the oligomeric fraction and unfractionated ACE2-728H-Fc have similar neutralization activities at higher concentrations (mean delta Ct-value at 0.8 µg/ml and 4 µg/ml: unfractionated = 14.5 and 18.8, oligomeric = 13.4 and 17.6), whereas the dimeric form is less potent in neutralizing SARS-CoV-2 (mean delta Ct-value at 0.8 µg/ml and 4 µg/ml: 4.0 and 9.6). Based on the results, we selected, unfractionated ACE2-728H-Fc expressed in *N. benthamiana* as our lead construct for further testing.

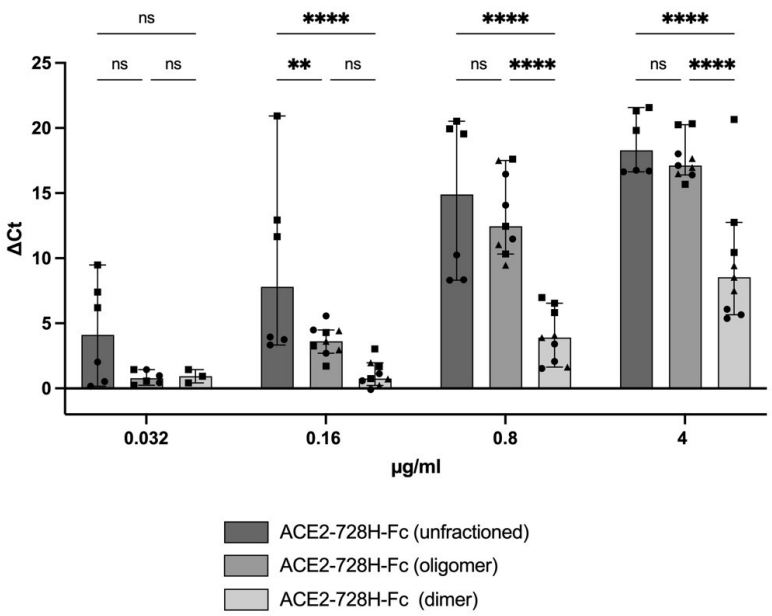

Figure 14 Unfractionated and oligomeric ACE2-728H-Fc have higher neutralization activity compared to dimeric ACE2-728H-Fc. Unfractionated, oligomeric, and dimeric ACE2-728H-Fc were pre-incubated with SARS-CoV-2 (de21) prior to infection of Calu-3 cells. Supernatants were harvested 48 hpi and viral RNA was quantified by RT-qPCR. Ct-values were normalized to an infected, untreated control. Data refer to two to three independent experiments (symbol shape) performed in triplicates. Bars represent median values with 95 % CI. P values were determined by two-way ANOVA followed by Tukey post hoc test. *ns = p > 0.05; * = p 0.01–0.05; ** = p 0.001–0.01; *** = p 0.0001–0.001; **** = p ≤ 0.0001.*

The physical instability of recombinant proteins means that storage conditions can affect the extent to which they unfold, aggregate, or degrade, which could hamper their effectiveness and raise safety concerns (103). Many recombinant proteins require storage at low temperatures ranging from 4°C to -80°C, to preserve their integrity and functionality. However, it is challenging to maintain these cooling conditions during transport and storage, and multiple freeze-thaw cycles may also compromise protein integrity (103,104).

Therefore, we examined how the storage temperature affects the neutralizing activity of ACE2-728H-Fc. ACE2-728H-Fc was stored either at -80°C or at room temperature. After five and nine months, IC_{50} values were determined by CPE assays with VeroE6 cells. ACE2-728H-Fc stored at room temperature demonstrated stable neutralization activity for a duration of up to nine months (Figure 15).

a

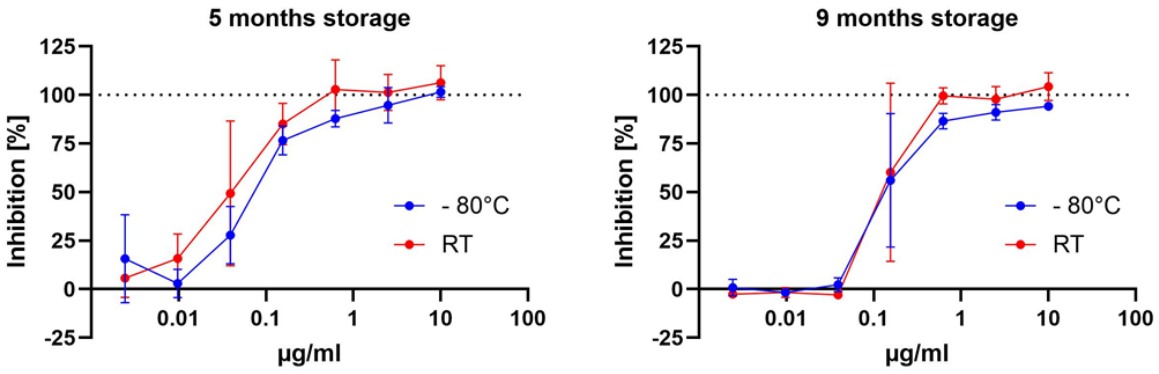

b

IC50 [µg/ml]

	5 months	9 months
-80°C	0.08	0.15
RT	0.04	0.15

Figure 15 ACE2-728H-Fc stored at room temperature, demonstrates stable neutralization activity for up to 9 months. ACE2-728H-Fc was either stored at -80°C (blue) or at room temperature (RT, red) in the dark. Neutralization activities were determined after five and nine months. a) Dose response curves of ACE2-728H-Fc against SARS-CoV-2 (de21) assessed by CPE assays with VeroE6 cells. Data are presented as arithmetic mean values ± SD and refer to one experiment performed in triplicates. b) IC_{50} concentrations calculated from dose response curves.

Next, we examined the antiviral activity of ACE2-728H-Fc in a primary air-liquid interface (ALI) culture model. ALI cultures closely simulate the human respiratory epithelium and are considered a physiologically relevant model for studying respiratory virus infections. Pre-treatment of SARS-CoV-2 (de21) with 20 µg/ml ACE2-728H-Fc significantly inhibited viral infection in primary ALI cultures. This was evidenced by immunohistochemical detection of the SARS-CoV-2 nucleocapsid protein and quantification of both intracellular and extracellular viral RNA levels (Figure 16).

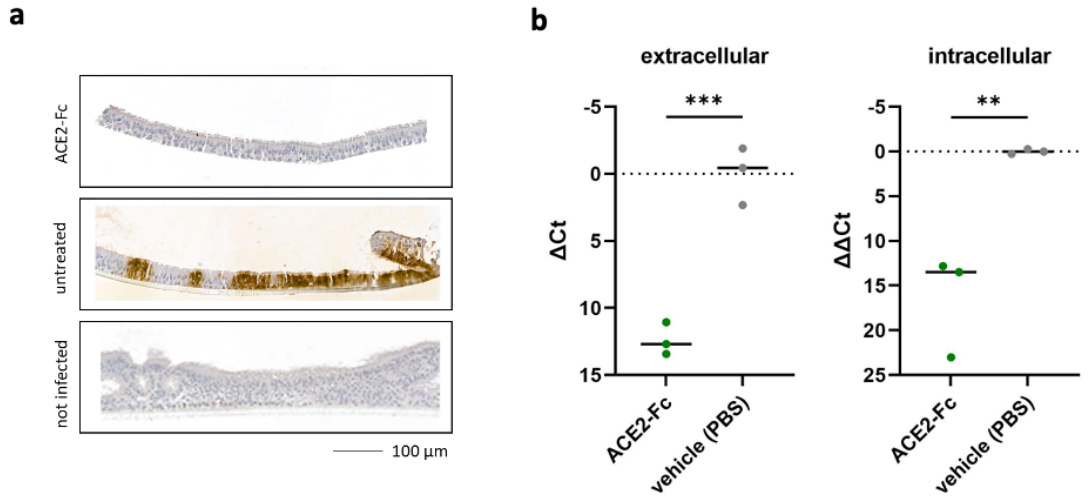

Figure 16 ACE2-728H-Fc prevents SARS-CoV-2 (de21) infection of primary ALI cultures a) Immunohistochemical detection of the viral nucleocapsid protein and b) detection of viral RNA by RT-qPCR. Extracellular virus RNA levels are presented as ΔCt. Intracellular virus RNA levels were quantified by ΔΔCt analysis of SARS-CoV-2 N gene expression, normalized to the house keeping gene HPRT1, and relative to infected, untreated controls. Dots represent independent cultures and bars the median values. P values were calculated by unpaired t-tests. *ns = p > 0.05;* * p < 0.05; ** p < 0.01; *** p < 0.001; **** p < 0.0001. Adapted from Föderl-Höbenreich et al. (2025).

3.2.3. ACE2-728H-Fc broadly neutralizes SARS-CoV-2 variants of concern

A broad neutralization spectrum is crucial for antiviral drugs to ensure a sustainable efficacy against emerging variants. We compared the neutralization activity of Nirmetalvir, a viral main protease inhibitor (PF-332), a pool of convalescent COVID-19 sera and ACE2-728H-Fc against early and late SARS-CoV-2 variants of concern (VOCs). We determined the IC_{50} against an ancestral SARS-CoV-2 strain (wh19) and three VOCs: a Delta variant (de21), an earlier Omicron variant (om21) and a later Omicron variant (om23).

ACE2-Fc robustly neutralized all tested VOCs, with even increased neutralization activity against later variants compared to the ancestral variant wh19 (Figure 17). In contrast, convalescent sera exhibited reduced neutralization activity against the more recent Omicron isolates. Nirmatrelvir robustly neutralized all tested VOCs, consistent with its previously reported broad efficacy (105).

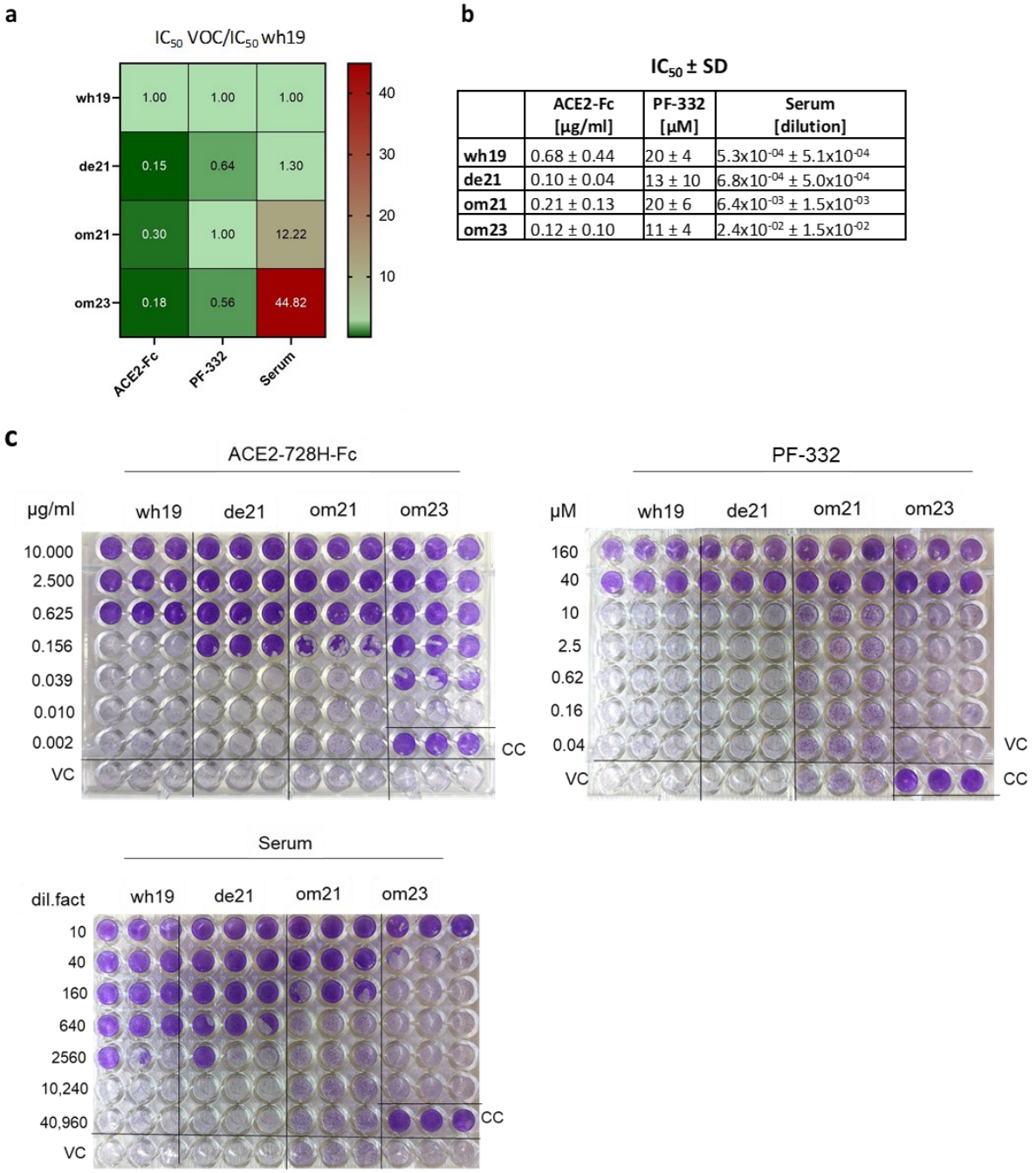

Figure 17 Broad neutralization spectrum of in planta expressed ACE2-728H-Fc against VOCs. The antiviral activity of ACE2-728H-Fc, viral protease inhibitor (PF332), and a pool of convalescent sera against the ancestral Wuhan strain (wh19), a Delta strain (de21) and two Omicron strains (om21, om23) was assessed by CPE assays with VeroE6 cells. IC_{50} values were determined by inhibitory dose-response curve analysis. a) Values indicate the fold change of IC_{50} concentrations, relative to the wild-type strain (wh19). b) Absolute IC_{50} values. c) Representative images of CPE assay plates after crystal violet staining. Violet-stained wells indicate no CPE, whereas transparent wells indicate CPE. VC: virus control, CC: cell control. Adapted from Föderl-Höbenreich et al. (2025).

3.2.4. Development of a non-binding ACE2-728H-Fc mutant to control for Fc-domain mediated effects in *in vivo* experiments

To demonstrate the specificity of the antiviral activity of ACE-728H-Fc *in vivo*, we designed a mutated ACE2-728H-Fc variant (mutACE2-728H-Fc), that allowed us to control for potential non-SARS-CoV-2 specific effects induced by the Fc-domain. To do so, eight amino acids of the human ACE2 sequence (Q24; D30; K31; H34; L79; M82; Y83; K353) were replaced with their mouse counterparts (N24; N30; N31; Q34; T79; S82; F83; H353) (106) (Sequence 2). It has been demonstrated that early SARS CoV-2 variants are unable to bind to murine ACE2 due to a receptor mismatch. This explains why mice are not susceptible to early SARS-CoV-2 variants (106). Nevertheless, recent studies demonstrated that the affinity of murine ACE2 to the RBD of Omicron variants is similar to that of human ACE2 (107).

Sequence 2. Sequence of non-neutralizing mutACE2-728H-Fc. The changed residues (N24, N30, N31, Q34, T79, S82, F83, H353) are marked in red. The hinge region of human IgG1 Fc is highlighted by italic letters.

QSTIEENAKTFLNNFNQEAEDLFYQSSLASWNYNTNITEENVQNMNNAGDKWSAFLKEQSTTAQSFPLQEIQNLT
VKLQLQALQQNGSSVLSEDKSKRLNTILNTMSTIYSTGKVCNPDNPQECLLLEPGLNEIMANSLDYNERLWAWES
WRSEVGKQLRPLYEEYVVLKNEMARANHYEDYGDYWRGDYEVNGVDGYDYSRGQLIEDVEHTFEEIKPLYEHL
HAYVRAKLMNAYPSYISPIGCLPAHLLGDMWGRFWTNLYSLTVPFGQKPNIDVTDAMVDQAWDAQRIFKEAEKFF
VSVGLPNMTQGFWENSMLTDPGNVQKAVCHPTAWDLGHGDFRILMCTKVTMDDFLTAHHEMGHIQYDMAYAA
QPFLLRNGANEGFHEAVGEIMSLSAATPKHLKSIGLLSPDFQEDNETEINFLLKQALTIVGTLPFTYMLEKWRWMV
FKGEIPKDQWMKKWWEMKREIVGVVEPVPHDETYCDPASLFHVSNDYSFIRYYTRTLYQFQFQEALCQAAKHEG
PLHKCDISNSTEAGQKLFNMLRLGKSEPWTLALENVVGAKNMNVRPLLNYFEPLFTWLKDQNKNSFVGWSTDWS
PYADQSIKVRISLKSALGDKAYEWNDNEMYLFRSSVAYAMRQYFLKVKNQMILFGEEDVRVANLKPRISFNFFVTA
PKNVSDIIPRTEVEKAIRMSRSRINDAFRLNDNSLEFLGIQTHTCPPCPAPELLGGP*SVFLFPPKPKDTLMISRTPEV*
TCVVVDVSHEDPEVKFNWYVDGVEVHNAKTKPREEQYNSTYRVVSVLTVLHQDWLNGKEYKCKVSNKALPAPIE
KTISKAKGQPREPQVYTLPPSRDELTKNQVSLTCLVKGFYPSDIAVEWESNGQPENNYKTTPPVLDSDGSFFLYS
KLTVDKSRWQQGNVFSCSVMHEALHNHYTQKSLSLSPGK

Indeed, mutACE2-Fc cannot bind to the Wuhan RBD as shown in enzyme-linked immunosorbent assays (Figure 18a) and failed to prevent VeroE6 cells from becoming infected

with the Delta and Wuhan strains (Figure 18b-d). By contrast, we observed residual neutralizing activity against the two Omicron isolates that were tested (Figure 18d).

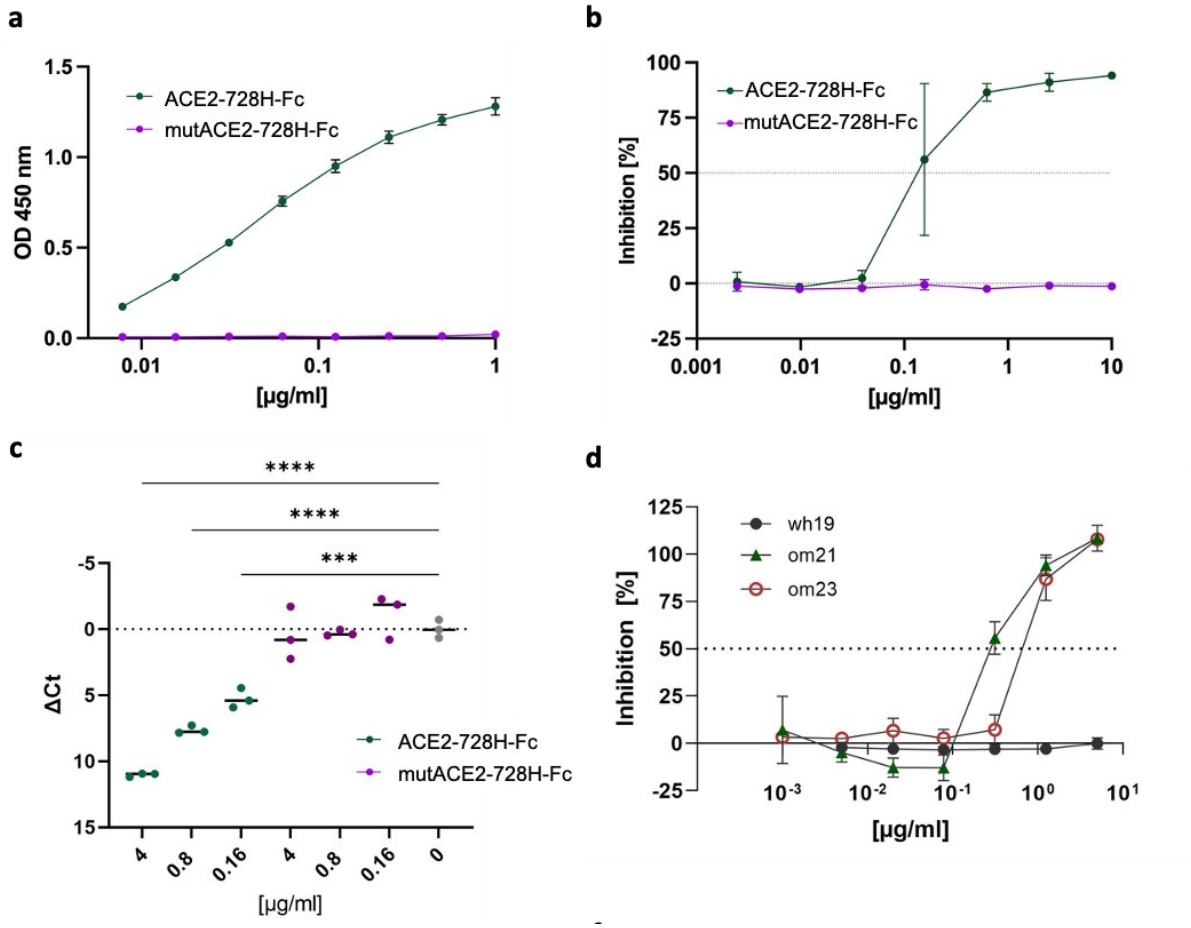

Figure 18 Neutralization and binding activity of mutACE2-728H-Fc. a) Binding affinity of wild-type ACE2-728H-Fc and mutACE2-728H-Fc for immobilized Wuhan RBD assessed by ELISA. Data shown represent arithmetic mean values ± SD of one representative experiment performed in technical duplicates. This experiment was repeated two times with similar results. b) Dose response curve of wild-type ACE2-Fc and mutACE2-Fc against SARS-CoV-2 (de21) assessed by CPE assays with VeroE6 cells. Data are presented as arithmetic mean values ± SD of one experiment performed in triplicates. c) Inhibition of SARS-CoV-2 (de21) replication was assessed by quantification of viral RNA in VeroE6 supernatants 24 hpi by RT-qPCR. Ct-values were normalized to an infected, untreated control. Data are presented as median values of a single experiment performed in triplicates. *P*-values were calculated by ANOVA followed by Dunnett post hoc test. *ns = p > 0.05;* * $p < 0.05$; ** $p < 0.01$; *** $p < 0.001$; **** $p < 0.0001$. d) Dose response curve of mutACE2-728H-Fc against different SARS-CoV-2 variants (wh19, om21, om23) in VeroE6 cells assessed by CPE assays. Data are presented as arithmetic mean values ± SD of one experiment performed in triplicates.

Differential scanning calorimetry revealed that the stability of the ACE2 and the C_H2 domains of mutACE2-728H-Fc was moderately reduced (Figure 19). However, the enzymatic activity of mutACE2-728H-Fc (18.6 ± 0.3 units per mg protein) and ACE2-728H-Fc (17.1 ± 0.4 units per mg protein) were comparable. Collectively, these findings establish mutACE2-Fc as an appropriate negative control for *in vivo* studies.

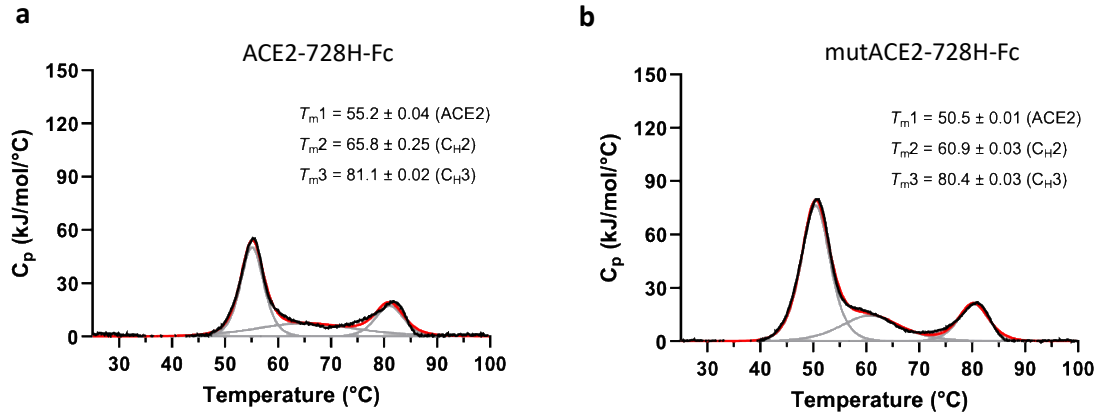

Figure 19 Thermal stability of wild-type and mutant ACE2-728H-Fc. Analysis of wild-type ACE2-728H-Fc (a) and mutACE2-728H-Fc (b) by differential scanning calorimetry. Raw data (black) were smoothened (red) and then fitted using a non-two-state thermal unfolding model (gray). Data are presented as mean ± SEM of three independent experiments. Cp, heat capacitance. Adapted from Föderl-Höbenreich et al. (2025).

3.2.5. Intranasal application of ACE2-728H-Fc reduces weight loss in SARS-CoV-2 infected hamsters

Based on the *in vitro* findings, we evaluated the therapeutic efficacy of plant-derived ACE2-728H-Fc in a Syrian hamster model. Hamsters were infected with 10^4 $TCID_{50}$/ml (50 µl/nostril) SARS-CoV-2 (Wuhan D614G, hCoV-19/France/GE1973/2020). In order to simulate a therapeutic setting, hamsters received daily intranasal administrations (50 µl/nostril) of either 2.5 mg/ml ACE2-728H-Fc, 2.5 mg/ml mutACE2-728H-Fc, or vehicle (PBS), starting 24 hpi (Figure 20).

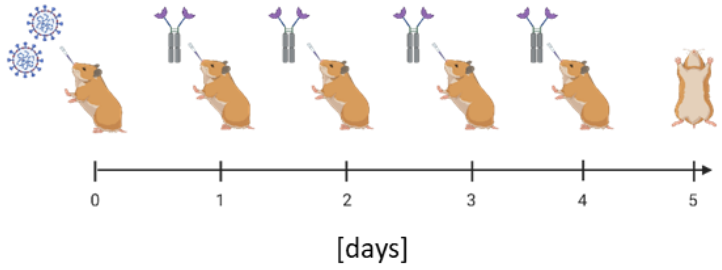

Figure 20 Experimental scheme for the *in vivo* efficacy test. Syrian gold hamsters were challenged with 10^4 $TCID_{50}$ authentic SARS-CoV-2. Starting at 24 hpi animals were daily treated with 100 µl (50 µl/nostril) of 2.5 mg/ml ACE2-728H-Fc, mutACE2-728H-Fc or vehicle (PBS).

Hamsters treated with wild-type ACE2-728H-Fc showed significantly reduced weight loss, with an average body weight change of -3.9 % five days post-infection compared to day 0. In contrast, the vehicle group lost 11.5 %. The group receiving non-binding mutACE2-728H-Fc exhibited a weight loss comparable to that of the vehicle group (-10.3 %) (Figure 21a). Furthermore, treatment with ACE2-728H-Fc significantly reduced the load of infectious viral particles in the lungs of hamsters (2.53 log_{10} decrease, Figure 21b) and decreased the transcriptional levels of pro-inflammatory cytokines (Figure 21c).

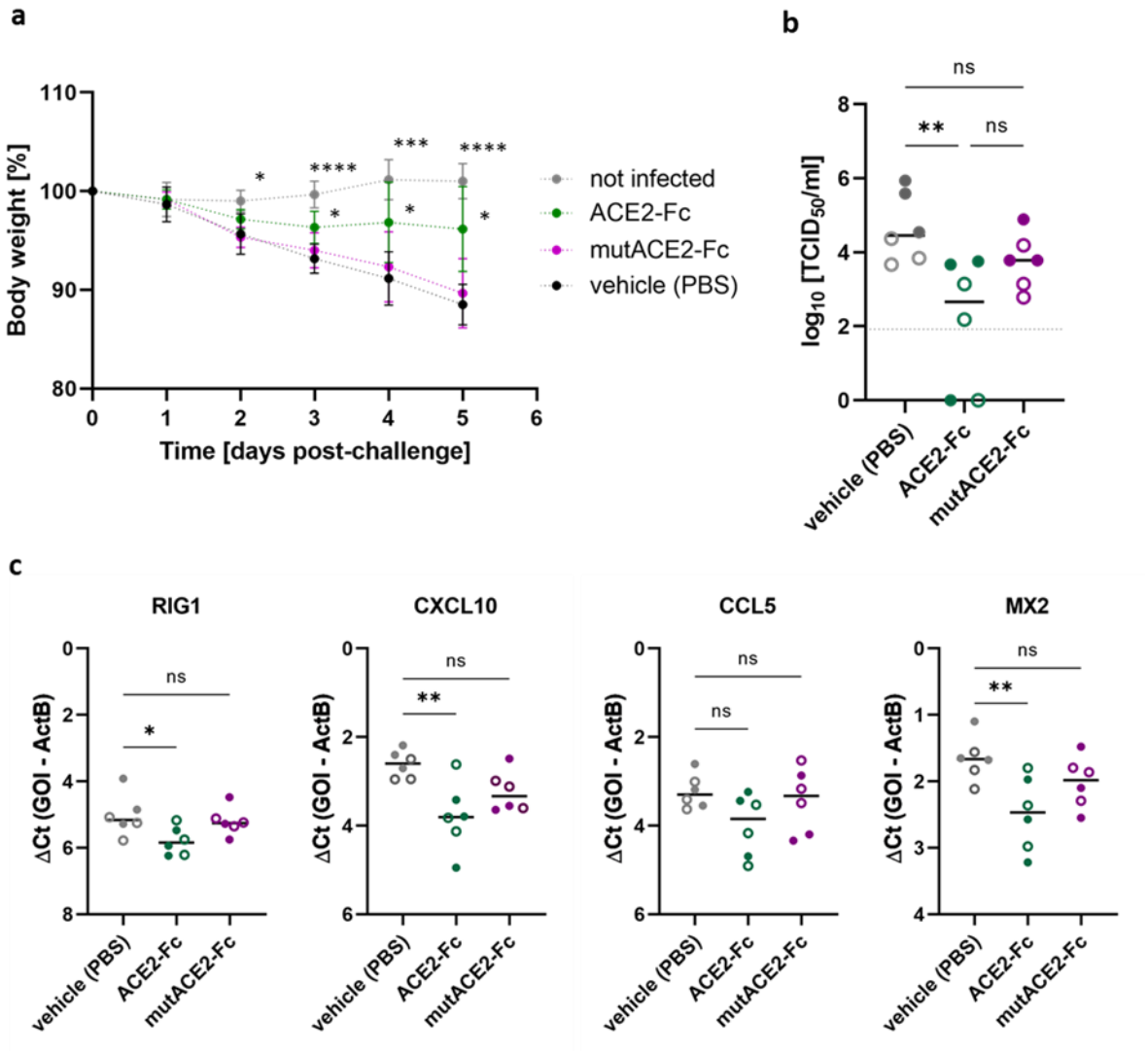

Figure 21 Intranasal application of ACE2-728H-Fc reduces body weight loss in SARS-CoV-2 infected hamsters. a) Percent of body weight relative to the day of infection. Data are shown as mean ± SD (n=6). P-values were determined by ANOVA with matched values followed by Bonferroni post hoc test. Asterisks indicate a statistically significant difference to the vehicle (PBS) treated, infected control group. b) Infectious virus titers in the lungs were compared five days post-infection and analyzed by ANOVA followed by Bonferroni post hoc test. c) Gene expression of inflammatory cytokines and chemokines in the lung tissue was quantified by RT-qPCR. Full circles represent male, empty circles female animals (n=6, n=3 for each sex). Data were analyzed using ANOVA followed by Bonferroni post hoc test. Bars represent median values. *ns = $p > 0.05$;* * $p < 0.05$; ** $p < 0.01$; *** $p < 0.001$; **** $p < 0.0001$. Adapted from Föderl-Höbenreich et al. (2025).

Strikingly, analysis of lung tissues stained for the SARS-CoV-2 nucleocapsid protein revealed a significant reduction in the number of virus-infected cells in animals that were treated with ACE2-728H-Fc. By contrast, the lung tissue of hamsters treated with mutACE2-728H-Fc

exhibited a comparable number of SARS-CoV-2-positive cells to those in the vehicle-treated group (Figure 22).

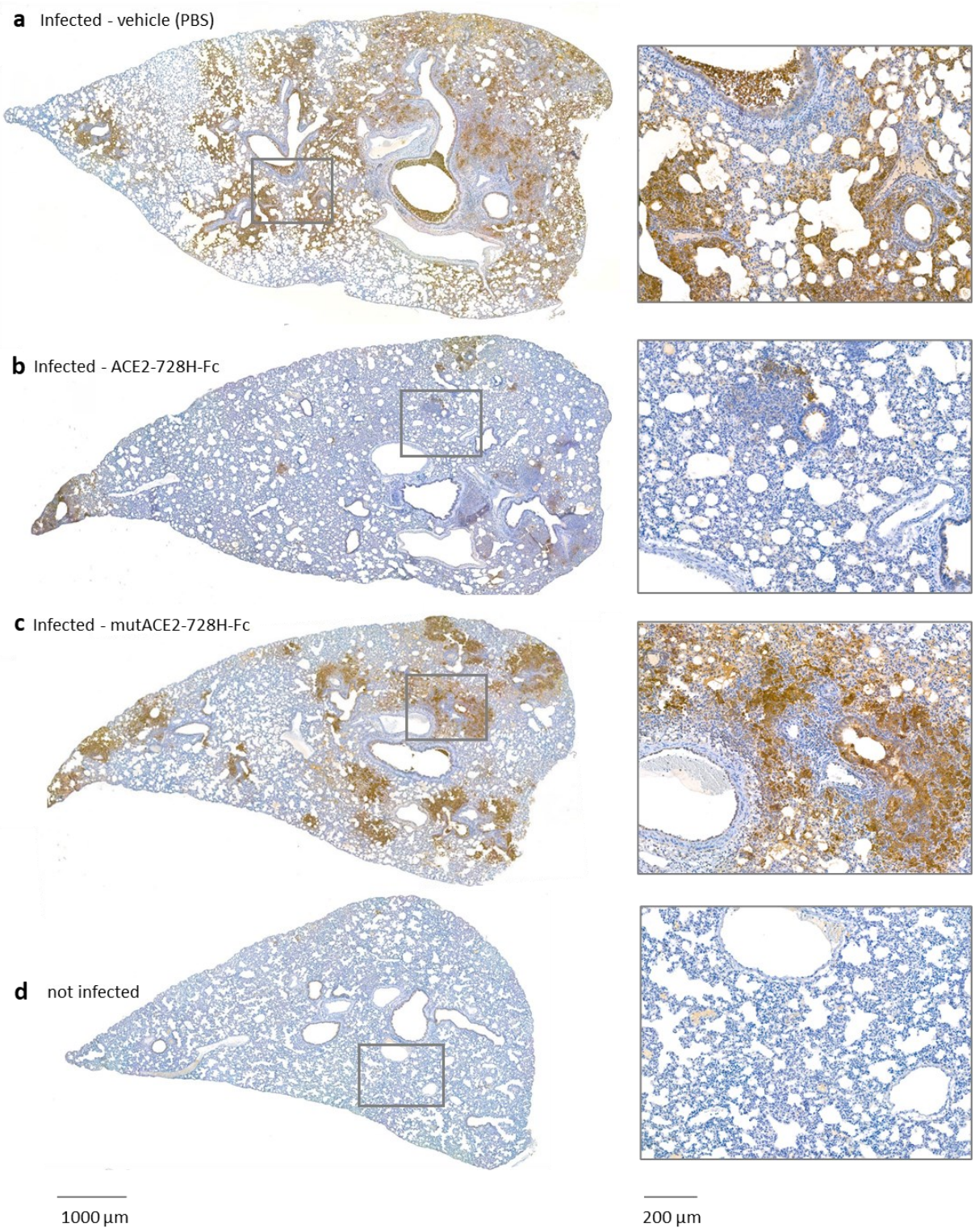

Figure 22 Intranasal administration of ACE2-728H-Fc decreases the number of infected cells in lung tissue. Representative immunohistochemical images showing SARS-CoV-2 nucleocapsid

protein in lung tissues five days post-infection, presented in two magnifications. a) infected vehicle group, b) infected ACE2-728H-Fc treated group, c) non-binding mutACE2-728H-Fc treated group and d) not infected group. Adapted from Föderl-Höbenreich et al. (2025).

3.2.6. Class-switching from IgG to IgA does not affect the neutralization activity of ACE2-728H-Fc

IgA is the main antibody class present on mucosal surfaces and is therefore adapted to the harsh environment in the upper respiratory tract. In terms of a nasal application route for future medical use of ACE2-Fc decoys, class-switching of the fused Fc domain from IgG to IgA might be advantageous in terms of degradation in the nasal cavity. We tested an ACE2-728H-Fc decoy containing an IgA Fc domain and compared the neutralization activity with that of a decoy containing an IgG Fc domain. No substantial differences were found in their neutralization activity (IC_{50} ACE2-728H-Fc (IgA): 0.30 µg/ml; IC_{50} ACE2-728H-Fc (IgG): 0.21 µg/ml).

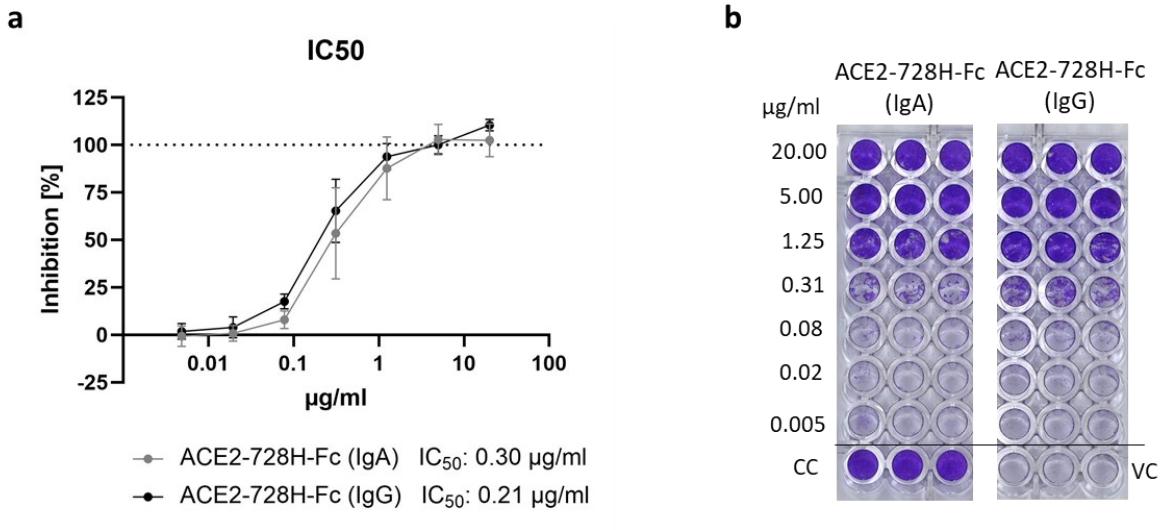

Figure 23 ACE2-728H-Fc (IgA) and ACE2-728H-Fc (IgG) have similar neutralization activity. a) IC_{50} values of ACE2-728H-Fc (IgA) and ACE2-728H-Fc (IgG) against SARS-CoV-2 (de21) were determined by CPE assays with VeroE6 cells and inhibitory dose-response curve analysis. Data are presented as arithmetic mean values ± SD of two experiments performed in triplicates. b) CPE assay plates after crystal violet staining. Violet-stained wells indicate no CPE, whereas transparent wells indicate CPE. VC: virus control, CC: cell control.

3.3. Fc-domain mediated crosstalk with hMDMs

The Fc domains of antibodies and Fc fusion proteins enable crosstalk with the innate immune system by binding to Fc receptors (FcRs). These interactions are critical for triggering effector functions such as antibody-dependent cellular phagocytosis, a process that supports the clearance of free virions or infected cells by promoting their uptake and degradation by phagocytic immune cells. In addition to engaging with FcRs (58), Fc domains can also interact with C1q, an essential component of the complement system (108).

We investigated the functional interplay between the Fc domain of ACE2-728H-Fc and FcRs using primary human monocyte-derived macrophages (hMDMs) as an *in vitro* model. Furthermore, we examined the potential role of complement factor C1q in mediating additional immune functions.

3.3.1. SARS-CoV-2 does not replicate in hMDMs

First, we tested whether SARS-CoV-2 could infect and replicate in hMDMs. Therefore, hMDMs were infected at a high MOI (2 $TCID_{50}$/cell) and intracellular virus loads were assessed over time. Additionally, a lung epithelial cell line (Calu-3), which is known to support SARS-CoV-2 propagation was infected at an MOI = 0.02 $TCID_{50}$/cell as control for replicative infection. Declining levels of intracellular SARS-CoV-2 RNA were observed in hMDMs over time, suggesting that these cells are not capable of supporting SARS-CoV-2 replication (Figure 24a). In contrast, Calu-3 cells supported the efficient replication of SARS-CoV-2, as evidenced by substantial increase in intracellular viral RNA levels (Figure 24a).

Next, we assessed the presence of intracellular viral proteins and RNA using immunofluorescent staining. Therefore, Calu-3 cells and hMDMs were infected at a MOI = 0.1 $TCID_{50}$/cell. After 24 hours, the cells were fixed and stained for the SARS-CoV-2 N protein and double-stranded RNA with antibodies. Calu-3 cells were positive for both, the N protein and double-stranded RNA, confirming viral replication. No double-stranded RNA was detected in hMDMs, which correlates with the absence of increasing viral RNA levels over time. However, positive N protein signals were detected in hMDMs, indicating attachment and/or uptake of viral particles (Figure 24b).

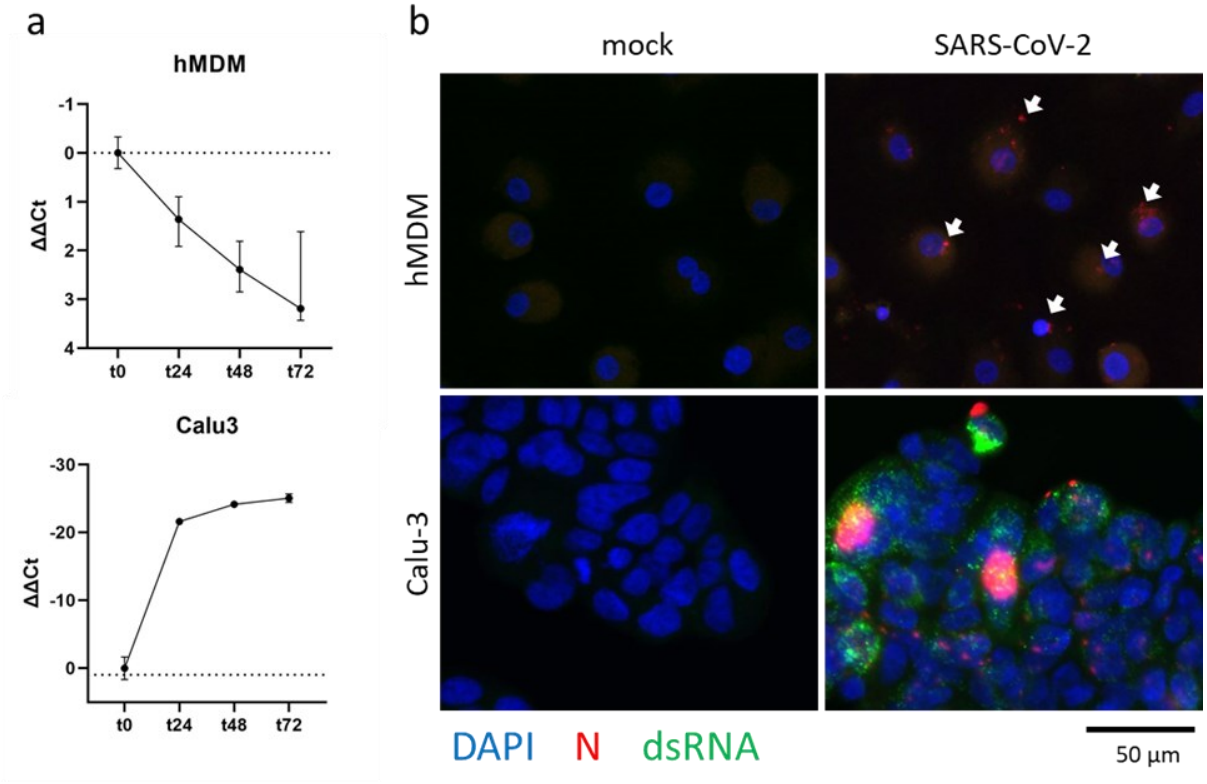

Figure 24 SARS-CoV-2 does not replicate in hMDMs. hMDMs and Calu-3 cells were infected with SARS-CoV-2. Cells were harvested 0, 24, 48 and 72 hpi. a) Intracellular virus RNA levels were quantified by ΔΔCt analysis. SARS-CoV-2 N gene was normalized to the house keeping gene HPRT1 and compared to the levels at timepoint t0. hMDMs from three different donors were infected in duplicates. Data a presented as arithmetic mean value ± SD. b) SARS-CoV-2 N protein (red) and double stranded RNA (green) were detected by immunofluorescence staining. Nuclei were stained with DAPI (blue). Arrows highlight positive N-protein signals detected in hMDMs.

As we found no evidence of SARS-CoV-2 replication in hMDMs, we examined the expression of the virus entry receptor ACE2. High levels were detected in both VeroE6 and Calu-3 cells, which are susceptible to replicative SARS-CoV-2 infection. However, ACE2 was undetectable in hMDMs from three different donors (Figure 25).

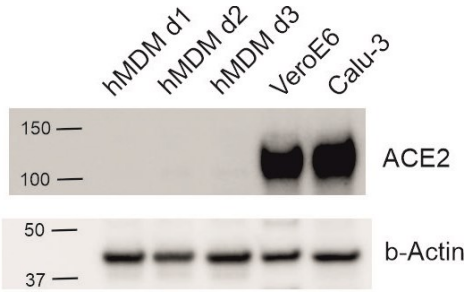

Figure 25 ACE2 expression in hMDMs, VeroE6 and Calu-3 cells. Immunoblot detecting ACE2 expression in hMDMs from three donors (hMDM d1, hMDM d2, hMDM d3), VeroE6 and Calu-3 cells. B-actin is detected as loading control.

Next, we examined whether hMDMs are stimulated upon exposure to SARS-CoV-2. hMDMs were infected at a MOI = 0.1 $TCID_{50}$/cell. After 24 hours, IFN-γ, IL-6, IL-10 and TNFα concentrations were measured in hMDM supernatants. No significant increase in pro-inflammatory cytokine release was observed following SARS-CoV-2 exposure. In contrast and as expected, treatment with 10 µg/ml LPS, induced a significant increase in TNFα levels (Figure 26).

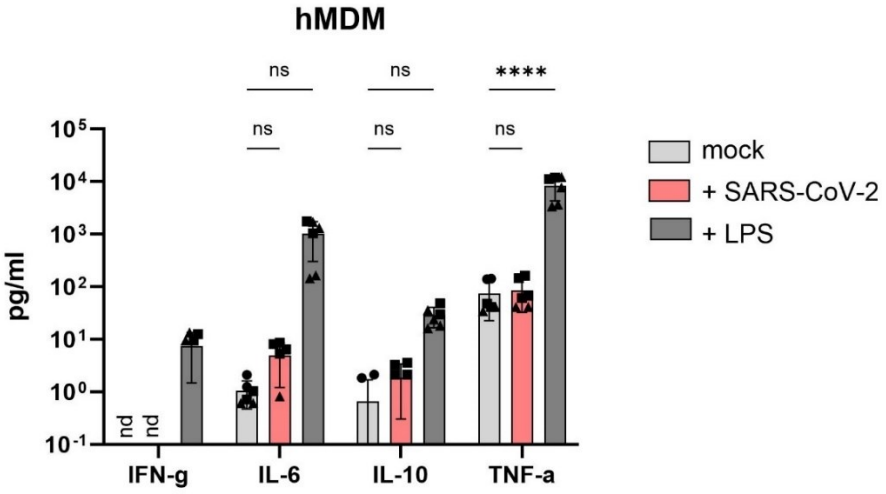

Figure 26 SARS-CoV-2 does not trigger cytokine release by hMDMs. hMDMs were infected at a MOI = 0.1 $TCID_{50}$/cell. After 24 hours, cytokine concentrations in hMDM culture supernatants were determined by Bioplex assays. Data refer to three different donors (symbol shape). Bars represent mean values ± SD. p values were determined by two-way ANOVA followed by Dunnett's post hoc test. *ns = p > 0.05; * = p 0.01–0.05; ** = p 0.001–0.01; *** = p 0.0001–0.001; **** = p ≤ 0.0001.*

3.3.2. ACE2-728H-Fc does not induce Fc-mediated enhancement of hMDM infection

Since ACE2-728H-Fc contains a human IgG1 domain, we investigated whether it could enhance the binding or uptake of SARS-CoV-2 via FcRs. To do so, hMDMs were infected in the presence of serially diluted ACE2-728H-Fc, ranging from 0.02 µg/ml to 20 µg/ml and intracellular viral RNA levels were compared to hMDMs infected in the absence of ACE2-728H-Fc. No significant changes in viral RNA levels were observed at any of the tested ACE2-728H-Fc concentrations (Figure 27). These results imply that ACE2-728H-Fc does not promote FcR-dependent enhancement of SARS-CoV-2 infection or attachment/phagocytosis.

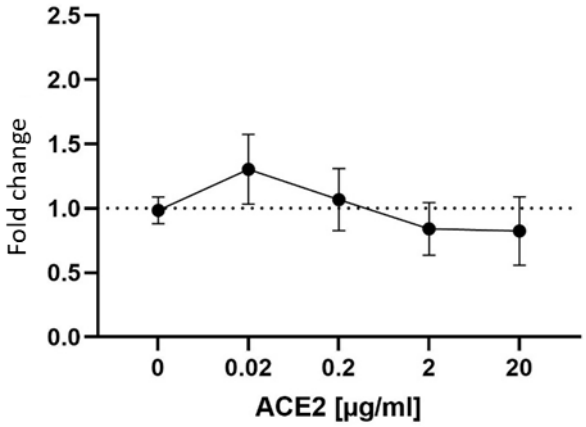

Figure 27 ACE2-Fc does not promote SARS-CoV-2 replication in hMDMs. hMDMs were infected with 4 x 10^4 $TCID_{50}$/ml (de21) in the presence of different concentrations of ACE2-728H-Fc for 24 hours. Intracellular viral RNA levels were quantified by ΔΔCt analysis. SARS-CoV-2 N gene was normalized to the house keeping gene HPRT1 and compared to infected, untreated cells. Data are presented as foldchange ($2^{\Delta\Delta Ct}$). hMDMs from three different donors were tested in duplicates. Data are presented as arithmetic mean value ± SD.

3.3.3. Crosstalk between ACE2-728H-Fc and C1q enhances attachment/uptake of SARS-CoV-2 to/by hMDMs *in vitro*

C1q is a key component of the complement system that can bind to antigen/antibody complexes by engaging with Fc domains. We therefore investigated whether adding C1q to ACE2-728H-Fc/SARS-CoV-2 complexes increases virus uptake or triggers a response in macrophages.

hMDMs were infected with SARS-CoV-2 in the presence of the following compounds: wild-type ACE2-728H-Fc (5 µg/ml), mutACE2-Fc (5 µg/ml), convalescent serum (1:50), either alone

or in combination with C1q (20 µg/ml). None of the tested compounds altered intracellular viral RNA levels in hMDMs. However, the combination of C1q with either ACE2-728H-Fc or convalescent serum significantly increased intracellular viral RNA loads by 3-fold. Conversely, the combination of C1q with mutACE2-728H-Fc did not increase viral RNA levels. We also confirmed the expression of the C1q receptor CD35 on hMDMs from three different donors by immunoblotting (Figure 28).

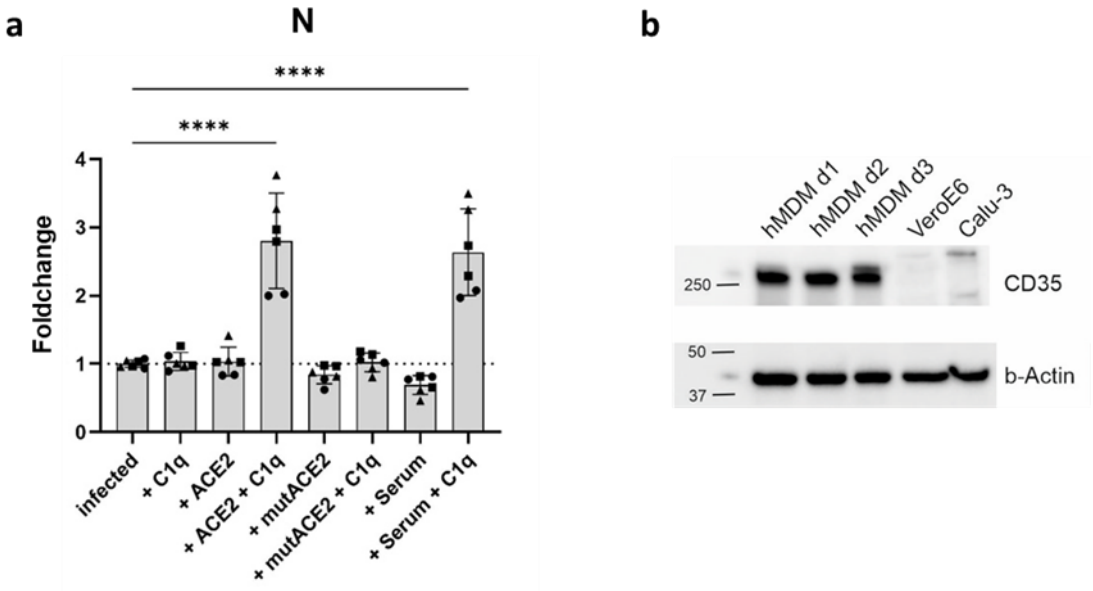

Figure 28 SARS-CoV-2 complexed with ACE-728H-Fc and C1q increases intracellular viral RNA levels in hMDMs, suggesting enhanced attachment and/or uptake. a**)** hMDMs were infected with SARS-CoV-2 in the presence of wild-type ACE2-728H-Fc (5 µg/ml), mutACE2-Fc (5 µg/ml), convalescent serum (1:50), either alone or in combination with C1q (20 µg/ml). Intracellular virus RNA levels were quantified by ΔΔCt analysis. SARS-CoV-2 N gene was normalized to the house keeping gene HPRT1 and compared to infected, untreated cells. Data are presented as fold change ($2^{\Delta\Delta Ct}$) and refer to three different donors (symbol shape). Bars represent arithmetic mean values ± SD. Right: Immunoblot detecting CD35 expression in hMDMs from three donors (hMDM d1, hMDM d2, hMDM d3), VeroE6 and Calu-3 cells. Beta-Actin (b-Actin) was used as loading control. P values were determined by one-way ANOVA followed by Dunnett's post hoc test. *ns = P > 0.05; * = P 0.01–0.05; ** = P 0.001–0.01; *** = P 0.0001–0.001; **** = P ≤ 0.0001.*

However, we found that increased attachment/phagocytosis of SARS-CoV-2/ACE2-728H-Fc/C1q complexes did not alter the expression of the pro-inflammatory genes CXCL8, TNFα and CXCL10 or release of the pro-inflammatory cytokines IL6, TNFα and IL8. This suggests that increased attachment/uptake is not accompanied by macrophage activation (Figure 29).

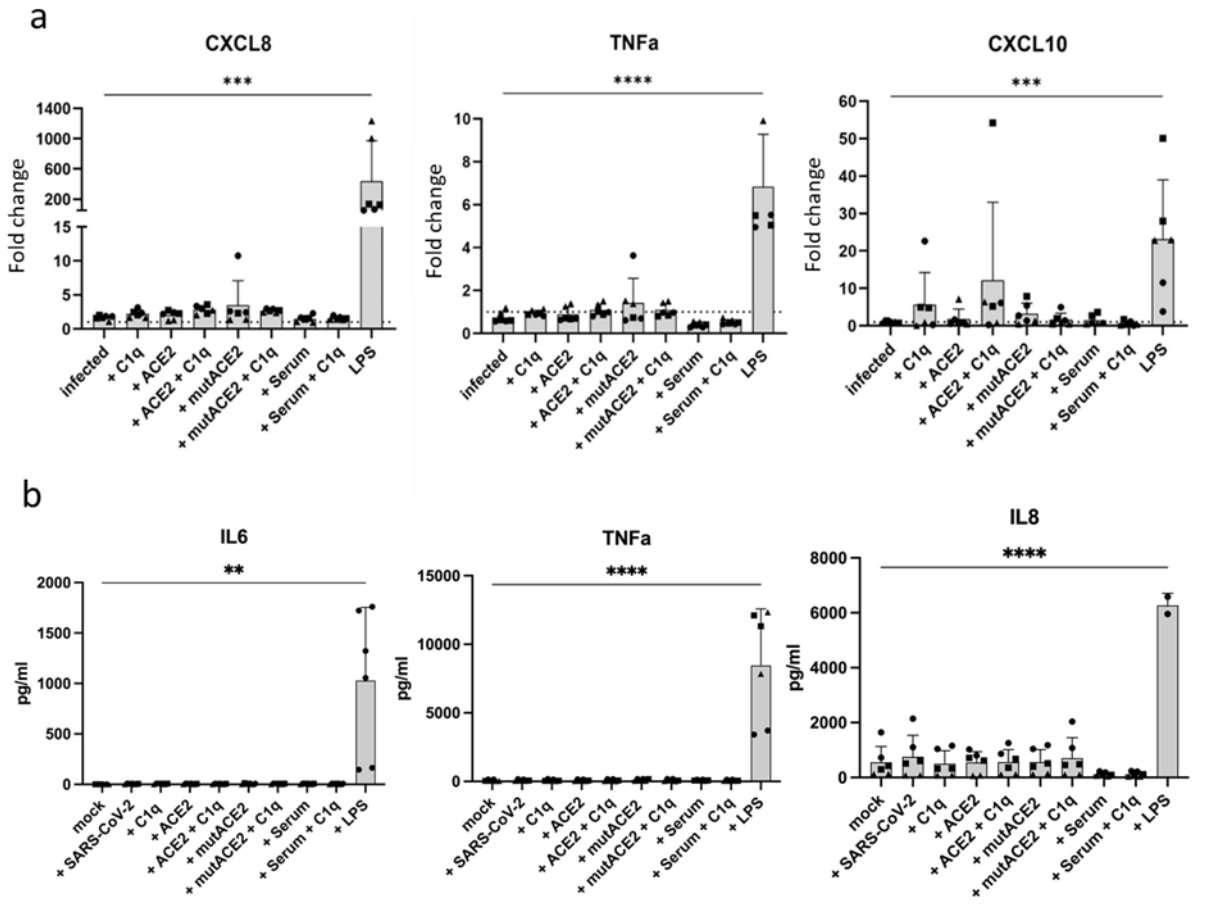

Figure 29 Increased attachment/uptake of SARS-CoV-2/ACE2-728H-Fc/C1q complexes does not enhance proinflammatory gene expression or trigger cytokine release. hMDMs were infected with SARS-CoV-2 in the presence of wild-type ACE2-728H-Fc (5 µg/ml), mutACE2-Fc (5 µg/ml), convalescent serum (1:50), either alone or in combination with C1q (20 µg/ml). a) Intracellular RNA was isolated 24 hpi and proinflammatory gene expression was quantified by RT-qPCR. Gene expression was normalized to the house keeping gene HPRT1 and compared to not infected, untreated cells. Data are presented as fold-change ($2^{\Delta\Delta Ct}$). b) Cytokine concentrations in supernatants of hMDMs were measured 24 hpi. Data refer to three different donors (symbol shape). Bars represent arithmetic mean values ± SD. p values were determined by two-way ANOVA followed by Dunnett's post hoc test. *ns = p > 0.05; * = p 0.01–0.05; ** = p 0.001–0.01; *** = p 0.0001–0.001; **** = p ≤ 0.0001.*

3.3.4. hMDMs respond to paracrine signals released by a infected lung epithelial cell line

Hyperactivated macrophages are supposed to contribute to the cytokine storm observed in severe COVID-19 cases (35). However, we found no direct activation of hMDMs by SARS-

CoV-2 (Figure 26). We hypothesized that macrophages might be activated by paracrine signals released by infected epithelial cells.

SARS-CoV-2 infection of immune-competent Calu-3 cells triggered the expression of several pro-inflammatory genes including IL-6, TNFα, CXCL10 and IFN1b and the level of gene induction correlated with the initial infectious dose (Figure 30).

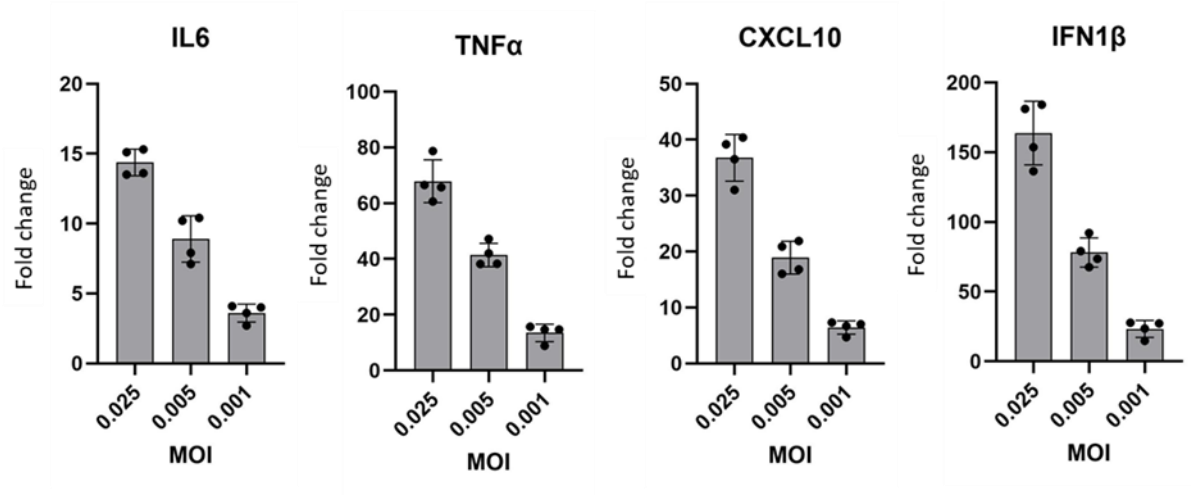

Figure 30 SARS-CoV-2 infection induces the expression of pro-inflammatory genes in Calu-3 cells. Calu-3 cells were infected at three different MOIs. Intracellular RNA was isolated 24 hpi and gene expression was quantified via RT-qPCR. Gene expression levels were normalized to the housekeeping gene GAPDH and compared to not infected cells. Data are presented as foldchange ($2^{\Delta\Delta Ct}$). Data refer to a single experiment performed in quadruplicates. Bars represent arithmetic mean values ± SD.

To simulate paracrine signalling, we prepared conditioned media using two cell lines: immune-competent Calu-3 cells and VeroE6 cells, the latter being deficient in IFN production (109,110). We hypothesized that supernatants from infected Calu-3 cells would contain not only newly released SARS-CoV-2 virions but also high levels of paracrine signals like interferons and cytokines. In contrast, supernatants from VeroE6 cells were expected to lack interferons. Conditioned media were collected 24 hpi when cell monolayers were still intact, and minimal CPE was detected, in order to limit the release of damage-associated molecular patterns. Additionally, supernatants from uninfected cells were collected to control for any secretory products that might be released independently of SARS-CoV-2 infection. A schematic illustration of the preparation of conditioned media is shown in Figure 31.

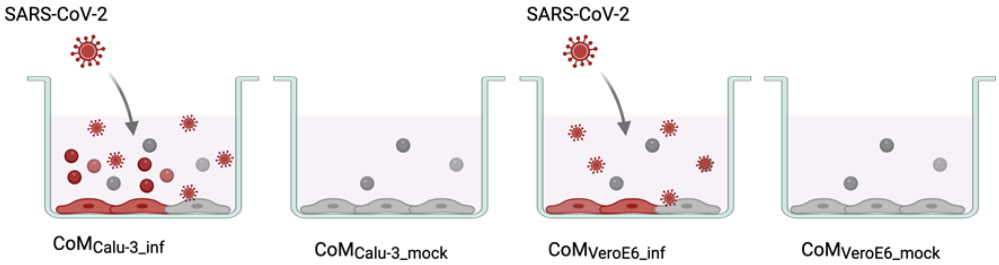

Figure 31 Preparation of conditioned media. Calu-3 cells and VeroE6 cells were mock infected (CoM_{Calu3_mock}, CoM_{VeroE6_mock}) or infected at an MOI = 0.005 (CoM_{Calu3_inf}, CoM_{VeroE6_inf}). Cell free supernatants were harvested 24 hpi. Conditioned media from infected Calu-3 cells are expected to contain not only newly released SARS-CoV-2 virions but also high levels of paracrine signals such as interferons. In contrast, VeroE6 cells, which are deficient in interferon production, are expected to release newly synthesized SARS-CoV-2 virions, but no interferons.

Next, hMDMs were treated with the different conditioned media to determine whether paracrine signals released by the infected cell lines could stimulate macrophage activation. Incubation of hMDMs with conditioned media from infected Calu-3 cells (CoM_{Calu3_inf}), significantly induced the expression of IFN-stimulated genes like IFIT1, MX1 and Siglec1. Nevertheless, inflammatory genes including TNFα, CXCL8, and CCL5 were not induced. Interestingly, treatment with conditioned media from infected VeroE6 cells (CoM_{VeroE6_inf}), induced the expression of IFN-stimulated genes in two out of five donors. Importantly, neither conditioned media from mock infected VeroE6 cells (CoM_{VeroE6_mock}) nor from mock infected Calu-3 cells (CoM_{Calu3_mock}) induced the expression of IFN-stimulated genes in hMDMs (Figure 32).

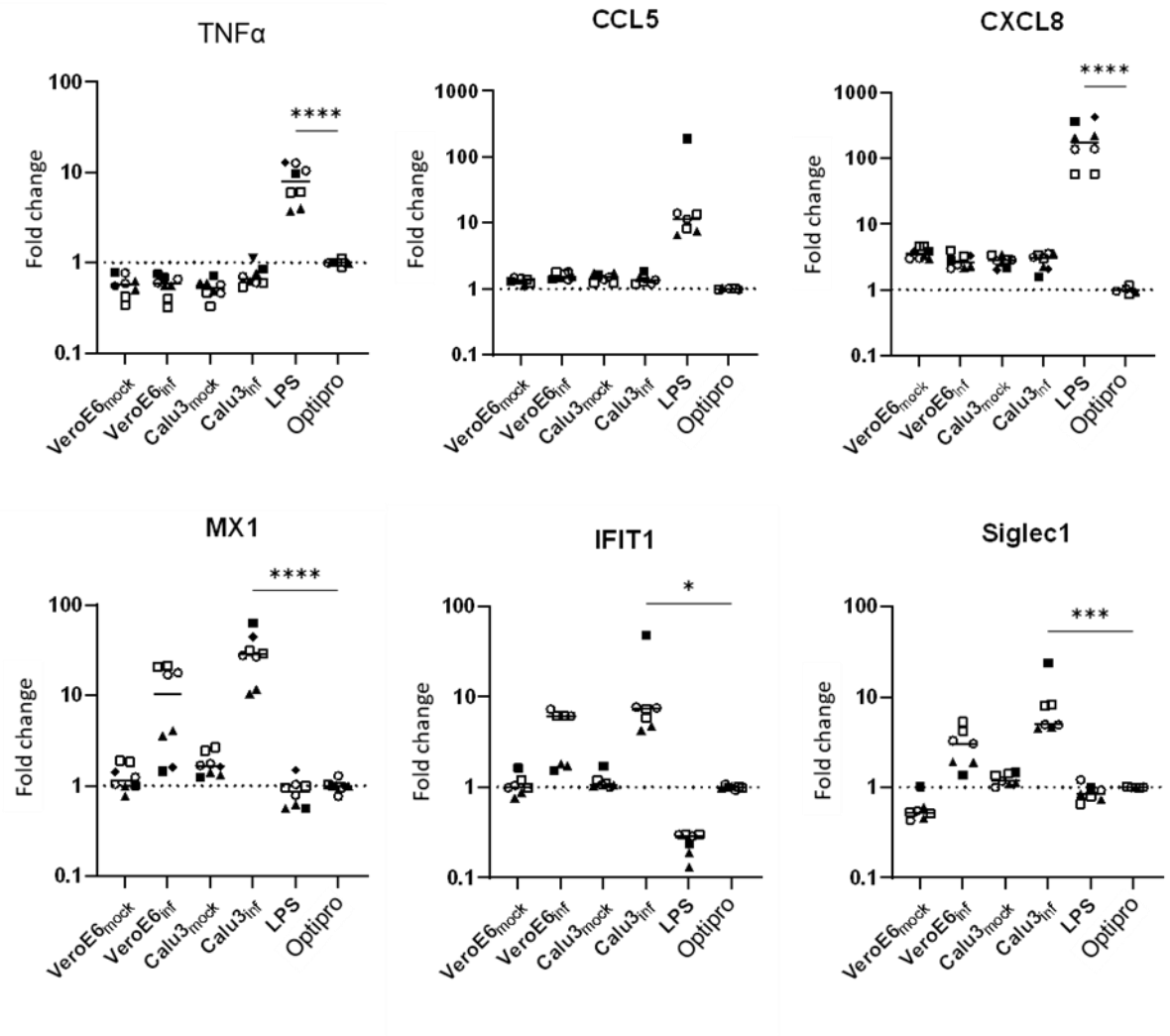

Figure 32 Conditioned media from SARS-CoV-2 infected Calu-3 cells induce expression of IFN-stimulated genes in hMDMs. hMDMs were treated with conditioned media from infected and mock infected Calu-3 and VeroE6 cells. Intracellular RNA was isolated 24 hpi and proinflammatory gene expression was quantified by RT-qPCR. Genes were normalized to the housekeeping gene HPRT1 and compared to cells treated with unconditioned Optipro SFM medium. Data are presented as fold-change ($2^{\Delta\Delta Ct}$). Data refer to five different donors (symbol shape). Bars represent median values. p values were determined by one-way ANOVA followed by Dunnett's post hoc test. *ns = p > 0.05; * = p 0.01–0.05; ** = p 0.001–0.01; *** = p 0.0001–0.001; **** = p ≤ 0.0001.*

4. Discussion

Stability of diagnostic specimens

Molecular diagnostics, particularly RT-qPCR were the gold standard for detecting SARS-CoV-2 during the COVID-19 pandemic (100). Maintaining SARS-CoV-2 RNA integrity from collection to analysis is critical, to ensure diagnostic accuracy and reliability, and to avoid false-negative results. Rapid and intensive testing played a pivotal role in revealing the dimensions of the COVID-19 pandemic, enabling governments and healthcare systems to respond effectively. Furthermore, reliable testing of SARS-CoV-2 infection is a prerequisite for specific therapies with drugs (e.g., Paxlovid), therapeutic antibodies or alternative antivirals such as ACE2 decoys.

Pre-analytical factors such as storage temperature, storage time and the choice of collection solution can directly impact the quality of the collected specimen. The World Health Organization recommends storing specimens intended for SARS-CoV-2 testing at temperatures between 2°C and 8°C (14). However, if cold-chain logistics are unavailable or overburdened, particularly during the summer months, fluctuations in temperature could affect RNA integrity. Inappropriate storage conditions could also facilitate bacterial growth and further compromise RNA integrity. Depending on their intended use, commercial swab systems are designed to maintain the viability of bacteria, viruses or fungi and usually consist of a buffered solution and a sterile swab. Sample collection systems specifically designed for viral samples (e.g., UTM, VTM) typically contain antibiotics to suppress bacterial overgrowth and protect viral RNA from degradation by bacterial nucleases.

We tested different swab systems and simulated critical pre-analytical factors including storage time and temperature and monitored the detectability of SARS-CoV-2 by RT-qPCR. Our data show that the choice of the swab system, in combination with sub-optimal storage conditions has significant impact on downstream diagnostic performance. However, since we used a sterile spike matrix, it is not possible to draw conclusions regarding the impact of bacterial contaminations on the stability of SARS-CoV-2 RNA.

Although RT-qPCR is considered the gold standard in SARS-CoV-2 diagnostics, it presents several challenges. The method requires trained personnel, is both time-intensive and costly, and demands specialized equipment. To address these limitations, rapid antigen diagnostic tests, such as lateral flow assays, have been developed. These assays are relatively cheap, provide results within minutes and are also intended for home use. However, they have a lower diagnostic sensitivity (111,112) and improper sampling by untrained individuals may

compromise the reliability of the test. However, rapid antigen tests served as a crucial complement to RT-qPCR, enabling broader testing coverage and a quicker response in pandemic management.

Advantage of ACE2 decoys versus monoclonal antibody therapies

Within months after the start of the pandemic, multiple vaccines, small-molecule antiviral drugs, and monoclonal antibodies (mAbs) had been authorized for emergency use (74). However, the rapid evolution of SARS-CoV-2 posed significant challenges to the efficacy and sustainability of these therapies (113,114). The virus's mutation rate, driven by selective pressure, replication errors, and occasional recombination events has led to changes in epitopes targeted by antibodies and rendered many of them ineffective (7,113). Several first-generation mAbs had to be withdrawn from clinical use because they were ineffective against newer VOCs (74). The rapid evolution of the virus has outpaced the development of new mAbs. This time lag poses a fundamental challenge, as the process of developing, testing and approving mAbs is much slower than the evolution of SARS-CoV-2 variants. These limitations highlight the need for more robust antiviral therapies.

Mutations enhancing the binding affinity to the host cell receptor ACE2 increase viral infectivity and transmission and play a crucial role in the emergence of new variants (115). Because an increased affinity for host cell ACE2 also implies an increased affinity for ACE2-based decoys (76,116), the neutralizing capacity of ACE2-based decoys is largely unaffected by viral escape mechanisms.

We demonstrated the robustness of an ACE2-Fc decoy against recent VOCs and found that it exhibited increased neutralization activity against later variants compared to the ancestral SARS-CoV-2 (Figure 17). The enhanced neutralization activity of several ACE2-based decoys against VOCs has also been reported by others (117–119). However, sera from convalescent COVID-19 patients showed reduced neutralizing activity against Omicron variants, in line with previous studies (120,121).

Enzymatic activity of ACE2 decoys

ACE2 is not only the SARS-CoV-2 entry receptor but also a key regulator of the renin-angiotensin system (RAS), which regulates blood pressure, fluid balance and cardiovascular function. ACE2 targets angiotensin II (Ang II) and converts it into the heptapeptide Ang 1-7, which in turn has vasodilatory, anti-inflammatory and antifibrotic properties. In the context of COVID-19, elevated levels of Ang II have been observed in plasma samples from patients and have been found to correlated with disease severity (122).

It has been demonstrated that ACE2 expression is reduced as a result of its interaction with the SARS-CoV-2 spike protein. This leads to an imbalance between Ang II and Ang 1-7 resulting in an accumulation of Ang II (123,124). Ang II promotes the recruitment of macrophages and their polarisation towards a pro-inflammatory M1 phenotype, thereby supporting the development of ARDS and associated organ damage (125).

A meta-analysis of sixteen randomized controlled trials evaluated the effects of RAS blockers in COVID-19 patients and found no evidence of a beneficial effects (126). There are also concerns about the safety of RAS inhibitors due to their potential to increase ACE2 expression, which could theoretically enhance infection (126). While studies have not conclusively demonstrated that RAS inhibitors worsen the outcomes of patients with SARS-CoV-2 infection, this remains a cause for concern.

Soluble ACE2 decoys, on the other hand, can be expressed in enzymatically active forms and do not affect ACE2 expression on host cells. Therefore, in addition to their virus neutralization activity, they could be a safe option to counteract SARS-CoV-2-induced downregulation of cellular ACE2 and restore the conversion of Ang II to Ang 1-7.

ACE2 in clinical trials

Human recombinant soluble ACE2 (hrsACE2) has already been tested in clinical trials. A Phase 1 clinical trial (NCT00886353) proved the tolerance and safety of intravenously administered hrsACE2 in healthy volunteers (79). In a randomized, double-blinded Phase 2 clinical trial (NCT04335136), 88 COVID-19 patients were treated intravenously with hrsACE2 twice daily. Although fewer deaths were observed in the intervention group compared to the placebo group, the difference was not significant. The half-life for intravenously administered hrsACE2 is ten hours (79), suggesting that systemic delivery might be suboptimal. A phase 1 dose-escalation study (NCT05065645) demonstrated that administration by inhalation, achieved high local ACE2 concentrations in the lung and could increase the plasma half-life to up to 52 hours (127). Further, a pharmacokinetic study in mice showed that fusion of an IgG Fc-domain to ACE2 greatly extended the half-life from 8.5 hours to 29.2 hours when administered intraperitoneally (128).

These data indicate that delivering hrsACE2 as an Fc-fusion protein via inhalation could significantly enhance the therapeutic efficacy of ACE2-based decoys, thereby increasing their clinical applicability. Furthermore, targeted optimization of post-translational modifications of the ACE2-decoy, could further enhance its performance. Both, ACE2 and the SARS-CoV-2 spike protein, are extensively glycosylated, which shields large parts of the surface area

(129,130). Hence, engineering the glycan patterns on ACE2, can improve its binding affinity to the RBD of the virus, further increasing its therapeutic potential.

Modification of ACE2 glycosylation by site-directed mutagenesis

Human ACE2 has seven N-glycosylation sites (N53, N90, N103, N322, N432, N546, and N690) (101), which mainly contain complex-type glycans with terminal sialic acid residues (22). Molecular dynamics simulations suggest that glycosylation and sialylation have a critical impact on the binding affinity between ACE2 and the RBD of the spike protein of SARS-CoV-2 (77).

We therefore examined the neutralization activity of ACE2-Fc constructs with modified glycosylation patterns that were predicted to enhance affinity for the viral RBD. We found that removal of the N-glycosylation site at position N90 increased the neutralizing activity of ACE2-Fc to a similar extent as complete enzymatic deglycosylation. This suggests that removal of the N90 glycan is primarily responsible for the enhanced neutralizing activity, which is consistent with previous studies (129) (131). While ACE2 variants with mutated N-glycosylation sites had increased neutralization capacities, enzymatic removal may be preferable, as glycosylation is essential for proper protein folding during biosynthesis. Furthermore, introducing non-natural mutations potentially increases the immunogenicity of ACE2-Fc.

Modification of ACE2 glycosylation by changing the expression system

In order to address the challenges of pandemic preparedness, the establishment of flexible and scalable production systems capable of meeting the global demand for recombinant proteins such as ACE2-Fc is essential. Recombinant proteins are vital not only for therapeutic treatment but also for diagnostic assays and test kits to screen for novel antiviral substances.

Plant molecular pharming has been established as efficient platform for producing pharmaceutical proteins. Using plants as expression system has several advantages compared to mammalian cell lines that are nowadays commonly used in the biopharmaceutical industry. Firstly, plant molecular pharming enables the rapid, large-scale production of recombinant proteins (132). Secondly, the production costs of plant biopharming processes are typically around 0.1 % of those associated with mammalian cell-based technologies (133). Furthermore, human pathogens are unable to replicate in plants, significantly mitigating safety risks associated with contaminations (134).

Expression systems that are commonly used for the production of recombinant protein therapeutics include mammalian cell lines, such as Chinese hamster ovary (CHO) cells and human embryonic kidney (HEK293) cells. Although those systems are well established and frequently used by industry, the biosynthesis of tailored post-translational modifications including glycosylation remains challenging in these systems. This is because mammalian cells produce heterogeneous N-glycans, which complicates product characterization (135,136). By contrast, plants produce more homogeneous N-glycans. However, these N-glycans typically contain β1,2-xylose and core α1,3-fucose residues, which are absent on mammalian N-glycans. Eliminating the endogenous beta 1,2-xylosyltransferase and alpha 1,3-fucosyltransferase activities in plants prevents the formation of potentially immunogenic plant-specific post-translational modifications. This enables the production of therapeutic proteins with “humanized” post-translational modifications in plants (89).

Castilho et al. demonstrated that ACE2-Fc can be expressed efficiently in such glycoengineered *N. benthamiana* plants, and that it is mainly decorated with human-type N-glycans (93). Given that glycosylation patterns influence the binding affinity of ACE2 to the viral RBD, we compared the neutralization activity of sequence-identical ACE2-Fc decoys expressed in both HEK293 cells and in glycoengineered *N. benthamiana.* We found that there was no significant difference in the neutralization activity of the two constructs (Figure 8), which is consistent with the observation of Castilho et al. (93).

Modification of ACE2 – optimization of the sequence for the expression in plants

A previous study reported, that the hinge region of mAbs is susceptible to proteolytic attack by endogenous proteases when produced in *N. benthamiana* (137). To reduce proteolytic degradation, we tested a synthetic linker, which is considered to be more resistant to proteolytic cleavage, to connect the Fc and ACE2 domains. Although, substituting the hinge region with a synthetic linker reduced proteolytic cleavage, a significant proportion of the protein was still degraded. As the hinge region occurs naturally in humans, it is less likely to provoke immunogenic reactions. For this reason, it was selected as linker sequence connecting the ACE2 and Fc domain.

ACE2-615-Fc consists of a truncated ACE2 ectodomain (amino acids 18-615), that lacks the collectrin-like domain. We hypothesized that expressing the full-length ACE2 ectodomain (amino acids 18 – 740) would enhance resistance to proteolytic cleavage. Our findings revealed that the full-length ACE2-740-Fc decoy exhibited greater resistance to proteolytic fragmentation *in N.benthamiana* and furthermore had enhanced neutralization activity (Figure 9). These findings align with the results by Torchia et al., who showed that the collectrin-like

domain enhances the affinity for the viral S protein and is essential for the *in vivo* activity of ACE2-Fc (138).

We investigated the differences in post-translational modifications of ACE2-740H-Fc when expressed in glycoengineered plants versus human HEK293 cells. We found that the hinge region and parts of the ACE2 domain undergo undesirable non-human post-translational modifications (Figure 10). To address this issue, we developed a modified ACE2-Fc decoy (ACE2-728H-Fc), that lacks several proline residues that are hydroxylated when the protein is expressed in *N. benthamiana*, but not in HEK293 cells. These hydroxyproline residues are subject to plant-specific O-glycosylation, which introduces heterogeneity and could contribute to immunogenicity (139). Furthermore, we removed an unpaired cysteine residue in the hinge region to reduce the tendency towards higher oligomer formation. Overall, we have designed an ACE2 decoy with superior biochemical and biophysical properties compared to the canonical variant, ACE2-740H-Fc (95).

Antiviral activity of ACE2-Fc *in vivo*

The next step was to examine the *in vivo* efficacy of the optimized ACE2-728H-Fc variant in a golden Syrian hamster model. Syrian hamsters are considered an appropriate small animal model for studying SARS-CoV-2 infection due to their natural susceptibility to SARS-CoV-2 (62). Syrian hamsters develop a lung pathology that closely resembles human COVID-19 pneumonia, accompanied by moderate weight loss, which is a key indicator of disease severity (69,70). However, more recent variants, such as Omicron, typically do not cause significant weight loss in hamsters (71). For this reason, we utilized an ancestral variant of the virus to facilitate phenotypic monitoring. Notably, ACE2-Fc was shown to neutralize a wide range of VOCs, including Omicron variants, *in vitro* (Figure 17). This indicates that the *in vivo* results are relevant to both current and emerging VOCs.

Several other groups have explored the concept of soluble ACE2 decoys in hamsters, using different decoy designs and experimental protocols (117,138,140–145). Most studies administered ACE2 decoys between two and twelve hpi, thus focusing on the early stage of infection (138,140,141,143). In our study the first dose of ACE2-728H-Fc was administered 24 hpi, when disease progression and viral replication were already advanced.

Daily intranasal administration of 250 µg ACE2-Fc significantly reduced SARS-CoV-2 replication, weight loss, and lung infection, although it did not prevent lung damage and edema. Similarly, Liu and colleagues (142) reported a 3-log10 reduction in lung viral titers and a 4 % decrease in body weight loss in hamsters treated with a daily lung-delivered dose of 4 mg/kg

of HH-120 (a mixture of pentameric and hexameric ACE2-Fc). These findings are consistent with our results, which showed a 2-log10 reduction in lung virus loads and an 8 % decrease in body weight loss with a daily intranasal application of 2.5 mg/kg of ACE2-Fc (Figure 21).

ACE2-Fc comprises a human IgG1 Fc-domain, that can be recognized by FcRs on immune cells, triggering FcR functions that contribute to virus clearance (58). Interestingly, Clark et al. found evidence that non-binding antibodies can protect mice through Fc-mediated interaction with immune cells and the complement system (146). Torchia et. al observed that ACE2-Fc decoys capable of inducing FcR functions provided greater therapeutic benefits in mice than those with impaired FcR binding capability (138). Furthermore, Chen and colleagues enhanced the *in vivo* efficacy of an ACE2-Fc decoy by introducing a mutation to the Fc-domain that increased its affinity for FcRs (147). Taken together, these data suggest that, in addition to extending the half-life, the Fc domain exerts positive effects by inducing FcR functions. However, concerns about the potential side effects of therapeutically administered Fc-fusion proteins remain a topic of ongoing debate (148,149).

To address this issue, we generated a mutated ACE2-Fc decoy (mutACE2-728H-Fc), which is designed to prevent binding to SARS-CoV-2. This allowed us to control for non-specific binding and Fc domain-induced effects *in vivo*. Specifically, eight mutations were introduced into the RBD-binding region of human ACE2 based on the sequence of murine ACE2, given that mice are known to be resistant to infection by ancestral SARS-CoV-2 (62). We used mutACE2-728H-Fc as an *in vivo* isotype control to demonstrate the specific mode of action of ACE2-728H-Fc in hamsters. However, the applicability of mutACE2-Fc may be limited to studies using the Wuhan variant and early VOCs, such as Delta, since recent studies have shown that Omicron variants have acquired the ability to infect mice (64,150). This is consistent with the observation that mutACE2-728H-Fc can neutralize the Omicron strains om21 and om23 used in our study (Figure 18). Importantly, mutACE2-728H-Fc maintained its enzymatic activity (95). However, no significant differences were observed between the sham-treated and mutACE2-728H-Fc-treated animals, indicating that the effects observed in the group treated with wild-type ACE2-728H-Fc are exclusively attributed to the virus-neutralization activity of the protein. Although FcRs share a high degree of sequence homology (151), it is important to consider that ACE2-728H-Fc comprises a human IgG1 domain. Species mismatching with hamster FcRs could compromise Fc-domain mediated functions.

Class switching of the Fc-domain to IgA

The choice of the Fc domain in antiviral decoys is a critical factor influencing their functionality, pharmacokinetics and interaction with immune components. The Fc domain of IgG, the most

abundant antibody class in serum, is commonly used in recombinant proteins due to its robust Fc-mediated effector functions and long systemic half-life. However, the predominant antibody class found in secretory glands and mucosal tissues is IgA, which primarily neutralizes pathogens through immune exclusion by binding to and entrapping them. Another unique feature of IgA is its ability to neutralize viruses when it transits through infected epithelial cells. Additionally, IgA can modulate inflammatory responses by interacting with CD89 (152).

When considering nasal delivery and mucosal immunity, substituting the IgG Fc domain with that of IgA could present compelling advantages. For example, it has been demonstrated that monoclonal IgA antibodies with a secretory component are more stable in saliva than their IgG counterparts (153).

Class switching from IgG-Fc to IgA-Fc represents a promising avenue for future drug development, as IgA is reported to have prolonged retention in the nasal cavity and lungs, potentially improving drug pharmacokinetics and local efficacy. Ejemel et al. reported that isotype switching of a monoclonal antibody from IgG to IgA results in enhanced neutralization activity against SARS-CoV-2 (154). However, this effect was not observed with ACE2-728H-Fc, for which class switching from IgG to IgA had no impact on the *in vitro* neutralization activity (Figure 23).

Interaction of SARS-CoV-2 with hMDMs

Although SARS-CoV-2-positive macrophages were detected in lung autopsies and bronchial lavage fluid from COVID-19 patients (155,156) we found no evidence of virus replication in hMDMs *in vitro* (Figure 24), consistent with other studies (157–159).

Although we found no evidence for viral replication, we detected virus-positive foci in hMDMs, indicating either viral attachment to the cell surface or phagocytosis (Figure 24). Notably, we found no evidence for macrophage activation in response to SARS-CoV-2 exposure (Figure 26). This observation aligns with the hypothesis proposed by Labzin et al., which posits that active replication of SARS-CoV-2 is a prerequisite for effective viral sensing and subsequent cytokine release (157).

The resistance of hMDMs to replicative SARS-CoV-2 infection *in vitro* suggests that macrophages may indirectly take up virions *in vivo*, either through phagocytosis of infected cells or via mechanisms mediated by antibodies or components of the complement system.

ACE2-Fc – Crosstalk with hMDMs

The Fc-domain in ACE2-728H-Fc enables interaction with various components of the immune system. Firstly, the Fc domain binds to FcRs expressed on hMDMs, which could facilitate the uptake of virus particles complexed with ACE2-728H-Fc (148). Secondly, the Fc domain can bind to the complement factor C1q, which interacts with C1q receptors expressed on a wide range of cells and potentially modulates cellular responses (160). Additionally, C1q can bind directly to the RBD of SARS-CoV-2 (161). Figure 33 shows possible interactions of ACE2-Fc and C1q with receptors expressed on hMDMs.

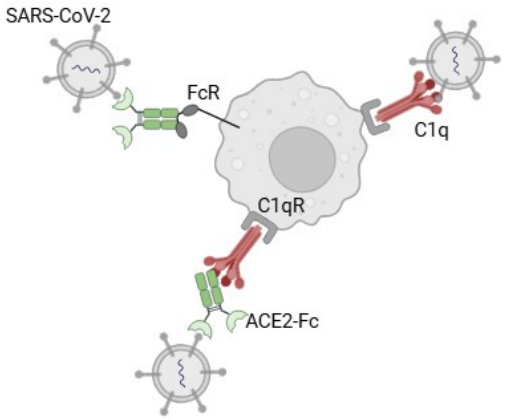

Figure 33 Potential crosstalk of ACE2-Fc and the immune system.

Despite potential beneficial effects conferred by the Fc domain, FcR-mediated uptake of ACE2-Fc or antibody-coated virus into immune cells may carry the risk of enhancing infection. This phenomenon is known as antibody-dependent enhancement (ADE) and was described for several viruses including dengue (162), but also for Betacoronaviruses like MERS (163) and SARS-CoV-1 (164,165). However, the role of ADE in COVID-19 remains a subject of controversy, with conflicting findings. While a study by García-Nicolás et al. found no evidence for ADE (166), others reported increased infection mediated by convalescent serum or monoclonal antibodies (54,56,167).

Since macrophages naturally express FcR on their surface, we investigated whether SARS-CoV-2/ACE2-728H-Fc complexes enable replicative infection of hMDMs via FcR–Fc domain interactions. RT-qPCR revealed no evidence for increased virus uptake or replication.

Okuya et al. observed C1q-dependent ADE in addition to FcR-dependent ADE by convalescent antibodies (56). As C1q can interact with the Fc domain of ACE2-728H-Fc, we investigated whether this interaction impacts viral uptake or supports ADE. Adding C1q to the SARS-CoV-2/ACE2-728H-Fc complex, resulted in a significant increase in intracellular viral RNA levels in hMDMs was observed (Figure 28). This may be clinically relevant, since

receptors for C1q are expressed on various cell types and increased levels of C1q have been detected in COVID-19 lungs (50,168). Nevertheless, we found no evidence that the increased binding of the SARS-CoV-2/ACE2-728H-Fc/C1q complex triggers cytokine release in hMDMs. Further investigations are needed to determine whether the reported 3-fold increase in viral RNA loads is due to enhanced attachment and phagocytosis, or occasional replicative infection of hMDMs.

Macrophages are considered a key source of proinflammatory cytokines and their hyperactivation has been associated with the development of ARDS (40). Given that hMDMs were neither directly activated by SARS-CoV-2 nor indirectly activated via FcR or C1qR, we hypothesized that hMDMs might respond to paracrine signals released from epithelial cells. Indeed, incubation of hMDMs with conditioned media (CoM) from infected Calu-3 cells induced the expression of IFN-stimulated genes, which is in line with previously published data (158). However, the expression of pro-inflammatory genes such as TNFα, CXCL8 and CCL5 was not induced. Interestingly, García-Nicolás and colleagues demonstrated that phagocytosis of SARS-CoV-2 infected cells triggered the secretion of IL-6 and TNFα in hMDMs, a response that was further enhanced in the presence of plasmacytoid dendritic cells (169).

Zheng et. al reported a direct induction of proinflammatory genes by SARS-CoV-2, which contradicts our observations (170). However, the virus stock used in that study was prepared in Calu-3 2B4 cells, which is an immune-competent cell line. Therefore, the observed effects may have been induced by signals released from the cells used for virus propagation. This observation is important for virus stock preparations, as contamination with IFNs makes it difficult to distinguish between virus-induced effects and paracrine effects triggered by signals released from the cell line used for virus propagation.

Nevertheless, we observed an induction of IFN-stimulated genes in two out of five donors when hMDMs were treated with CoM from infected VeroE6 cells that was supposed to be free of type I IFNs. A recent study demonstrated that re-stimulation of hMDMs isolated from convalescent patients who had previously experienced mild COVID-19 led to an exaggerated expression of multiple IFN-stimulated genes (171). Similar findings were reported in airway-resident macrophages from mice previously infected with SARS-CoV-2, where poly(I:C) and LPS triggered a hyper-induction of IFN-stimulated genes (172). We hypothesize that a preceding SARS-CoV-2 infection of donors might explain the induction of IFN-stimulated genes in hMDMs upon treatment with CoM from infected VeroE6 cells.

Limitations of the study

This study has several limitations that should be addressed in future research.

- Unfractionated ACE2-728H-Fc containing different multimeric forms of the protein was used in both *in vivo* and *in vitro* experiments. This may have introduced variability to the results. The experiments might be repeated with purified dimeric ACE2-728H-Fc to confirm the findings.
- No pharmacokinetic data were collected during the *in vivo* experiment. The half-life of ACE2-728H-Fc in lung tissue following intranasal application should be determined, along with the Ang II/Ang 1-7 ratios.
- For future experiments, an ACE2-728H-Fc construct with abrogated FcR binding capacity would be advantageous to further investigate the effects mediated by the Fc domain.
- The antibody-dependent enhancement assay in the hMDM model lacked a positive control, which limits the ability to fully validate the assay and interpret the absence of ADE in our experiments.
- The conditioned media produced to study paracrine signalling were not further characterized.
- hMDM donors were characterized only by their date of collection, with no detailed patient history available. The absence of donor-specific information, particularly regarding recent SARS-CoV-2 infections, limits the interpretation of the results.

Outlook

- Future research could focus on further optimization of ACE2-728H-Fc to enhance its therapeutic potential and pharmacokinetics. Class switching from IgG-Fc to IgA-Fc presents a promising avenue, as IgA is reported to have prolonged retention in the nasal cavity and lungs, potentially improving drug pharmacokinetics and local efficacy. Therefore, it should be explored whether replacing the IgG-Fc domain with the IgA-Fc domain could enhance retention times in the respiratory tract. Pharmacokinetic studies should also include monitoring of Ang II and Ang 1-7 levels to analyse the impact of the enzymatic activity of the ACE2 domain on the renin-angiotensin system.
- Co-housing experiments could provide valuable insights into the efficacy of preventive application of ACE2-728H-Fc by assessing its ability to limit viral transmission.
- Additional studies on interactions with the complement system are necessary, with a particular focus on the potential formation of the membrane attack complex in the

presence of complement convertases. Further investigations are needed to determine whether the observed increase of viral RNA levels in hMDMs results from enhanced attachment and phagocytosis or occasional replicative infection.

These studies will be essential to fully understand the mechanisms underlying ACE2-728H-Fc activity and to refine its design for both therapeutic and prophylactic applications.

References

1. Piret J, Boivin G. Pandemics Throughout History. Front Microbiol. 2021 Jan 15;11:988058.
2. Parvez MK, Parveen S. Evolution and Emergence of Pathogenic Viruses: Past, Present, and Future. Intervirology. 2017 Aug 4;60(1–2):1–7.
3. Reid AH, Taubenberger JK, Fanning TG. Evidence of an absence: the genetic origins of the 1918 pandemic influenza virus. Nat Rev Microbiol. 2004 Nov;2(11):909–14.
4. Ye ZW, Yuan S, Yuen KS, Fung SY, Chan CP, Jin DY. Zoonotic origins of human coronaviruses. Int J Biol Sci. 2020 Mar 3;16(10):1686–97.
5. Zhou P, Shi ZL. SARS-CoV-2 spillover events. Science (1979). 2021 Jan 8;371(6525):120–2.
6. Parra-Lucares A, Segura P, Rojas V, Pumarino C, Saint-Pierre G, Toro L. Emergence of SARS-CoV-2 Variants in the World: How Could This Happen? Life. 2022 Jan 28;12(2):194.
7. Markov P V., Ghafari M, Beer M, Lythgoe K, Simmonds P, Stilianakis NI, et al. The evolution of SARS-CoV-2. Nat Rev Microbiol. 2023 Jun 5;21(6):361–79.
8. Ozono S, Zhang Y, Ode H, Sano K, Tan TS, Imai K, et al. SARS-CoV-2 D614G spike mutation increases entry efficiency with enhanced ACE2-binding affinity. Nat Commun. 2021 Feb 8;12(1):848.
9. Barton MI, MacGowan SA, Kutuzov MA, Dushek O, Barton GJ, van der Merwe PA. Effects of common mutations in the SARS-CoV-2 Spike RBD and its ligand, the human ACE2 receptor on binding affinity and kinetics. Elife. 2021 Aug 26;10:e70658.
10. World Health Organization. Recommendations for national SARS-CoV-2 testing strategies and diagnostic capacities [Internet]. 2021 [cited 2025 May 23].

Available from: https://iris.who.int/bitstream/handle/10665/342002/WHO-2019-nCoV-lab-testing-2021.1-eng.pdf?sequence=1

11. Smith-Jeffcoat SE, Mellis AM, Grijalva CG, Talbot HK, Schmitz J, Lutrick K, et al. SARS-CoV-2 Viral Shedding and Rapid Antigen Test Performance — Respiratory Virus Transmission Network, November 2022–May 2023. MMWR Morb Mortal Wkly Rep. 2024 Apr 25;73(16):365–71.

12. Chheda U, Pradeepan S, Esposito E, Strezsak S, Fernandez-Delgado O, Kranz J. Factors Affecting Stability of RNA – Temperature, Length, Concentration, pH, and Buffering Species. J Pharm Sci. 2024 Feb;113(2):377–85.

13. Payne D, Newton D, Evans P, Osman H, Baretto R. Preanalytical issues affecting the diagnosis of COVID-19. J Clin Pathol. 2021 Apr;74(4):207–8.

14. World Health Organization. Laboratory testing for coronavirus disease (COVID-19) in suspected human cases [Internet]. 2020 Mar [cited 2025 May 23]. Available from: https://iris.who.int/bitstream/handle/10665/331501/WHO-COVID-19-laboratory-2020.5-eng.pdf?sequence=1&isAllowed=y

15. Yang H, Rao Z. Structural biology of SARS-CoV-2 and implications for therapeutic development. Nat Rev Microbiol. 2021 Nov 17;19(11):685–700.

16. Jackson CB, Farzan M, Chen B, Choe H. Mechanisms of SARS-CoV-2 entry into cells. Nat Rev Mol Cell Biol. 2022 Jan 5;23(1):3–20.

17. V'kovski P, Kratzel A, Steiner S, Stalder H, Thiel V. Coronavirus biology and replication: implications for SARS-CoV-2. Nat Rev Microbiol. 2021 Mar 28;19(3):155–70.

18. Yan R, Zhang Y, Li Y, Xia L, Guo Y, Zhou Q. Structural basis for the recognition of SARS-CoV-2 by full-length human ACE2. Science (1979). 2020 Mar 4;367(6485):1444–8.

19. Beyerstedt S, Casaro EB, Rangel ÉB. COVID-19: angiotensin-converting enzyme 2 (ACE2) expression and tissue susceptibility to SARS-CoV-2 infection. European Journal of Clinical Microbiology & Infectious Diseases. 2021 May 3;40(5):905–19.

20. Scialo F, Daniele A, Amato F, Pastore L, Matera MG, Cazzola M, et al. ACE2: The Major Cell Entry Receptor for SARS-CoV-2. Lung. 2020 Dec 10;198(6):867–77.

21. Hikmet F, Méar L, Edvinsson Å, Micke P, Uhlén M, Lindskog C. The protein expression profile of ACE2 in human tissues. Mol Syst Biol. 2020 Jul 26;16(7):e9610.

22. Gong Y, Qin S, Dai L, Tian Z. The glycosylation in SARS-CoV-2 and its receptor ACE2. Signal Transduct Target Ther. 2021 Nov 15;6(1):396.

23. Parasher A. COVID-19: Current understanding of its Pathophysiology, Clinical presentation and Treatment. Postgrad Med J. 2021 May 1;97(1147):312–20.

24. Polak SB, Van Gool IC, Cohen D, von der Thüsen JH, van Paassen J. A systematic review of pathological findings in COVID-19: a pathophysiological timeline and possible mechanisms of disease progression. Modern Pathology. 2020 Nov;33(11):2128–38.

25. Lamers MM, Haagmans BL. SARS-CoV-2 pathogenesis. Nat Rev Microbiol. 2022 May 30;20(5):270–84.

26. Upadhya S, Rehman J, Malik AB, Chen S. Mechanisms of Lung Injury Induced by SARS-CoV-2 Infection. Physiology. 2022 Mar 1;37(2):88–100.

27. Zanza C, Romenskaya T, Manetti A, Franceschi F, La Russa R, Bertozzi G, et al. Cytokine Storm in COVID-19: Immunopathogenesis and Therapy. Medicina (B Aires). 2022 Jan 18;58(2):144.

28. Park A, Iwasaki A. Type I and Type III Interferons – Induction, Signaling, Evasion, and Application to Combat COVID-19. Cell Host Microbe. 2020 Jun;27(6):870–8.

29. Yang L, Xie X, Tu Z, Fu J, Xu D, Zhou Y. The signal pathways and treatment of cytokine storm in COVID-19. Signal Transduct Target Ther. 2021 Dec 1;6(1):255.

30. Chen R, Lan Z, Ye J, Pang L, Liu Y, Wu W, et al. Cytokine Storm: The Primary Determinant for the Pathophysiological Evolution of COVID-19 Deterioration. Front Immunol. 2021 Apr 28;12:589095.

31. Montazersaheb S, Hosseiniyan Khatibi SM, Hejazi MS, Tarhriz V, Farjami A, Ghasemian Sorbeni F, et al. COVID-19 infection: an overview on cytokine storm and related interventions. Virol J. 2022 May 26;19(1):92.

32. Mann ER, Menon M, Knight SB, Konkel JE, Jagger C, Shaw TN, et al. Longitudinal immune profiling reveals key myeloid signatures associated with COVID-19. Sci Immunol. 2020 Sep 18;5(51):eabd6197.

33. García-González P, Tempio F, Fuentes C, Merino C, Vargas L, Simon V, et al. Dysregulated Immune Responses in COVID-19 Patients Correlating With Disease Severity and Invasive Oxygen Requirements. Front Immunol. 2021 Oct 21;12:769059.

34. Bassler K, Schulte-Schrepping J, Warnat-Herresthal S, Aschenbrenner AC, Schultze JL. The Myeloid Cell Compartment—Cell by Cell. Annu Rev Immunol. 2019 Apr 26;37(1):269–93.

35. Merad M, Martin JC. Pathological inflammation in patients with COVID-19: a key role for monocytes and macrophages. Nat Rev Immunol. 2020 Jun 17;20(6):355–62.

36. Meidaninikjeh S, Sabouni N, Marzouni HZ, Bengar S, Khalili A, Jafari R. Monocytes and macrophages in COVID-19: Friends and foes. Life Sci. 2021 Mar 15;269:119010.

37. Muntjewerff EM, Meesters LD, van den Bogaart G. Antigen Cross-Presentation by Macrophages. Front Immunol. 2020 Jul 8;11:1276.

38. Labonte AC, Tosello-Trampont AC, Hahn YS. The Role of Macrophage Polarization in Infectious and Inflammatory Diseases. Mol Cells. 2014 Apr;37(4):275–85.

39. Biswas SK, Chittezhath M, Shalova IN, Lim JY. Macrophage polarization and plasticity in health and disease. Immunol Res. 2012 Sep;53(1–3):11–24.

40. Kosyreva A, Dzhalilova D, Lokhonina A, Vishnyakova P, Fatkhudinov T. The Role of Macrophages in the Pathogenesis of SARS-CoV-2-Associated Acute Respiratory Distress Syndrome. Front Immunol. 2021 May 10;12:682871.

41. Ma M, Jiang W, Zhou R. DAMPs and DAMP-sensing receptors in inflammation and diseases. Immunity. 2024 Apr;57(4):752–71.

42. Sievers BL, Cheng MTK, Csiba K, Meng B, Gupta RK. SARS-CoV-2 and innate immunity: the good, the bad, and the “goldilocks.” Cell Mol Immunol. 2023 Nov 20;21(2):171–83.

43. Le Pen J, Rice CM. The antiviral state of the cell: lessons from SARS-CoV-2. Curr Opin Immunol. 2024 Apr;87:102426.

44. Minkoff JM, tenOever B. Innate immune evasion strategies of SARS-CoV-2. Nat Rev Microbiol. 2023 Jan 11;21(3):178–94.

45. Zhang Q, Bastard P, Liu Z, Le Pen J, Moncada-Velez M, Chen J, et al. Inborn errors of type I IFN immunity in patients with life-threatening COVID-19. Science (1979). 2020 Oct 23;370(6515):eabd4570.

46. Agrawal P, Nawadkar R, Ojha H, Kumar J, Sahu A. Complement Evasion Strategies of Viruses: An Overview. Front Microbiol. 2017 Jun 16;8:1117.

47. Afzali B, Noris M, Lambrecht BN, Kemper C. The state of complement in COVID-19. Nat Rev Immunol. 2022 Feb 15;22(2):77–84.

48. Kishore U, Ghebrehiwet B. Editorial: C1q: A Molecular Bridge to Innate and Adaptive Immunity. Front Immunol. 2020 Mar 17;11:417.

49. Macor P, Durigutto P, Mangogna A, Bussani R, De Maso L, D'Errico S, et al. Multiple-Organ Complement Deposition on Vascular Endothelium in COVID-19 Patients. Biomedicines. 2021 Aug 12;9(8):1003.

50. Zacharias M, Kashofer K, Wurm P, Regitnig P, Schütte M, Neger M, et al. Host and microbiome features of secondary infections in lethal covid-19. iScience. 2022 Sep;25(9):104926.

51. Ma L, Sahu SK, Cano M, Kuppuswamy V, Bajwa J, McPhatter J, et al. Increased complement activation is a distinctive feature of severe SARS-CoV-2 infection. Sci Immunol. 2021 May 28;6(59):eabh2259.

52. Wells TJ, Esposito T, Henderson IR, Labzin LI. Mechanisms of antibody-dependent enhancement of infectious disease. Nat Rev Immunol. 2024 Aug 9;6–21.

53. Bournazos S, Gupta A, Ravetch J V. The role of IgG Fc receptors in antibody-dependent enhancement. Nat Rev Immunol. 2020 Oct 11;20(10):633–43.

54. Shimizu J, Sasaki T, Koketsu R, Morita R, Yoshimura Y, Murakami A, et al. Reevaluation of antibody-dependent enhancement of infection in anti-SARS-CoV-2 therapeutic antibodies and mRNA-vaccine antisera using FcR- and ACE2-positive cells. Sci Rep. 2022 Sep 16;12(1):15612.

55. Shen XR, Li Q, Li HL, Wang X, Wang Q, Zheng XS, et al. Antibody-Dependent Enhancement of SARS-CoV-2 Infection of Human Immune Cells: In Vitro Assessment Provides Insight in COVID-19 Pathogenesis. Viruses. 2021 Dec 11;13(12):2483.

56. Okuya K, Hattori T, Saito T, Takadate Y, Sasaki M, Furuyama W, et al. Multiple Routes of Antibody-Dependent Enhancement of SARS-CoV-2 Infection. Microbiol Spectr. 2022 Apr 27;10(2):e0155321.

57. Qi H, Liu B, Wang X, Zhang L. The humoral response and antibodies against SARS-CoV-2 infection. Nat Immunol. 2022 Jul 27;23(7):1008–20.

58. Zhang A, Stacey HD, D'Agostino MR, Tugg Y, Marzok A, Miller MS. Beyond neutralization: Fc-dependent antibody effector functions in SARS-CoV-2 infection. Nat Rev Immunol. 2023 Jun 19;23(6):381–96.

59. Mellors J, Dhaliwal R, Longet S, Tipton T, McInnes I, Siebert S, et al. Complement-mediated enhancement of SARS-CoV-2 antibody neutralisation potency in vaccinated individuals. Nat Commun. 2025 Mar 18;16(1):2666.

60. Corthésy B. Multi-Faceted Functions of Secretory IgA at Mucosal Surfaces. Front Immunol. 2013 Jul 12;4:185.

61. Pilapitiya D, Wheatley AK, Tan HX. Mucosal vaccines for SARS-CoV-2: triumph of hope over experience. EBioMedicine. 2023 Jun;92:104585.

62. Chu H, Chan JFW, Yuen KY. Animal models in SARS-CoV-2 research. Nat Methods. 2022 Apr 8;19(4):392–4.

63. Muñoz-Fontela C, Dowling WE, Funnell SGP, Gsell PS, Riveros-Balta AX, Albrecht RA, et al. Animal models for COVID-19. Nature. 2020 Oct 22;586(7830):509–15.

64. Tarrés-Freixas F, Trinité B, Pons-Grífols A, Romero-Durana M, Riveira-Muñoz E, Ávila-Nieto C, et al. Heterogeneous Infectivity and Pathogenesis of SARS-CoV-2 Variants Beta, Delta and Omicron in Transgenic K18-hACE2 and Wildtype Mice. Front Microbiol. 2022 May 4;13:840757.

65. Enkirch T, von Messling V. Ferret models of viral pathogenesis. Virology. 2015 May 1;479–480:259–70.

66. Kim Y Il, Kim SG, Kim SM, Kim EH, Park SJ, Yu KM, et al. Infection and Rapid Transmission of SARS-CoV-2 in Ferrets. Cell Host Microbe. 2020 May 13;27(5):704-709.e2.

67. Chang MC, Hild S, Grieder F. Nonhuman primate models for SARS-CoV-2 research: Consider alternatives to macaques. Lab Anim (NY). 2021 May 30;50(5):113–4.

68. Lemaitre J, Naninck T, Delache B, Creppy J, Huber P, Holzapfel M, et al. Non-human primate models of human respiratory infections. Mol Immunol. 2021 Jul 1;135:147–64.

69. Imai M, Iwatsuki-Horimoto K, Hatta M, Loeber S, Halfmann PJ, Nakajima N, et al. Syrian hamsters as a small animal model for SARS-CoV-2 infection and countermeasure development. Proc Natl Acad Sci U S A. 2020 Jul 14;117(28):16587–95.

70. Sia SF, Yan LM, Chin AWH, Fung K, Choy KT, Wong AYL, et al. Pathogenesis and transmission of SARS-CoV-2 in golden hamsters. Nature. 2020 Jul 30;583(7818):834–8.

71. McMahan K, Giffin V, Tostanoski LH, Chung B, Siamatu M, Suthar MS, et al. Reduced pathogenicity of the SARS-CoV-2 omicron variant in hamsters. Med. 2022 Apr 8;3(4):262-268.e4.

72. Yuan S, Ye ZW, Liang R, Tang K, Zhang AJ, Lu G, et al. Pathogenicity, transmissibility, and fitness of SARS-CoV-2 Omicron in Syrian hamsters. Science (1979). 2022 Jul 22;377(6604):428–33.

73. Jeong GU, Song H, Yoon GY, Kim D, Kwon YC. Therapeutic Strategies Against COVID-19 and Structural Characterization of SARS-CoV-2: A Review. Front Microbiol. 2020 Jul 14;11:1723.

74. Li G, Hilgenfeld R, Whitley R, De Clercq E. Therapeutic strategies for COVID-19: progress and lessons learned. Nat Rev Drug Discov. 2023 Jun 19;22(6):449–75.

75. Corti D, Purcell LA, Snell G, Veesler D. Tackling COVID-19 with neutralizing monoclonal antibodies. Cell. 2021 Jun 10;184(12):3086–108.

76. Zhang H, Lv P, Jiang J, Liu Y, Yan R, Shu S, et al. Advances in developing ACE2 derivatives against SARS-CoV-2. Lancet Microbe. 2023 May 1;4(5):e369–78.

77. Capraz T, Kienzl NF, Laurent E, Perthold JW, Föderl-Höbenreich E, Grünwald-Gruber C, et al. Structure-guided glyco-engineering of ACE2 for improved potency as soluble SARS-CoV-2 decoy receptor. Elife. 2021 Dec 20;10:e73641.

78. Chan KK, Dorosky D, Sharma P, Abbasi SA, Dye JM, Kranz DM, et al. Engineering human ACE2 to optimize binding to the spike protein of SARS coronavirus 2. Science (1979). 2020 Sep 4;369(6508):1261–5.

79. Haschke M, Schuster M, Poglitsch M, Loibner H, Salzberg M, Bruggisser M, et al. Pharmacokinetics and pharmacodynamics of recombinant human angiotensin-converting enzyme 2 in healthy human subjects. Clin Pharmacokinet. 2013 Sep 1;52(9):783–92.

80. Strohl WR. Fusion Proteins for Half-Life Extension of Biologics as a Strategy to Make Biobetters. BioDrugs. 2015 Aug 16;29(4):215–39.

81. Fahad S, Khan FA, Pandupuspitasari NS, Ahmed MM, Liao YC, Waheed MT, et al. Recent developments in therapeutic protein expression technologies in plants. Biotechnol Lett. 2015 Feb 18;37(2):265–79.

82. The PREVAIL II Writing Group for the MNPIST. A Randomized, Controlled Trial of ZMapp for Ebola Virus Infection. New England Journal of Medicine. 2016 Oct 13;375(15):1448–56.

83. Chichester JA, Green BJ, Jones RM, Shoji Y, Miura K, Long CA, et al. Safety and immunogenicity of a plant-produced Pfs25 virus-like particle as a transmission blocking vaccine against malaria: A Phase 1 dose-escalation study in healthy adults. Vaccine. 2018 Sep 18;36(39):5865–71.

84. Phoolcharoen W, Shanmugaraj B, Khorattanakulchai N, Sunyakumthorn P, Pichyangkul S, Taepavarapruk P, et al. Preclinical evaluation of immunogenicity, efficacy and safety of a recombinant plant-based SARS-CoV-2 RBD vaccine formulated with 3M-052-Alum adjuvant. Vaccine. 2023 Apr 24;41(17):2781–92.

85. Hager KJ, Pérez Marc G, Gobeil P, Diaz RS, Heizer G, Llapur C, et al. Efficacy and Safety of a Recombinant Plant-Based Adjuvanted Covid-19 Vaccine. New England Journal of Medicine. 2022 Jun 2;386(22):2084–96.

86. Huafang Lai QC, Jake Stahnke JH. Agroinfiltration as an Effective and Scalable Strategy of Gene Delivery for Production of Pharmaceutical Proteins. Adv Tech Biol Med. 2014 Jul 28;01(01):103.

87. Nosaki S, Hoshikawa K, Ezura H, Miura K. Transient protein expression systems in plants and their applications. Plant Biotechnology. 2021 Sep 25;38(3):21.0610a.

88. Strasser R. Plant glycoengineering for designing next-generation vaccines and therapeutic proteins. Biotechnol Adv. 2023 Oct;67:108197.

89. Strasser R, Stadlmann J, Schähs M, Stiegler G, Quendler H, Mach L, et al. Generation of glyco-engineered Nicotiana benthamiana for the production of monoclonal antibodies with a homogeneous human-like N-glycan structure. Plant Biotechnol J. 2008 May;6(4):392–402.

90. CDC 2019-Novel Coronavirus (2019-nCoV) Real-Time RT-PCR Diagnostic Panel [Internet]. Centers for Disease Control and Prevention Division of Viral Diseases; 2023 [cited 2025 Jun 26]. Available from: https://www.fda.gov/media/134922/download

91. Welch SR, Davies KA, Buczkowski H, Hettiarachchi N, Green N, Arnold U, et al. Analysis of Inactivation of SARS-CoV-2 by Specimen Transport Media, Nucleic Acid Extraction Reagents, Detergents, and Fixatives. Loeffelholz MJ, editor. J Clin Microbiol. 2020 Oct 21;58(11):e01713-20.

92. Riddell S, Goldie S, Hill A, Eagles D, Drew TW. The effect of temperature on persistence of SARS-CoV-2 on common surfaces. Virol J. 2020 Oct 7;17(1):145.

93. Castilho A, Schwestka J, Kienzl NF, Vavra U, Grünwald-Gruber C, Izadi S, et al. Generation of enzymatically competent SARS-CoV-2 decoy receptor ACE2-Fc in glycoengineered Nicotiana benthamiana. Biotechnol J. 2021 Jun 12;16(6):2000566.

94. Izadi S, Vavra U, Melnik S, Grünwald-Gruber C, Föderl-Höbenreich E, Sack M, et al. In planta deglycosylation improves the SARS-CoV-2 neutralization activity of recombinant ACE2-Fc. Front Bioeng Biotechnol. 2023 May 3;11:1180044.

95. Föderl-Höbenreich E, Izadi S, Hofacker L, Kienzl NF, Castilho A, Strasser R, et al. An ACE2-Fc decoy produced in glycoengineered plants neutralizes ancestral and newly emerging SARS-CoV-2 variants and demonstrates therapeutic efficacy in hamsters. Sci Rep. 2025 Apr 2;15(1):11307.

96. Lei C, Yang J, Hu J, Sun X. On the Calculation of TCID50 for Quantitation of Virus Infectivity. Virol Sin. 2021 Feb 26;36(1):141–4.

97. Klausberger M, Kienzl NF, Stadlmayr G, Grünwald-Gruber C, Laurent E, Stadlbauer K, et al. Designed SARS-CoV-2 receptor binding domain variants form stable monomers. Biotechnol J. 2022 May 3;17(5).

98. Livak KJ, Schmittgen TD. Analysis of Relative Gene Expression Data Using Real-Time Quantitative PCR and the 2−ΔΔCT Method. Methods. 2001 Dec;25(4):402–8.

99. Hardt M, Föderl-Höbenreich E, Freydl S, Kouros A, Loibner M, Zatloukal K. Pre-analytical sample stabilization by different sampling devices for PCR-based COVID-19 diagnostics. N Biotechnol. 2022 Apr 8;70:19–27.

100. Kevadiya BD, Machhi J, Herskovitz J, Oleynikov MD, Blomberg WR, Bajwa N, et al. Diagnostics for SARS-CoV-2 infections. Nat Mater. 2021 May 15;20(5):593–605.

101. Zhao P, Praissman JL, Grant OC, Cai Y, Xiao T, Rosenbalm KE, et al. Virus-Receptor Interactions of Glycosylated SARS-CoV-2 Spike and Human ACE2 Receptor. Cell Host Microbe. 2020 Oct;28(4):586-601.e6.

102. Suryamohan K, Diwanji D, Stawiski EW, Gupta R, Miersch S, Liu J, et al. Human ACE2 receptor polymorphisms and altered susceptibility to SARS-CoV-2. Commun Biol. 2021 Apr 12;4(1):475.

103. Krause ME, Sahin E. Chemical and physical instabilities in manufacturing and storage of therapeutic proteins. Curr Opin Biotechnol. 2019 Dec 1;60:159–67.

104. Akbarian M, Chen SH. Instability Challenges and Stabilization Strategies of Pharmaceutical Proteins. Pharmaceutics. 2022 Nov 20;14(11):2533.

105. Abdelnabi R, Foo CS, Jochmans D, Vangeel L, De Jonghe S, Augustijns P, et al. The oral protease inhibitor (PF-07321332) protects Syrian hamsters against infection with SARS-CoV-2 variants of concern. Nat Commun. 2022 Feb 15;13(1):719.

106. Li Y, Wang H, Tang X, Fang S, Ma D, Du C, et al. SARS-CoV-2 and Three Related Coronaviruses Utilize Multiple ACE2 Orthologs and Are Potently Blocked by an Improved ACE2-Ig. J Virol. 2020 Oct 27;94(22):e01283-20.

107. Li L, Han P, Huang B, Xie Y, Li W, Zhang D, et al. Broader-species receptor binding and structural bases of Omicron SARS-CoV-2 to both mouse and palm-civet ACE2s. Cell Discov. 2022 Jul 12;8(1):65.

108. Gadjeva MG, Rouseva MM, Zlatarova AS, Reid KBM, Kishore U, Kojouharova MS. Interaction of Human C1q with IgG and IgM: Revisited. Biochemistry. 2008 Dec 9;47(49):13093–102.

109. Desmyter J, Melnick JL, Rawls WE. Defectiveness of interferon production and of rubella virus interference in a line of African green monkey kidney cells (Vero). J Virol. 1968 Oct;2(10):955–61.

110. Felgenhauer U, Schoen A, Gad HH, Hartmann R, Schaubmar AR, Failing K, et al. Inhibition of SARS–CoV-2 by type I and type III interferons. Journal of Biological Chemistry. 2020 Oct 9;295(41):13958–64.

111. Heskin J, Pallett SJC, Al-Hindawi A, Davies GW, Rayment M, Mughal N, et al. Evaluating the performance characteristics of five lateral flow assays for the detection of the SARS-CoV-2 nucleocapsid antigen. Sci Rep. 2022 Dec 1;12(1):8811.

112. Peto T, Affron D, Afrough B, Agasu A, Ainsworth M, Allanson A, et al. COVID-19: Rapid antigen detection for SARS-CoV-2 by lateral flow assay: A national systematic

evaluation of sensitivity and specificity for mass-testing. EClinicalMedicine. 2021 Jun 1;36:100924.

113. Carabelli AM, Peacock TP, Thorne LG, Harvey WT, Hughes J, de Silva TI, et al. SARS-CoV-2 variant biology: immune escape, transmission and fitness. Nat Rev Microbiol. 2023 Jan 18;162–77.

114. VanBlargan LA, Errico JM, Halfmann PJ, Zost SJ, Crowe JE, Purcell LA, et al. An infectious SARS-CoV-2 B.1.1.529 Omicron virus escapes neutralization by therapeutic monoclonal antibodies. Nat Med. 2022 Mar 1;28(3):490–5.

115. Huo J, Dijokaite-Guraliuc A, Liu C, Zhou D, Ginn HM, Das R, et al. A delicate balance between antibody evasion and ACE2 affinity for Omicron BA.2.75. Cell Rep. 2023 Jan 31;42(1):111903.

116. Arimori T, Ikemura N, Okamoto T, Takagi J, Standley DM, Hoshino A. Engineering ACE2 decoy receptors to combat viral escapability. Trends Pharmacol Sci. 2022 Oct 1;43(10):838–51.

117. Havranek B, Lindsey GW, Higuchi Y, Itoh Y, Suzuki T, Okamoto T, et al. A computationally designed ACE2 decoy has broad efficacy against SARS-CoV-2 omicron variants and related viruses in vitro and in vivo. Commun Biol. 2023 May 12;6(1):513.

118. Monteil V, Eaton B, Postnikova E, Murphy M, Braunsfeld B, Crozier I, et al. Clinical grade ACE2 as a universal agent to block SARS-CoV -2 variants . EMBO Mol Med. 2022 Aug 8;14(8):e15230.

119. Urano E, Itoh Y, Suzuki T, Sasaki T, Kishikawa J ichi, Akamatsu K, et al. An inhaled ACE2 decoy confers protection against SARS-CoV-2 infection in preclinical models. Sci Transl Med. 2023 Aug 30;15(711):16.

120. Rössler A, Riepler L, Bante D, von Laer D, Kimpel J. SARS-CoV-2 Omicron Variant Neutralization in Serum from Vaccinated and Convalescent Persons. New England Journal of Medicine. 2022 Feb 17;386(7):698–700.

121. Carreño JM, Alshammary H, Tcheou J, Singh G, Raskin AJ, Kawabata H, et al. Activity of convalescent and vaccine serum against SARS-CoV-2 Omicron. Nature. 2022 Feb 24;602(7898):682–8.

122. Wu Z, Hu R, Zhang C, Ren W, Yu A, Zhou X. Elevation of plasma angiotensin II level is a potential pathogenesis for the critically ill COVID-19 patients. Crit Care. 2020 Jun 5;24(1):290.

123. Lu Y, Zhu Q, Fox DM, Gao C, Stanley SA, Luo K. SARS-CoV-2 down-regulates ACE2 through lysosomal degradation. Mol Biol Cell. 2022 Dec 1;33(14):ar147.

124. Gao X, Zhang S, Gou J, Wen Y, Fan L, Zhou J, et al. Spike-mediated ACE2 down-regulation was involved in the pathogenesis of SARS-CoV-2 infection. Journal of Infection. 2022 Oct 1;85(4):418–27.

125. Banu N, Panikar SS, Leal LR, Leal AR. Protective role of ACE2 and its downregulation in SARS-CoV-2 infection leading to Macrophage Activation Syndrome: Therapeutic implications. Life Sci. 2020 Sep 1;256:117905.

126. Lee MMY, Kondo T, Campbell RT, Petrie MC, Sattar N, Solomon SD, et al. Effects of renin–angiotensin system blockers on outcomes from COVID-19: a systematic review and meta-analysis of randomized controlled trials. Eur Heart J Cardiovasc Pharmacother. 2024 Jan 5;10(1):68–80.

127. Bauer M, Jorda A, al-Jalali V, Wölfl-Duchek M, Bergmann F, Nussbaumer-Pröll A, et al. Phase I dose-escalation study to assess the safety, tolerability, pharmacokinetics and pharmacodynamics of an inhaled recombinant human ACE2. ERJ Open Res. 2024 Jan;10(1):00567–2023.

128. Zhang Z, Zeng E, Zhang L, Wang W, Jin Y, Sun J, et al. Potent prophylactic and therapeutic efficacy of recombinant human ACE2-Fc against SARS-CoV-2 infection in vivo. Cell Discov. 2021 Dec 1;7(1):65.

129. Isobe A, Arai Y, Kuroda D, Okumura N, Ono T, Ushiba S, et al. ACE2 N-glycosylation modulates interactions with SARS-CoV-2 spike protein in a site-specific manner. Commun Biol. 2022 Dec 1;5(1):1188.

130. Mehdipour AR, Hummer G. Dual nature of human ACE2 glycosylation in binding to SARS-CoV-2 spike. Proceedings of the National Academy of Sciences. 2021 May 11;118(19):e2100425118.

131. Chu H, Hu B, Huang X, Chai Y, Zhou D, Wang Y, et al. Host and viral determinants for efficient SARS-CoV-2 infection of the human lung. Nat Commun. 2021 Jan 8;12(1):134.

132. Liu H, Timko MP. Improving Protein Quantity and Quality-The Next Level of Plant Molecular Farming. Int J Mol Sci. 2022 Feb 1;23(3):1326.

133. Yao J, Weng Y, Dickey A, Wang K. Plants as Factories for Human Pharmaceuticals: Applications and Challenges. Int J Mol Sci. 2015 Dec 2;16(12):28549–65.

134. Buyel JF. Plant Molecular Farming – Integration and Exploitation of Side Streams to Achieve Sustainable Biomanufacturing. Front Plant Sci. 2019 Jan 18;9:1893.

135. Yang Z, Wang S, Halim A, Schulz MA, Frodin M, Rahman SH, et al. Engineered CHO cells for production of diverse, homogeneous glycoproteins. Nat Biotechnol. 2015 Aug 10;33(8):842–4.

136. Jaroentomeechai T, Karlsson R, Goerdeler F, Teoh FKY, Grønset MN, de Wit D, et al. Mammalian cell-based production of glycans, glycopeptides and glycomodules. Nat Commun. 2024 Dec 1;15(1):9668.

137. Niemer M, Mehofer U, Torres Acosta JA, Verdianz M, Henkel T, Loos A, et al. The human anti-HIV antibodies 2F5, 2G12, and PG9 differ in their susceptibility to proteolytic degradation: Down-regulation of endogenous serine and cysteine proteinase activities could improve antibody production in plant-based expression platforms. Biotechnol J. 2014 Apr;9(4):493–500.

138. Torchia JA, Tavares AH, Carstensen LS, Chen DY, Huang J, Xiao T, et al. Optimized ACE2 decoys neutralize antibody-resistant SARS-CoV-2 variants through functional receptor mimicry and treat infection in vivo. Sci Adv. 2022 Dec 9;8(49):eabq6527.

139. Göritzer K, Kallolimath S, Strasser R. Posttranslational modifications of heterologous proteins expressed in Nicotiana benthamiana. Plant Biotechnol J. 2025 Jun 8;pbi.70176.

140. Higuchi Y, Suzuki T, Arimori T, Ikemura N, Mihara E, Kirita Y, et al. Engineered ACE2 receptor therapy overcomes mutational escape of SARS-CoV-2. Nat Commun. 2021 Dec 21;12(1):3802.

141. Ikemura N, Taminishi S, Inaba T, Arimori T, Motooka D, Katoh K, et al. An engineered ACE2 decoy neutralizes the SARS-CoV-2 Omicron variant and confers protection against infection in vivo. Sci Transl Med. 2022 Jun 22;14(650):eabn7737.

142. Liu J, Mao F, Chen J, Lu S, Qi Y, Sun Y, et al. An IgM-like inhalable ACE2 fusion protein broadly neutralizes SARS-CoV-2 variants. Nat Commun. 2023 Aug 25;14(1):5191.

143. Ferrari M, Mekkaoui L, Ilca FT, Akbar Z, Bughda R, Lamb K, et al. Characterization of a Novel ACE2-Based Therapeutic with Enhanced Rather than Reduced Activity against SARS-CoV-2 Variants. J Virol. 2021 Sep 9;95(19):e0068521.

144. Merigeon E, Yang D, Ihms E, Bassit L, Fitzpatrick E, Jonsson C, et al. An ACE2-IgG4 Fc Fusion Protein Demonstrates Strong Binding to All Tested SARS-CoV-2 Variants and Reduced Lung Inflammation in Animal Models of SARS-CoV-2 and Influenza. Pathog Immun. 2022 Aug 23;7(1):104–21.

145. Kim CM, Kim DM, Bang MS, Seo JW, Kim DY, Yun NR, et al. Efficacy of Plant-Made Human Recombinant ACE2 against COVID-19 in a Golden Syrian Hamster Model. Viruses. 2023 Apr 14;15(4):964.

146. Clark JJ, Hoxie I, Adelsberg DC, Sapse IA, Andreata-Santos R, Yong JS, et al. Protective effect and molecular mechanisms of human non-neutralizing cross-reactive spike antibodies elicited by SARS-CoV-2 mRNA vaccination. Cell Rep. 2024 Nov;43(11):114922.

147. Chen Y, Sun L, Ullah I, Beaudoin-Bussières G, Anand SP, Hederman AP, et al. Engineered ACE2-Fc counters murine lethal SARS-CoV-2 infection through direct neutralization and Fc-effector activities. Sci Adv. 2022 Jul 15;8(28).

148. Czajkowsky DM, Hu J, Shao Z, Pleass RJ. Fc-fusion proteins: new developments and future perspectives. EMBO Mol Med. 2012 Oct 26;4(10):1015–28.

149. Duivelshof BL, Murisier A, Camperi J, Fekete S, Beck A, Guillarme D, et al. Therapeutic Fc-fusion proteins: Current analytical strategies. J Sep Sci. 2021 Jan 29;44(1):35–62.

150. Liu S, Selvaraj P, Sangare K, Luan B, Wang TT. Spike protein-independent attenuation of SARS-CoV-2 Omicron variant in laboratory mice. Cell Rep. 2022 Sep;40(11):111359.

151. Yamin R, Jones AT, Hoffmann HH, Schäfer A, Kao KS, Francis RL, et al. Fc-engineered antibody therapeutics with improved anti-SARS-CoV-2 efficacy. Nature. 2021 Nov 18;599(7885):465–70.

152. Bakema JE, van Egmond M. Immunoglobulin A. MAbs. 2011 Jul 27;3(4):352–61.

153. Göritzer K, Groppelli E, Grünwald-Gruber C, Figl R, Ni F, Hu H, et al. Recombinant neutralizing secretory IgA antibodies for preventing mucosal acquisition and transmission of SARS-CoV-2. Molecular Therapy. 2024 Mar 6;32(3):689–703.

154. Ejemel M, Li Q, Hou S, Schiller ZA, Tree JA, Wallace A, et al. A cross-reactive human IgA monoclonal antibody blocks SARS-CoV-2 spike-ACE2 interaction. Nat Commun. 2020 Aug 21;11(1):4198.

155. Grant RA, Morales-Nebreda L, Markov NS, Swaminathan S, Querrey M, Guzman ER, et al. Circuits between infected macrophages and T cells in SARS-CoV-2 pneumonia. Nature. 2021 Feb 25;590(7847):635–41.

156. Sefik E, Qu R, Junqueira C, Kaffe E, Mirza H, Zhao J, et al. Inflammasome activation in infected macrophages drives COVID-19 pathology. Nature. 2022 Jun 16;606(7914):585–93.

157. Labzin LI, Chew KY, Eschke K, Wang X, Esposito T, Stocks CJ, et al. Macrophage ACE2 is necessary for SARS-CoV-2 replication and subsequent cytokine responses that restrict continued virion release. Sci Signal. 2023 Apr 25;16(782):eabq1366.

158. Thorne LG, Reuschl A, Zuliani-Alvarez L, Whelan MVX, Turner J, Noursadeghi M, et al. SARS-CoV-2 sensing by RIG-I and MDA5 links epithelial infection to macrophage inflammation. EMBO J. 2021 Aug 2;40(15):e107826.

159. Boumaza A, Gay L, Mezouar S, Bestion E, Diallo AB, Michel M, et al. Monocytes and Macrophages, Targets of Severe Acute Respiratory Syndrome Coronavirus 2: The Clue for Coronavirus Disease 2019 Immunoparalysis. J Infect Dis. 2021 Aug 2;224(3):395–406.

160. Son M, Diamond B, Santiago-Schwarz F. Fundamental role of C1q in autoimmunity and inflammation. Immunol Res. 2015 Dec 26;63(1–3):101–6.

161. Beirag N, Varghese PM, Neto MM, Al Aiyan A, Khan HA, Qablan M, et al. Complement Activation-Independent Attenuation of SARS-CoV-2 Infection by C1q and C4b-Binding Protein. Viruses. 2023 May 29;15(6):1269.

162. Halstead SB. Dengue Antibody-Dependent Enhancement: Knowns and Unknowns. Microbiol Spectr. 2014 Nov 21;2(6):10.1128.

163. Wan Y, Shang J, Sun S, Tai W, Chen J, Geng Q, et al. Molecular Mechanism for Antibody-Dependent Enhancement of Coronavirus Entry. J Virol. 2020 Feb 14;94(5):e02015.

164. Liu L, Wei Q, Lin Q, Fang J, Wang H, Kwok H, et al. Anti-spike IgG causes severe acute lung injury by skewing macrophage responses during acute SARS-CoV infection. JCI Insight. 2019 Feb 21;4(4):e123158.

165. Luo F, Liao FL, Wang H, Tang HB, Yang ZQ, Hou W. Evaluation of Antibody-Dependent Enhancement of SARS-CoV Infection in Rhesus Macaques Immunized with an Inactivated SARS-CoV Vaccine. Virol Sin. 2018 Apr 14;33(2):201–4.

166. García-Nicolás O, V'kovski P, Zettl F, Zimmer G, Thiel V, Summerfield A. No Evidence for Human Monocyte-Derived Macrophage Infection and Antibody-Mediated Enhancement of SARS-CoV-2 Infection. Front Cell Infect Microbiol. 2021 Apr 12;11:644574.

167. Maemura T, Kuroda M, Armbrust T, Yamayoshi S, Halfmann PJ, Kawaoka Y. Antibody-Dependent Enhancement of SARS-CoV-2 Infection Is Mediated by the IgG Receptors FcgRIIA and FcgRIIIA but Does Not Contribute to Aberrant Cytokine Production by Macrophages. mBio. 2021 Oct 1;12(5):e0198721.

168. GHIRAN I, Tyagi SR, Klickstein LB, Nicholson-Weller A. Expression and Function of C1q Receptors and C1q Binding Proteins at the Cell Surface. Immunobiology. 2002 Sep;205(4–5):407–20.

169. García-Nicolás O, Godel A, Zimmer G, Summerfield A. Macrophage phagocytosis of SARS-CoV-2-infected cells mediates potent plasmacytoid dendritic cell activation. Cell Mol Immunol. 2023 May 30;20(7):835–49.

170. Zheng J, Wang Y, Li K, Meyerholz DK, Allamargot C, Perlman S. Severe Acute Respiratory Syndrome Coronavirus 2-Induced Immune Activation and Death of Monocyte-Derived Human Macrophages and Dendritic Cells. Journal of Infectious Diseases. 2021 Mar 1;223(5):785–95.

171. Bohnacker S, Hartung F, Henkel F, Quaranta A, Kolmert J, Priller A, et al. Mild COVID-19 imprints a long-term inflammatory eicosanoid- and chemokine memory in monocyte-derived macrophages. Mucosal Immunol. 2022 Mar 1;15(3):515–24.

172. Lercher A, Cheong JG, Bale MJ, Jiang C, Hoffmann HH, Ashbrook AW, et al. Antiviral innate immune memory in alveolar macrophages following SARS-CoV-2 infection ameliorates secondary influenza A virus disease. Immunity. 2024 Nov 12;57(11):2530-2546.e13.